UNIVERSITY OF CALIFORNIA, MERCED

Evaluating water balance components in the Sierra Nevada: Snowpack sensitivity to climate warming and forest evapotranspiration reduction potential

A dissertation submitted in partial satisfaction of the requirements
for the degree Doctor of Philosophy

in

Environmental Systems

by

James William Roche

Committee in charge:

Professor Roger C. Bales, Chair
Professor Martha H. Conklin
Professor Teamrat A. Ghezzehei
Professor Jessica D. Lundquist

2017

The Dissertation of James William Roche is approved, and it is acceptable in quality and form for publication on microfilm and electronically:

Dr. Jessica D. Lundquist

Dr. Teamrat A. Ghezzehei

Dr. Martha H. Conklin

Dr. Roger C. Bales, Chair

University of California, Merced

2017

Table of Contents

List of Tables

List of Figures

Acknowledgements

I am thankful for the many people who guided me in this endeavor. My advisor, Roger Bales, kept me moving through the process, always with the challenge: “How does this work build our intuition?”. Martha Conklin offered encouragement and was instrumental in securing and maintaining funding for tuition. Teamrat Ghezzehei taught one of the best groundwater classes there is and gave me early confidence running spatial hydrologic process models. Lastly, Jessica Lundquist first suggested that I pursue a doctorate almost a decade ago and has encouraged me along the way.

Special thanks to the Yosemite Conservancy for providing substantial funding that supported me financially in my position with Yosemite National Park, as well as funding the University of California Merced to support this research. The Merced Irrigation District through the California Integrated Regional Watershed Management Program provided tuition support as did a fellowship from the Southern California Edison Company. Finally, thanks to Yosemite National Park for providing early tuition costs until other funding became available.

Finally, I would like to acknowledge colleagues, friends, and family for their patient support over the past six years. Joseph Meyer, Linda Mazzu, and Niki Nicholas of Yosemite National Park provided encouragement and material support by allowing an alternate work schedule to accommodate pursuit of this degree. I wish to acknowledge the substantial technical assistance and advice I received from Danny Marks, Adam

Winstral, Scott Havens, Mike Goulden, Xiande Meng, Patrick Womble, Erin Stacy, Safeeq Mohammed, Bob Rice, Phil Saksa, Jan van Wagtendonk, and Yanjun Su. I am grateful for the encouragement, advice, and friendship that I received from Mike Yochim, Kelly Redmond, Greg Stock, Peter Kirchner, Michael Pickard, Jodi Bailey, Katy Warner, Rachel Mazur, Andi Heard, Sylvia Haultain, Sue Beatty, and Bruce McGurk. I must also acknowledge the Physical Science and Landscape Ecology group at Yosemite National Park who supported and covered for me throughout this process. Special thanks and love to my parents, James E. and Krista Roche, and my wife, Sally Sprouse, without whom none of this would have been possible.

Curriculum Vitae

James W. Roche
Park Hydrologist
Yosemite National Park
P.O. Box 700W
El Portal, CA 95318

Education

Ph.D. Environmental Systems. University of California, Merced. 2017
Advisor: Dr. Roger Bales, Director Sierra Nevada Research Institute

M.S. Geology. University of Washington. 1994.
Advisor: Dr. Bernard Hallet, Professor of Geology

B.S. Chemistry. Louisiana State University. 1990.

Publications

Peer-reviewed

2017

Forrester, H.A, Clow, D.W., **Roche, J.W.**, Heyvaert, A.C., and Battaglin, W.A., Effects of backpacker use, pack stock trail use, and pack stock grazing on water quality in Yosemite National Park, California. *J. Environmental Management.* doi:10.1007/s00267-017-0899-z

2016

Lundquist, J. D., **Roche, J. W.**, Forrester, H., Moore, C., Keenan, E., Perry, G., Cristea, N., Henn, B., Lapo, K., McGurk, B., Cayan, D.R., and Dettinger, M. D., Yosemite Hydroclimate Network: Distributed stream and atmospheric data for the Tuolumne River watershed and surroundings. *Water Resources Research*, *52*(9), 7478–7489. doi: 10.1002/2016WR019261

2015

Holmquist, J.G., Schmidt-Gengenbach, J. and **Roche, J.W.**, Stream macroinvertebrates and habitat below and above two wilderness fords used by mules, horses, and hikers in Yosemite National Park. Western North American Naturalist, **75(3)**, pp.311-324. doi: 10.3398/064.075.0308

Cooper, D.J., Wolf, E.C., Ronayne, M.J. and **Roche, J.W.**, Effects of groundwater pumping on the sustainability of a mountain wetland complex, Yosemite National Park, California. *Journal of Hydrology*: Regional Studies, **3**, pp. 87-105. doi: 10.1016/j.ejrh.2014.10.002

2014

Ostoja, S.M., Brooks, M.L., Moore, P.E., Berlow, E.L., Blank, R., **Roche, J.**, Chase, J. and Haultain, S., 2014. Potential environmental effects of pack stock on meadow ecosystems of the Sierra Nevada, USA. *The Rangeland Journal* **36(5)**, pp. 411-427. doi: 10.1071/RJ14050

2012

Russo, T.A., Fisher, A.T., and **Roche, J.W.**, Improving riparian wetland conditions based on infiltration and drainage behavior during and after controlled flooding. *Journal of Hydrology*, **432**, pp. 98-111. doi: 10.1016/j.jhydrol.2012.02.022

2011

Clow, D. W., Peavler, R. S., **Roche, J.**, Panorska, A. K., Thomas, J. M., and Smith, S., 2011. Assessing possible visitor-use impacts on water quality in Yosemite National Park, California. *Environmental monitoring and assessment*, **183(1-4)**, pp. 197-215. doi: 10.1007/s10661-011-1915-z

Other publications

2009

Lundquist, J. and **Roche, J.**, 2009. Climate change and water supply in western national parks. *Park Science,* **26(1)**, pp. 31-34. ISSN 1090-9966

2006

Bacon, J., **Roche J.**, Elliot, C., Nicholas, N., 2006. VERP: Putting Principles into Practice in Yosemite National Park. *The George Wright Forum*, **23(2)**, pp. 73-83.

Cooper, D.J., Lundquist, J.D, King, J., Flint, A., Flint, L., Wolf, E., Lott, F.C. and **Roche, J.W.**, Effects of the Tioga Road on Hydrologic Processes and Lodgepole Pine Invasion into Tuolumne Meadows, Yosemite National Park. National Park Service, 146 pp. https://www.nps.gov/yose/learn/management/upload/Tuolumne-Meadows-Hydrology-Impacts-Report-FINAL.pdf

Submitted manuscript

Roche, J.W., Bales, R.C., Rice, R., and Marks, D., Management implications of snowpack sensitivity to temperature and atmospheric-moisture changes in Yosemite National Park, CA. Submitted to the Journal of the American Water Resources Association, June 4, 2017.

Manuscripts in preparation

Roche, J.W., Rice, R., Meng, X., Cayan, D.R., Dettinger, M.D., Alden, D., Bales, R.C., Patel, S.C., and Mason, M.A., Climate and snow data set for the Tuolumne and Merced River watersheds, California, USA.

Roche, J.W., Goulden, M.L., and Bales, R.C., Estimating evapotranspiration change due to forest treatment and fire at the basin scale in the Sierra Nevada, California.

Abstract

Evaluating water balance components in the Sierra Nevada: Snowpack sensitivity to climate warming and forest evapotranspiration reduction potential

by

James William Roche

Doctor of Philosophy in Environmental Systems

University of California, Merced, 2017

Professor Roger C. Bales, Chair

The work presented here was motivated by a need to better understand components of the water balance in the Sierra Nevada with respect to a warming climate. I present this as two case studies preceded by a summary of a climate data set prepared during the course of this work. The first case study examined the implications of climate warming on snowpack storage in the Merced and Tuolumne River watersheds, which encompass Yosemite National Park, using recent wet and cool (water year 2011) and warm and dry (WY2013) years as starting points. The second study focused on estimating the impact of forest treatment and fire on forest evapotranspiration (ET) at the patch to watershed scale in the American and Kings River basins.

Modeled April 1st snowpack storage in the Yosemite area declined 38, 73, and 90% for +2, 4, 6°C dry-year warming scenarios. Seasonal snowpack disappears below 2000 m elevation with 4°C warming in both wet and dry years. Assuming vapor pressure remains constant with increasing temperature resulted in up to 100 mm more late-spring snow water equivalent than the respective constant-relative-humidity scenario with 6°C warming. Reduced snowpack and snow-cover duration will mean less summer melt input to meadow and forest soils, resulting in loss of wetlands and longer forest fire seasons. Other management implications include reduced late-season streamflow for dependent downstream communities and wildlife.

Water-limited forests exhibited smaller changes in the normalized difference vegetation index (NDVI) per respective changes in basal area than less water-limited areas. Intensive thinning projects, which reduced forest density 40-50%, resulted in NDVI reductions of 0.09-0.12 units from control plot values of 0.7-0.8, corresponding to ET reductions of 152-216 mm yr^{-1}. The minimum observed change for treated areas was 0.07 NDVI units from an initial value of 0.7 units, associated with a basal area reduction of 9%. Net ET reduction due to forest fires in 1990-2008 in the American River watershed was about 5 times that in the Kings River (65 vs. 14 million m^3 yr^{-1}). In

addition to reducing the multiple impacts of catastrophic forest fire, forest thinning and managed fire offer the potential to offset water losses due to increased ET in a warming climate.

Summary Introduction

Water balance as the sum of precipitation inputs, soil and regolith storage, runoff, and evapotranspiration (ET) in mountain watersheds is changing, and expected temperature increases over the next century imply much greater changes are in store, particularly for snow-dominated systems. Yosemite National Park lies at the heart of the Sierra Nevada and has and will experience changes in the water cycle. Yosemite also serves a laboratory where changes are being observed with respect to runoff, snowpack, and tree mortality. Snowpack storage historically accounted for 40% of California's water supply (Roos, 1989) and has decreased significantly at elevations below 2600 m since 1950 in the Yosemite to Sequoia-Kings National Parks region (Andrews, 2012; Mote et al., 2005). Substantial decreases in snowpack are expected across the high Sierra Nevada over this century (Knowles & Cayan, 2002). As this source of storage decreases, forest water demand is expected to increase (Goulden & Bales, 2014), and as has been observed during the recent warm drought, forest mortality may also increase (Millar & Stephenson, 2015; Williams et al., 2013). Motivating the studies in this dissertation is a need to bridge research-grade methods with management needs to facilitate resources management planning in these rapidly changing conditions. That is, there is a critical need to examine changes to the water balance at the scale of mountain watersheds with sufficient spatial and temporal resolution to address questions of management concern (e.g. Curtis et al., 2014; Flint & Flint, 2012). I contribute to this effort through two case studies, one focused on potential snowpack storage changes in the Yosemite National Park region, and another that examines the potential for altering evapotranspiration from

mountain forests in order to mitigate changes in water storage due to warmer temperatures.

Chapter 1 introduces data sources used to model snowpack across the domain of the Merced and Tuolumne River watersheds where Yosemite National Park occupies the higher snow-dominated areas. This stand-alone data paper contains information on instrumentation, data limitations, and processing steps taken to quality control data for water years 2010-2014. The data set contains 23 high quality temperature and humidity station records that span the model domain and elevations from 333 to 2987 m. In addition to forcing data (temperature, humidity, solar radiation, wind speed and direction, and precipitation), there is also observed snow depth and water content, and spatial data including elevation, vegetation properties, and watershed polygons. The purpose of publishing this data set is to a) adhere to hydrologic community's effort to publish data sets used to force modeling studies such as Chapter 2, and b) make high-quality data sets available to others interested in building our understanding this ecosystem.

The purpose of Chapter 2 was to examine snowpack sensitivity to temperature increases under different atmospheric humidity scenarios in the Merced and Tuolumne River watersheds at a spatial resolution relevant to management concerns. A secondary purpose was to apply a modeling approach that minimized calibration so that the internal snowpack physics remained consistent under warming scenarios. Using the data set described in Chapter 1 to force an energy- and mass-balance snow model (iSnobal, Marks et al., 1999), I examined snowpack spatial and temporal variability in recent cool and wet

(WY2011) and warm and dry (WY2013) years. I then applied uniform temperature increases of +2, +4, and +6°C to these "base" years under two humidity scenarios: 1) constant relative humidity and 2) constant vapor pressure. The results were examined for implications regarding snowpack storage and melt, seasonal snowcover duration, recreational and fire management, and downstream runoff changes.

In Chapter 3, I examined the potential impacts of forest treatments and fire on evapotranspiration using a data-driven remote sensing approach. The methods take advantage of a robust relation between mean annual ET as measured at flux towers and mean annual greenness of windward vegetation measured using the Landsat 30-m resolution normalized difference vegetation index (NDVI). The full Landsat surface reflectance library has recently been made available and coupled with powerful cloud computing tools permits detailed spatial and temporal examination of changes in NDVI (or other metrics of interest) from the scale of an individual forest plot to entire watersheds. I examined NDVI change as a result of treatment or fire, estimated the potential change in ET, and then expanded the analysis to estimate the net ET change over the American (warm and wet) and the Kings (cool and dry) watersheds for the 1990-2008 period.

References

Andrews, E. D. (2012). Hydrology of the Sierra Nevada Network national parks: Status and trends. Natural Resource Report NPS/SIEN/NRR—2012/500. (pp. 192). National Park Service, Fort Collins, Colorado. Retrieved from https://irma.nps.gov/DataStore/Reference/Profile/2184307

Curtis, J. A., Flint, L. E., Flint, A. L., Lundquist, J. D., Hudgens, B., Boydston, E. E., & Young, J. K. (2014). Incorporating cold-air pooling into downscaled climate models increases potential refugia for snow-dependent species within the Sierra Nevada Ecoregion, CA. *PloS One*, *9*(9), e106984. doi: 10.1371/journal.pone.0106984

Flint, L., & Flint, A. (2012). Downscaling future climate scenarios to fine scales for hydrologic and ecological modeling and analysis. *Ecological Processes*, *1*(1), 1–15. doi: 10.1186/2192-1709-1-2

Goulden, M. L., & Bales, R. C. (2014). Mountain runoff vulnerability to increased evapotranspiration with vegetation expansion. *Proceedings of the National Academy of Sciences*, *111*(39), 14071–14075. doi: 10.1073/pnas.1319316111

Knowles, N., & Cayan, D. R. (2002). Potential effects of global warming on the Sacramento/San Joaquin watershed and the San Francisco estuary. *Geophysical Research Letters*, *29*(18), 4. doi: 10.1029/2001GL014339

Marks, D., Domingo, J., Susong, D., Link, T., & Garen, D. (1999). A spatially distributed energy balance snowmelt model for application in mountain basins. *Hydrological Processes*, *13*(February), 1935–1959. doi: 10.1002/(SICI)1099-1085(199909)13:12/13<1935::AID-HYP868>3.0.CO;2-C

Millar, C. I., & Stephenson, N. L. (2015). Temperate forest health in an era of emerging megadisturbance. *Science*, *349*(6250), 823–826. doi: 10.1126/science.aaa9933

Mote, P. M., Hamlet, A. F., Clark, M. P., & Lettenmaier, D. P. (2005). Declining Mountain Snowpack in Western North America. *Bulletin of the American Meteorological Society*, *86*(1), 39–49. doi: 10.1175/BAMS-86-1-39

Roos, M. (1989). Possible Climate Change and Its Impact On Water Supply In California (Vol. 1, pp. 247–249). doi: 10.1109/OCEANS.1989.592877

Williams, A. P., Allen, C. D., Macalady, A. K., Griffin, D., Woodhouse, C. A., Meko, D. M., … McDowell, N. G. (2013). Temperature as a potent driver of regional forest drought stress and tree mortality. *Nature Clim. Change*, *3*(3), 292–297. doi: 10.1038/nclimate1693

Chapter 1 Climate and snow data set for the Tuolumne and Merced River watersheds, California, USA

[1,2]James W. Roche, [3]Robert Rice, [3]Xiande Meng, [4]Daniel R. Cayan, [5]Mike D. Dettinger, [4]Douglas Alden, [6]Sarina C. Patel, [1]Megan A. Mason, and [3]Roger C. Bales

[1] Yosemite National Park, USDOI National Park Service, El Portal, CA, 95318, USA

[2] Environmental Systems Graduate Group, University of California, Merced, Merced, CA, 95340, USA

[3] Sierra Nevada Research Institute, University of California, Merced, Merced, CA, 95340, USA

[4] Climate, Atmospheric Sciences, and Physical Oceanography, Scripps Institution of Oceanography, University of California, San Diego, La Jolla, CA, 92093, USA

[5] US Geological Survey, Carson City, NV, 89701, USA

[6] Earth and Planetary Science, University of California, Berkeley, Berkeley, CA, 94720

Correspondence to: James W. Roche (jim_roche@nps.gov)

Abstract

We present hourly climate data to force land surface process models and assessments over the Merced and Tuolumne watersheds in the Sierra Nevada, California, for the water year 2010-2014 period. Climate data (number of stations) includes temperature and humidity (23), precipitation (13), solar radiation (8), and wind speed and direction (8) spanning an elevation range of 333 to 2987 m. Each data set contains raw data as obtained from the source (level 0), data that are serially continuous with noise and non-physical points removed (level 1), and, where possible, data that are gap-filled using linear interpolation or regression with a nearby station record (level 2). All stations chosen for this data set were known or documented to be regularly maintained and components checked and calibrated during the period. Additional time-series data included are available snow water equivalent records from automated stations (8) and manual snow courses (22), as well as distributed snow-depth and co-located soil-moisture measurements (2-6) from four locations spanning the rain-to-snow transition zone in the center of the domain. Spatial data layers pertinent to snowpack modeling in this data set are basin polygons and 100-m resolution rasters of elevation, vegetation type, forest basal area, tree height, and forest canopy cover, transmissivity, and extinction coefficient.

Keywords: climate data, Sierra Nevada, Yosemite National Park, soil-moisture data, distributed snow-depth measurements

Introduction

The snowpack of the Sierra Nevada mountains provides at least 40% of California's water (Roos, 1989) and has historically stored an amount of water equivalent to more than half of the available Sierra foothill reservoir storage (Bales et al., 2011). Snowpack in the western U.S. is highly vulnerable to climate warming, both in the recent past (Mote et al., 2005) and as expected in the coming decades, particularly at lower elevations (Fyfe et al., 2017; Miller et al., 2003; Young et al., 2009). Melting snow sustains soil moisture, streams, and other water sources well into the very dry and warm Mediterranean summer that typifies the area (e.g. Yarnell et al., 2010). Building our intuition about the sensitivity of the snowpack to current and future climates, as well as storm paths and timing, is critical to the future management of these areas. Snowpack water storage affects forest fire, forest health, invasive and threatened species, recreation, flooding, and local and downstream water supplies (Brekke et al., 2009; Dettinger, 2011; Ligare et al., 2012; Miller et al., 2009; Sala et al., 2000).

Soil moisture is the other major component of water storage in mountain ecosystems. As snowpack storage diminishes, it will be essential to understand changes in soil moisture as it pertains to plant-available water, evapotranspiration, and, ultimately, forest health (e.g. Bales et al., in review; Asner et al., 2016). The 2012-2016 California drought, including the 2015 "snow drought" (Harpold et al., 2017), and associated large-scale forest mortality highlight the importance of assessments that investigate the coupled changes in snowpack and soil moisture in mountain forests.

The purpose of this paper is to introduce climate, soil-moisture, snow, and spatial data that may be used for hydrologic or land-surface assessments and modeling in the Tuolumne and Merced watersheds in the Sierra Nevada mountains of central California (Figure 1-1; Tables 1-1, 1-2, and 1-3). Hourly climate data and snow and soil-moisture measurements were derived from stations within and immediately adjacent to the basins. Spatial data include basin polygon files and 100-m resolution raster files of elevation, and vegetation properties. We describe data sources, processing, limitations, and where to obtain the data.

Area Description

The study basins are west-draining watersheds on the broad western slope of the Sierra Nevada and ultimately tributaries to the San Joaquin River. The climate is generally characterized by cool, wet winters and long warm, dry summers. Winter storms derive from large synoptic systems from the northern Pacific and more-focused and moisture-laden atmospheric rivers from further south in the Pacific. Indeed, the latter may produce 20-50% of annual precipitation for the area, and just a few storms may determine the difference between above-average water years and drought (Dettinger, 2011). Within the seasonal snow zone above 1800 m elevation, much of the landscape consists of broad interfluves between deep river canyons on the Merced and Tuolumne Rivers, the area of Yosemite National Park. Most snowmelt runoff is generated between 2100 and 3000 m elevation, with up to 40% of runoff originating from elevations greater than 3000 m, above existing measurements (Rice et al., 2011). Nearly 60% of the snowpack zone lies between the elevations of 2000 and 3000 m (Rice et al., 2011) and small changes in

temperature during storms can result in large changes in runoff due to shifts in precipitation phase. This is illustrated in Figure 1-2 where wet-season winter temperatures in this zone hover close to 0ºC in representative wet and dry years in the data set.

Dominant vegetation ranges from moisture-limited grasslands and oak woodlands below 1000 m elevation through ponderosa, mixed-conifer (sugar pine, incense cedar, Jeffrey pine, and white fir), and red-fir forests, to energy-limited western white and lodgepole pine forests at and above 2500 m (Fites-Kaufman et al., 2007; Keeler-Wolf et al., 2012). Some of the largest and most productive forests in the world are located in the 1500-2000 m elevation range where there is neither moisture nor energy limitation (Kelly & Goulden, 2016; Matchett et al., 2015). Here, the mean winter temperature is a few degrees above freezing and precipitation averages 1100-1200 mm yr^{-1} (PRISM Climate Group, 2012).

Like all major river basins in California, the Tuolumne and Merced are vitally important water sources to the economy of the region. The watersheds provide water for a large agricultural region of the Central Valley between Merced in the south to Modesto in the north, fed primarily by Lake McClure on the Merced and Lake Don Pedro on the Tuolumne River. Further upstream on the Tuolumne River, the Hetch Hetchy water system supplies water to 2.6 million San Francisco and other Bay Area residents.

Climate Data

The original intent of assembling this dataset was to force the snow energy- and mass-balance model iSnobal (Marks et al., 1999) at an hourly time-step. The data represent the required parameters to drive the model: incoming solar radiation, temperature, relative humidity, wind speed and direction, and precipitation. That modeling effort (Roche et al., in review) employed a subset of this data archive, which is described is succeeding sections (bold parameters in Table S1). Data were obtained from the California Data Exchange Commission (CDEC) for California Department of Water Resources stations, Western Regional Climate Center for Fire Remote Access Weather Station (RAWS) network stations, and the Scripps Institution of Oceanography (SIO), which operates a transect of stations across the Sierra through the middle of the study domain. All raw data (Level 0) were processed to be serially continuous and to remove noise and non-physical data (Level 1) and gap-filled where possible using linear interpolation and regression with nearby stations (Level 2). Very few stations adequately measured all parameters and several stations have extensive periods with no data that precluded gap filling. As is typical in large mountain basins, instrumentation distribution is not uniform, often located where it is convenient to service, and heavily weighted to the lower elevations. More than two-thirds of the stations are below 2000 m elevation and no stations are located above 3000 m (Figures 1-1, 1-2). Above 1800m, where seasonal snowpack occurs, there are three precipitation measurement stations, two of which are rain-shadow affected (Figure 1-1).

Temperature and humidity. Paired temperature (°C) and relative humidity (KPa KPa^{-1}) used for snow modeling were measured at 23 stations in this dataset. Stations were

chosen for modeling given known maintenance records at each site that assured minimal drift and accurate subsequent calculation of dew point and vapor pressure. Figure 1-3 illustrates dew-point and air temperature variability as recorded at Crane Flat Lookout over a two-week period in late 2012 and early 2013. Also shown is the dew point lapse rate (using the methods of Marks et al. (1999)), which averaged -0.0055 and -0.0065°C m^{-1} during and between precipitation events. Temperature gradient varied from -0.0075 to -0.0044°C m^{-1} during wet periods and -0.0079 to -0.0016°C m^{-1} during dry periods.

Precipitation. Hourly precipitation (mm) was the most difficult parameter to obtain and process. The best quality records were those obtained from stations equipped with tipping-bucket gauges that were below 1000 m elevation where snow and ice are minimal. Weighing gauges in Yosemite Valley (1208 m), Yosemite South Entrance (1511 m), and Stanislaus Powerhouse (333 m), and Geonor™ gauges at Hetch Hetchy (1195 m) and the Crane Flat NOAA Climate Reference Network site (2017 m) were regularly maintained and appear to produce acceptable data. The only two high-elevation gauges were at Tuolumne Meadows (TUM) and Virginia Lakes Ridge (VLR) and both were accumulation-type gauges equipped with pressure transducers. The records from these gauges exhibit substantial diurnal expansion and contraction effects adding uncertainty to the hourly records. To process these records, we first established a daily record by extracting the midnight value to minimize heating and cooling effects, differencing from the previous day and removing any negative values. For days with zero midnight values, all hourly values were set to zero. For days with non-zero accumulation, we first set all negative incremental values to zero and we examined data from the

adjacent snow pillows, other stations with snow pillows in the vicinity, and compared the records of both TUM and VLR in order to weight the positive increments such that the sum equaled the daily total. Given that these gauges recorded 50-60% of PRISM estimates in their respective elevation bands in water years 2011 and 2013 (Figure 1-2), the use of these records may be primarily to weight snow-pillow records as approximate measures of precipitation elsewhere in the basin (e.g. Lundquist et al., 2016), or as simple measures of precipitation timing rather than quantity.

Wind speed and direction. For snow modeling, we selected wind data from eight sites that were primarily located on open ridge lines in order to avoid the terrain- or forest-influenced winds. Terrain and vegetation effects could then be modeled using methods such as those of Winstral et al. (2009). Additional stations such as Tioga Pass Entrance Station (TES) and Gin Flat (GIN) provided a reference for forest wind speeds.

Solar radiation. All stations measured solar radiation using pyranometers that introduce substantial aspherical effects at dawn and dusk. Moreover, their calibration history was not known. Hence, the sites chosen for snow modeling were those with a largely complete record that spanned the domain and that exhibited minimal vegetation and terrain shading. As such, this record is best used as an estimate of cloudiness when combined with an independent estimate of incoming clear-sky solar radiation at each site. Other stations in the dataset exhibit substantially more terrain and vegetation shading influences.

Snow Data

Snow water equivalent data. We extracted all available monthly snow course and daily snow pillow data from CDEC for purposes of evaluating snow modeling performance. Missing snow course data were not gap-filled given substantial inter-site variability. Snow pillow data were checked for serial completeness and outliers and gap-filled using linear interpolation only.

Snow depth data. Snow-depth data were collected at four locations spanning the rain-to-snow transition zone along the Tioga Road at the Merced Grove (1810 m), Gin Flat (2149 m), Smoky Jack (2182 m), and Olmsted Quarry (2604 m). Each site contained 2-6 operational snow depth sensors arranged to sample various aspects and tree canopy cover. Snow data were filtered to remove unrealistic depths and checked for serial continuity (Level 1) and then gap-filled using linear interpolation for periods of a few hours and regression with adjacent stations for larger gaps (Level 2). Soil-moisture data, included volumetric soil-moisture content and soil temperature, was collected at depths of 10, 30, 60, and, where possible, 90 cm below the ground surface at three of the snow depth measurement points within each of the four sites. Soil moisture data was processed in a manner similar to other parameters.

Spatial Data

Spatial data included in this data set are basin polygons and raster files. All spatial data are in Universal Transverse Mercator (UTM) Zone 11 projection with the 1983 North American Datum. Basin polygons are in Earth Systems Research Institute (ESRI) ArcGIS shapefile format while raster files are in ESRI ArcGIS ASCII grid format. Raster files include 100-m resolution elevation (m), canopy cover (proportion), generalized vegetation type, derived tree height (m), derived canopy transmissivity (dimensionless), and canopy extinction coefficient (m^{-1}) (Table 1-4). The digital elevation model (DEM) was derived by resampling the 10-meter U.S. Geological Survey National Elevation Dataset (NED) using bilinear interpolation. All other raster data sets were aligned with this DEM. The resulting raster contained 1296 columns and 1107 rows. Vegetation type, canopy cover, and tree basal area were derived from the U.S. Forest Service 30-meter resolution California Region 5 Vegetation Maps (U.S. Forest Service, 2014) by determining the dominant over-story vegetation in each raster cell (Wildlife Habitat Relation (WHR) Lifeform), or spatially averaging canopy cover or basal area within each raster cell. We calculated tree height using basal area and the allometric relation of Zhao et al. (2012). The WHR Lifeform designation was used to assign canopy transmissivity and extinction coefficients to each pixel as shown in Table 2 based on the values from Link and Marks (1999).

Data availability

All data presented in this paper will be available on the University of California Digital Library. Detailed metadata will be associated with each file including contact information.

Summary

The dataset assembled here represents the nature of data available in sparsely instrumented mountain basins coupled with the higher-quality SIO Sierra transect and complimentary snow depth and soil moisture dataset that has undergone quality control and gap filling. While it was used for one snow-modeling effort (Roche et al, in review), there are many opportunities to use the data for other applications, combining available raster datasets (PRISM, Basin Characterization Model, etc.), and testing the sensitivity of using more or fewer stations for estimating the parameter of interest. One outstanding use of the dataset is an assessment of the temporal evolution of soil moisture with respect to snow accumulation and ablation across the rain-to-snow transition zone. Given the stark lack of measured short- and long-wave radiation in the watershed, other estimates of these parameters may be used to explore the sensitivity of model results. It is important for these kinds of data to be available for longer periods of time and in other watersheds in order to apply data-driven land surface modeling efforts that seek to minimize calibration in order to more robustly assess stressors on ecosystems.

References

Asner, G. P., Brodrick, P. G., Anderson, C. B., Vaughn, N., Knapp, D. E., & Martin, R. E. (2016). Progressive forest canopy water loss during the 2012-2015 California drought. *Proceedings of the National Academy of Sciences of the United States of America*, *113*(2), E249-55. doi: 10.1073/pnas.1523397113

Bales, R. C., Battles, J. J., Chen, Y., Conklin, M. H., Holst, E., O'Hara, K. L., … Stewart, W. (2011). Forests and Water in the Sierra Nevada: Sierra Nevada Watershed Ecosystem Enhancement Project Forests and Water in the Sierra Nevada : Sierra Nevada Watershed Ecosystem Enhancement Project. *Sierra Nevada Research Institute Report*, *11.1*, 1–35.

Brekke, L. D., Maurer, E. P., Anderson, J. D., Dettinger, M. D., Townsley, E. S., Harrison, A., & Pruitt, T. (2009). Assessing reservoir operations risk under climate change. *Water Resources* Research, 45(4). doi: 10.1029/2008WR006941

Dettinger, M. (2011). Climate Change, Atmospheric Rivers, and Floods in California - A Multimodel Analysis of Storm Frequency and Magnitude Changes. *Journal of the American Water Resources Association*, *47*(3), 514–523. doi: 10.1111/j.1752-1688.2011.00546.x

Fites-Kaufman, J. A., Rundel, P., Stephenson, N., & Weixelman, D. A. (2007). Montane and subalpine vegetation of the Sierra Nevada and Cascade ranges (pp. 456–501). Berkeley, CA: University of California Press.

Fyfe, J. C., Derksen, C., Mudryk, L., Flato, G. M., Santer, B. D., Swart, N. C., … Jiao, Y. (2017). Large near-term projected snowpack loss over the western United States. *Nature Communications*, *8*, 14996. doi: 10.1038/ncomms14996

Harpold, A. A., Dettinger, M., & Rajagopal, S. (2017). Defining snow drought and why it matters. *Eos, Transactions American Geophysical Union*, *98*. doi: 10.1029/2017EO068775

Keeler-Wolf, T., Moore, P. E., Reyes, E. T., Menke, J. M., Johnson, D. N., & Karavidas, D. L. (2012). Yosemite National Park vegetation classification and mapping project report. *Natural Resource Technical Report NPS/YOSE/NRTR-2012/598*.

Kelly, A. E., & Goulden, M. L. (2016). A montane Mediterranean climate supports year-round photosynthesis and high forest biomass. *Tree Physiology*, *36*(4), 459–468. doi: 10.1093/treephys/tpv131

Ligare, S. T., Viers, J. H., Null, S. E., Rheinheimer, D. E., & Mount, J. F. (2012). Non-Uniform Changes to Whitewater Recreation in California's Sierra Nevada from Regional Climate Warming. *River Research and Applications*, *28*(8), 1299–1311. doi: 10.1002/rra.1522

Link, T., & Marks, D. (1999). Distributed simulation of snowcover mass‐ and energy‐balance in the boreal forest. *Hydrological Processes*, *13*(14‐15), 2439‐2452. doi: AID-HYP866>3.0.CO;2-1

Lundquist, J. D., Roche, J. W., Forrester, H., Moore, C., Keenan, E., Perry, G., … Dettinger, M. D. (2016). Yosemite Hydroclimate Network: Distributed stream and atmospheric data for the Tuolumne River watershed and surroundings. *Water Resources Research*, *52*(9), 7478–7489. doi: 10.1002/2016WR019261

Marks, D., Domingo, J., Susong, D., Link, T., & Garen, D. (1999). A spatially distributed energy balance snowmelt model for application in mountain basins. *Hydrological Processes*, *13*(February), 1935–1959. doi: 10.1002/(SICI)1099-1085(199909)13:12/13<1935::AID-HYP868>3.0.CO;2-C

Matchett, J. R., Lutz, J. A., Tarnay, L. W., Smith, D. G., Becker, K. M. L., & Brooks, M. L. (2015). Impacts of fire management on aboveground tree carbon stocks in Yosemite and Sequoia & Kings Canyon National Parks, Natural Resource Report NPS/SIEN/NRR—2015/910. . Fort Collins, Colorado. Retrieved from http://pubs.er.usgs.gov/publication/70140618

Miller, J. D., Safford, H. D., Crimmins, M., & Thode, A. E. (2009). Quantitative Evidence for Increasing Forest Fire Severity in the Sierra Nevada and Southern Cascade Mountains, California and Nevada, USA. *Ecosystems*, *12*(1), 16–32. doi: 10.1007/s10021-008-9201-9

Miller, N. L., Bashford, K. E., & Strem, E. (2003). Potential impacts of climate change on California Hydrology. *Journal of the American Water Resources Association*, *39*(4), 771–784. doi: 10.1111/j.1752-1688.2003.tb04404.x

Mote, P. M., Hamlet, A. F., Clark, M. P., & Lettenmaier, D. P. (2005). Declining Mountain Snowpack in Western North America. *Bulletin of the American Meteorological Society*, *86*(1), 39–49. doi: 10.1175/BAMS-86-1-39

PRISM Climate Group. (2012). United States Average Annual Precipitation, 1981-2010. . Oregon State University.

Rice, R., Bales, R. C., Painter, T. H., & Dozier, J. (2011). Snow water equivalent along elevation gradients in the Merced and Tuolumne River basins of the Sierra Nevada. *Water Resources Research*, *47*(8). doi: 10.1029/2010WR009278

Roos, M. (1989). Possible Climate Change and Its Impact On Water Supply In California (Vol. 1, pp. 247–249). doi: 10.1109/OCEANS.1989.592877

Sala, O. E., Chapin III, F. S., Armesto, J. J., Berlow, E., Bloomfield, J., Dirzo, R., … Wall, D. H. (2009). Global Biodiversity Scenarios for the Year 2100. *Science*, *287*(5459), 1770–1774. doi: 10.1126/science.287.5459.1770

U.S. Forest Service. (2014). Existing Vegetation - CALVEG, ESRI personal geodatabase. Retrieved from https://www.fs.usda.gov/detail/r5/landmanagement/resourcemanagement/?cid=stelprdb5347192.

Winstral, A., Marks, D., & Gurney, R. (2009). An efficient method for distributing wind speeds over heterogeneous terrain. *Hydrological Processes*, *23*(17), 2526–2535. doi: 10.1002/hyp.7141

Yarnell, S. M., Viers, J. H., & Mount, J. F. (2010). Ecology and Management of the Spring Snowmelt Recession. *BioScience*, *60*(2), 114–127. doi: 10.1525/bio.2010.60.2.6

Young, C. A., Escobar-Arias, M. I., Fernandes, M., Joyce, B., Kiparsky, M., Mount, J. F., … Yates, D. (2009). Modeling the Hydrology of Climate Change in California's

Sierra Nevada for Subwatershed Scale Adaptation1. *Journal of the American Water Resources Association*, *45*(6), 1409–1423. doi: 10.1111/j.1752-1688.2009.00375.x

Zhao, F., Guo, Q., & Kelly, M. (2012). Allometric equation choice impacts lidar-based forest biomass estimates: A case study from the Sierra National Forest, CA. *Agricultural and Forest Meteorology*, *165*, 64–72. doi: 10.1016/j.agrformet.2012.05.019

Table 1-1. Measurements, operator, and instrumentation at each site.

Measurement	Operator / Instruments[1]	Instrument height (m)
Air temperature	RAWS (various[2]) SIO, UCM (in-house-calibrated thermistors) CA-DWR (Vaisala HMP45A/H DUS, Dana Meadow; FTS THS-3, Mariposa Grove)	5
Relative humidity	RAWS (various[2]) SIO, UCM (Sensirion, SHT15DV) CA-DWR (Vaisala HMP45A/H DUS, Dana Meadow; FTS THS-3, Mariposa Grove)	5
Precipitation	RAWS (Tipping bucket (typical); various[2]) MID (Weighing-type, ETI Instrument Systems; tipping bucket, Briceburg) CRN (Geonor™) NRCS (storage with pressure transducer) DWR (storage with pressure transducer) PGE (Weighing-type, ETI Instrument Systems) HHWP (Geonor™)	3 3 3 5 5 3 3
Solar radiation	RAWS (Pyranometer, LICor 441A (typical)[2]) CA-DWR (LICor 441A)	5
Wind speed / direction	RAWS (various[2]) CA-DWR (Vaisala 425A Ultrasonic) UCM (3D sonic anemometer)	5
Snow depth	Judd ultrasonic depth sensor	n/a
Soil moisture	Decagon Devices, 5TE	n/a

[1]Operator abbreviations are: RAWS – Interagency Fire Remote Access Weather Station network managed by the Bureau of Land Management; SIO – Scripps Institution of Oceanography; UCM – University of California Merced; CA-DWR – California Department of Water Resources; MID – Merced Irrigation District; HHWP – Hetch Hetchy Water and Power; NRCS – Natural Resource Conservation Service; PGE – Pacific Gas and Electric; NOAA – National Oceanic and Atmospheric Administration Climate Reference Network.

[2] See RAWS (various; see https://famit.nwcg.gov/applications/RAWS) for a description of instrument types.

Table 1-2. Meteorological stations and data used to force model. Bold parameters indicate those selected for snow modeling in Chapter 2.

Station name[1]	Elev., m	UTM northing[2], m	UTM easting[2], m	Measurements used[3]	Operator[4]
Green Springs (GRN)	311	4193067	191966	**t, rh, p,** sr, w	RAWS
Stanislaus Powerhouse (SPW)	333	4225930	204880	**p**	PGE
Cathey's Valley (CVR)	366	4151342	224905	**t, rh, p**	RAWS
Briceburg (MBB)[5]	670	4153062	238501	**p**	MID
Mariposa (MRP)	680	4154996	235967	**t, rh, p**	RAWS
Priest Reservoir (PRR-SIO)	709	4189078	212647	**t, rh**	SIO
Metcalf Gap (MCF)	938	4143892	255011	**t, rh,** sr, w	RAWS
Batterson (BTT)	943	4140575	268301	**p**	RAWS
Dudley Ranch (DUC)	1114	4151264	224864	**p**	MID
Smith Peak (SEW)	1168	4188222	226980	**sr, w,** p, t, rh	RAWS
Smith Peak (SEW-SIO)	1168	4188222	226980	**t, rh**	SIO
Jerseydale (JSD)	1189	4158967	249214	**t, rh,** sr, w	RAWS
Hetch Hetchy (HEM)	1195	4203412	255489	**p**	HHWP
Wawona (WWN)	1235	4158119	265654	**t, rh, sr**	RAWS
Yosemite Valley (YYV)	1208	4181238	271843	**p**	MID
Miami Mountain (MIA)	1321	4144912	257059	**t, rh, sr, w**	RAWS
Sunset Inn (SUN-SIO)	1371	4188288	245001	**t, rh**	SIO
Hodgdon (HDG-SIO)	1397	4187075	248304	**t, rh**	SIO
Mount Elizabeth (MTE)	1504	4217791	215134	**t, rh, sr, w**	RAWS
Yosemite South Entrance (YOW)	1511	4154480	267291	**p**	MID
Forty Mile (FTY-SIO)	1723	4184565	247936	**t, rh**	SIO
Pinecrest (PNW)	1738	4230750	236322	**t, rh, sr, w**	RAWS
Merced Grove (MEG-SIO)	1810	4183446	249675	**t, rh**	SIO
Mariposa Grove (MPG)	1951	4154932	269754	**t, rh,** w, sr, p	RAWS
Crane Flat (CFL-CRN)	2017	4182829	251510	**p**	NOAA
Crane Flat Lookout (CFL)	2026	4182878	251530	**t, rh, sr, w,** p	RAWS
Gin Flat (GIN-SIO)	2149	4183578	255577	**t, rh**	SIO
Gin Flat (GIN)	2149	4183578	255577	t, rh, w, p, sr	CA-DWR
Fresno Dome (FRS)	2177	4149346	275698	**t, rh, w**	UCM
Smoky Jack (SMK-SIO)	2182	4188935	261192	**t, rh**	SIO
White Wolf (WHW)	2408	4193540	266732	**t, rh, sr, w**	RAWS
Ostrander Lake (STR)	2499	4168599	274999	t, rh, w	CA-DWR

Table 1-2. (cont.)

Station name[1]	Elev., m	UTM easting[2], m	UTM northing[2], m	Measurements used[3]	Operator[4]
Horse Meadow (HRS)	2560	4226695	266766	t	CA-DWR
Olmsted Quarry (OLM-SIO)	2604	4187768	279089	**t, rh**	SIO
Tuolumne Meadows (TUM)	2622	4194700	293480	**p,** t, sr	CA-DWR
Virginia Lakes Ridge (VRG)	2879	4215567	304085	**p**	NRCS
Dana Meadow (DAN)	2988	4196683	301507	**t, rh, sr, w**	CA-DWR
Tioga Pass Entry Station (TES)	3041	4198329	301461	t, rh, w	CA-DWR

[1]Station name abbreviations: Three letter abbreviations are derived from conventions in the California Data Exchange Commission database (http://cdec.water.ca.gov/). Abbreviations ending with "-SIO" indicate stations operated by Scripps Institution of Oceanography that are not currently available through CDEC. CFL-CRN indicates the NOAA Climate Reference Network Station located near the Crane Flat Lookout.

[2]Geographic coordinates are in Universal Transverse Mercator (UTM) projection, North American 1983 Datum, Zone 11.

[3]Variable abbreviations: p, precipitation; rh, relative humidity; sr, solar radiation; t, air temperature; w, wind speed and direction.

[4]Operator abbreviations are: RAWS – Interagency Fire Remote Access Weather Station network managed by the Bureau of Land Management; SIO – Scripps Institution of Oceanography; UCM – University of California Merced; CA-DWR – California Department of Water Resources; MID – Merced Irrigation District; HHWP – Hetch Hetchy Water and Power; NRCS – Natural Resource Conservation Service; PGE – Pacific Gas and Electric; NOAA – National Oceanic and Atmospheric Administration Climate Reference Network.

[5]Actually located in the town of Mariposa, CA.

Table 1-3. Snow and soil-moisture data sources.

Station name[1]	Elev., m	UTM northing[2], m	UTM easting[2], m	Data type[3]
Merced Grove (MEG-SIO)	1810	4183446	249675	distributed snow depth, soil moisture
Bell Meadow (BEM)	1981	4228435	242260	monthly swe
Beehive Meadow (BHV)	1981	4208908	255883	monthly swe
Lower Kibbie (LKB)	2042	4213387	247407	monthly swe
Lake Vernon (VNN)	2042	4211186	261488	monthly swe
Upper Kibbie Ridge (UKR)	2042	4214521	246651	monthly swe
Kerrick Ranch (KRC)	2134	4229596	240718	monthly swe
Gin Flat (GFL)	2134	4183363	255739	monthly swe
	2134	4183578	255576	daily swe
Gin Flat (GIN-SIO)	2134	4183350	255550	distributed snow depth, soil moisture
Peregoy Meadow (PGM)	2134	4172111	268473	monthly swe
Smoky Jack (SMK-SIO)	2182	4188935	261192	distributed snow depth, soil moisture
Paradise Meadow (PDS)	2332	4214396	265710	monthly swe
	2332	4214326	265612	daily swe
Huckleberry Lake (HCL)	2377	4220692	259308	monthly swe
Spotted Fawn Lake (SPF)	2377	4219616	258135	monthly swe
Sachse Spring (SAS)	2408	4219048	251182	monthly swe
White Wolf (WHW)	2408	4193540	266732	daily swe
Wilma Lake (WLW)	2438	4218298	269071	monthly swe
Tenaya Lake (TNY)	2484	4190665	284584	monthly swe
	2484	4190534	284349	daily swe
Ostrander Lake (STR)	2499	4168599	274999	monthly swe
	2499	4168565	274701	daily swe
Horse Meadow (HRS)	2560	4226695	266766	monthly swe
	2560	4227164	266940	daily swe
Olmsted Quarry (OLM-SIO)	2604	4187768	279089	distributed snow depth, soil moisture
Tuolumne Meadow (TUM)	2621	4194327	293307	monthly swe
Snow Flat (SNF)	2652	4189558	280239	monthly swe

Table 1-3. (cont.)

Station name[1]	Elev., m	UTM northing[2], m	UTM easting[2], m	Data type[3]
New Grace Meadow (NGM)	2713	4225694	270684	monthly swe
Slide Canyon (SLI)	2797	4218724	286737	daily swe
Bond Pass (BNP)	2835	4228817	270246	monthly swe
Rafferty Meadow (RFM)	2865	4190277	295406	monthly swe
Dana Meadow (DAN)	2987	4196789	301552	monthly swe
	2987	4196756	301486	daily swe

[1]See footnote 1 in Table 1-2.

[2]See footnote 2 in Table 1-2.

[3]Data type explanations: monthly swe denotes manually measured snow courses, hourly swe indicates a snow-pillow site, and distributed snow depth indicates sites with 4-6 snow depth sensors distributed across an area of approximately 100 meters square.

Table 1-4. Canopy parameters (adapted from Link and Marks, 1999).

Vegetation class	tau (τ)	mu (μ)
Herbaceous, sparse shrub, non-vegetated	1	0
Conifer forest/woodland	0.2	0.040
Mixed conifer and hardwood	0.3	0.033
Hardwood forest/woodland	0.4	0.025

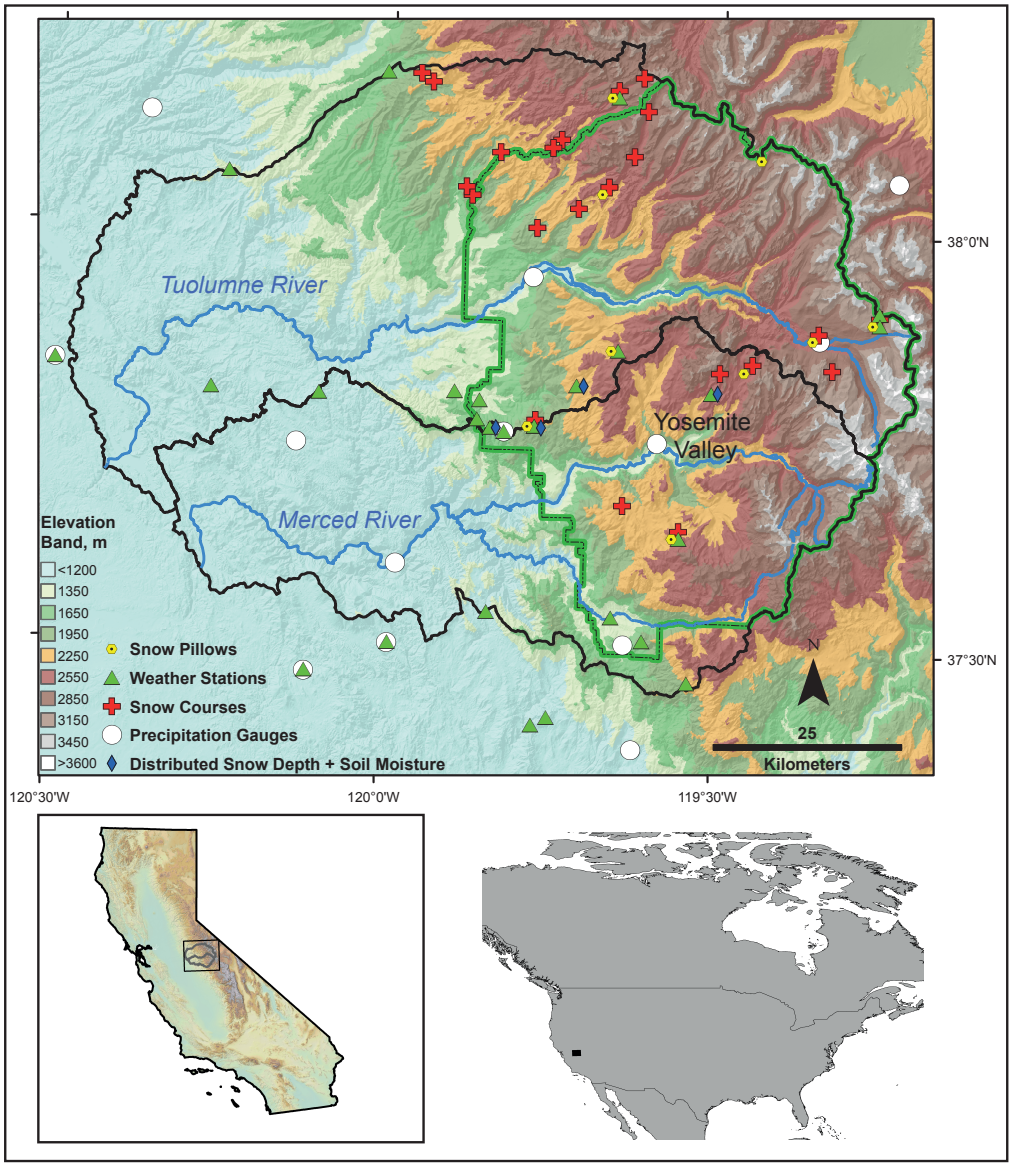

Figure 1-1. Hydrometeorological stations in and adjacent to the Merced and Tuolumne watersheds used in this data set. Co-located station types are offset for clarity. Yosemite National Park is demarked by the green boundary.

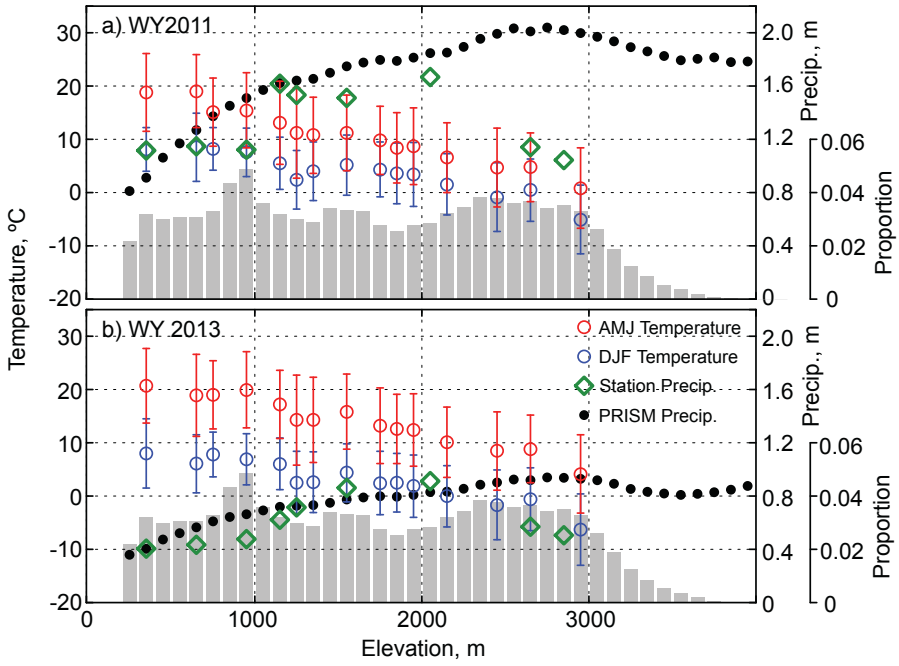

Figure 1-2. Elevation transects of temperature and precipitation in a) wet and cold water year 2011, and b) dry and warm 2013. Temperatures are three-month means and standard deviations during the main snowpack accumulation period (December-February) and the main snowmelt season (April-June). Precipitation and temperature station data were averaged by 100-m elevation band. Shaded area is the proportional basin area in each 100-m elevation band.

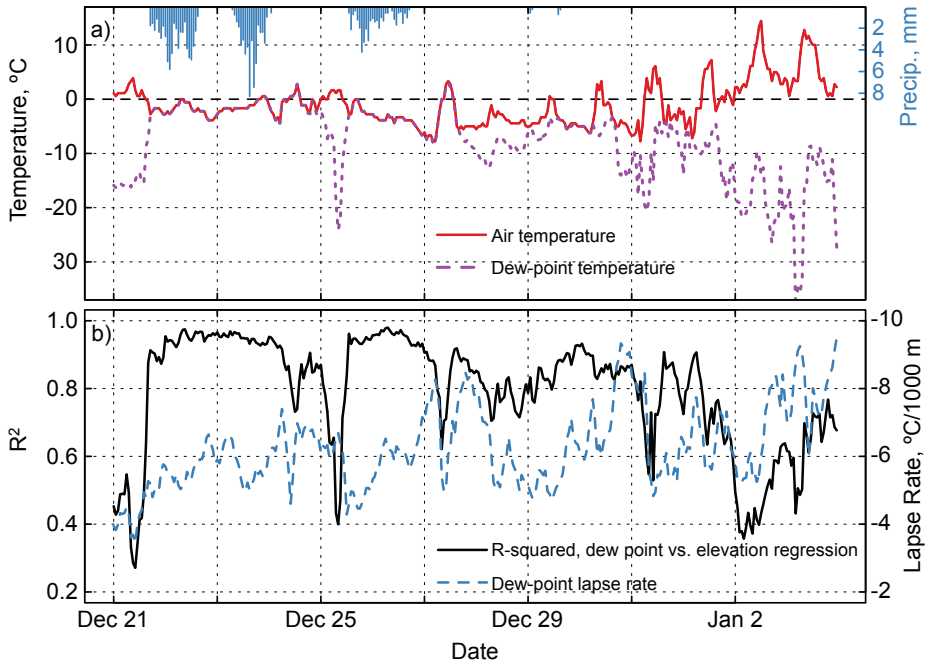

Figure 1-3. a) Hourly time-series of air temperature, dew-point temperature, and precipitation as recorded at Crane Flat Lookout RAWS and Crane Flat CRN stations for a two-week period from December 21, 2012 through January 3, 2013. b) Dew-point lapse rate and corresponding coefficient of determination for the same period.

Chapter 2 Management Implications of Snowpack Sensitivity to Temperature and Atmospheric-Moisture Changes in Yosemite National Park, California

James W. Roche[1,2], Roger C. Bales[3], Robert Rice[3], Danny Marks[4]

[1]Yosemite National Park, USDOI National Park Service, El Portal, California

[2]Environmental Systems Graduate Group, University of California, Merced, California

[3]Sierra Nevada Research Institute, University of California Merced, Merced, California

[4]USDA Agricultural Research Service Northwest Research Center, Boise, Idaho

Corresponding author: James W. Roche

E-mail: jim_roche@nps.gov

Abstract

In order to investigate snowpack sensitivity to temperature increases and end-member atmospheric-moisture conditions, we applied a well-constrained energy- and mass-balance snow model (iSnobal) across the full elevation range of seasonal snowpack using forcing data from recent wet and dry years. We imposed uniform temperature increases of 2, 4, and 6°C over observed values and examined end-member humidity scenarios of constant relative humidity and constant vapor pressure between storms. Forced by distributed ground-based measurements of temperature, precipitation, vapor pressure, and wind speed as well as modeled solar and thermal radiation, the model captured the observed magnitude and timing of snowmelt for water years 2011 and 2013. April 1 SWE losses of 38, 73, and 90% with temperature increases of 2, 4, and 6°C in a dry year centered on areas of greatest SWE accumulation. Each 2°C increment of warming also resulted in seasonal snowline moving upslope by 300 m. The zone of maximum melt was compressed upwards 100-500 m with 6°C warming, with the range reflecting differences in basin hypsometry. Melt contribution by elevations below 2000 m disappeared with 4°C warming. The constant-relative-humidity scenario resulted in 0-100 mm less snowpack in late spring versus the constant-vapor-pressure scenario in a wet year, a difference driven by increased thermal radiation (+1.2 W m^{-2}) and turbulent energy fluxes (+1.2 W m^{-2}) to the snowpack for the constant-relative-humidity case. Loss of snowpack storage and potential increases in forest evaporative demand due to warming will result in a substantial shift in forest water balance and present major challenges to land management in this mountainous region.

Keywords: snow hydrology; Sierra Nevada; simulation; watershed management

Introduction

Changes in snowpack profoundly affect ecological processes in mountainous regions, including annual evapotranspiration, stream flow and peak timing, wetland health, and wildlife (McMenamin et al., 2008; Stewart et al., 2005; Trujillo et al., 2012). Western North America is projected to experience warming of approximately 2-6°C, assuming representative concentration pathways of greenhouse gas concentrations that increase radiative forcing 2.6 to 8.5 W m^{-2}, by the end of this century (Diffenbaugh & Field, 2013) and the impact that this will have on regional snowpack has been shown in many publications (e.g. Bales et al., 2006; Dettinger et al., 2004; Knowles & Cayan, 2004). Documented snowpack changes, over the past century, (Andrews, 2012; Mote et al., 2005) are projected to continue in the future and include decreased annual peak snow water equivalent (SWE) (Barnett et al., 2005), increased winter runoff as snow transitions to rain (Stewart et al., 2004), earlier annual snowpack disappearance (Brown & Mote, 2009), and negative glacial mass balance (Moore et al., 2009).

There is a need for land managers to understand how changes in snowpack associated with the ongoing warming of the earth's climate affect forest health and fire, wildlife populations, and recreation (e.g. Flint et al., 2013). Specifically, there is a need to understand in fine-grained spatial and temporal detail how snowpacks may change, and the factors that may mitigate that change, in order to develop management responses that address ecological transitions necessary for at-risk populations (e.g. Hannah et al., 2014). Moreover, in order to be ecologically relevant, estimates of snowpack changes should be done at the watershed scale, including the entire rain-to-snow transition zone that usually

contains the largest areas of resources of concern. In this zone, the shift from snow to rain precipitation and concomitantly reduced snowpack depth and duration will profoundly affect the rate and timing of water delivery to soils, which in turn will affect plant-available water in forest, wetland, riparian, and aquatic habitats during the snow-free season (Bales et al., 2006; Schimel et al., 2002).

The work of Sproles et al. (2012) and Cooper et al. (2016) illustrate the challenges of applying physically based snow models over large watersheds in the Pacific Northwest. These challenges include sparse instrumentation with which to drive models and to validate or evaluate results, and the methods chosen to distribute point data spatially. Application of these models often requires substantial calibration in order to fit observed conditions at snow pillows or snow courses. Similar works by Flint et al. (2013) and Curtis et al. (2014) employ the SNOW-17 model, a hybrid empirical and physically based model (Anderson, 2006). Both methods rely heavily on the assumption that calibrations necessary to achieve results that match observed conditions do not affect representation of physical processes under future conditions that are beyond the range of variation for which the model was calibrated. There remains a persistent need to fully evaluate the effect of model calibration on internal energy dynamics and how this may affect warming-scenario results. An alternative approach is to physically model the snowpack without calibration, potentially sacrificing a better model fit to observations for more-consistent physics under warmer-climate scenarios. Research reported in this paper builds on prior work mentioned above by using a full snow energy- and mass-balance model

with minimal calibration to estimate the sensitivity of snowpack to temperature changes in wet and dry years.

Most snowpack or watershed modeling efforts assume constant relative humidity, implying increasing specific humidity with a warming climate, reflecting the ability of warmer air to hold more water vapor and in line with global land trends (Dai, 2006). In contrast, Pierce et al. (2013) predicted decreases in relative humidity over the western United States due to temperature increases outpacing atmospheric-moisture increases as the climate warms. Feld et al. (2013) demonstrated that errors in dew point temperature of +/-2°C advanced/extended the snow disappearance date by 3 days in the snow-dominated Tuolumne Meadows watershed in 2005, a relatively wet year with late-melting snow. The extent of the modeled change they observed was muted by offsetting changes in latent heat release through sublimation and longwave atmospheric radiation. Despite the small changes modeled by Feld et al. (2013), a necessary extension of their work is the examination of differences in snow accumulation and melt patterns with end-member atmospheric moisture assumptions over entire watersheds and for the full range of expected temperature increases.

Three main questions motivated the research. First, by how much will snowpack storage across the current snow-covered elevation range change under mid- to end-of-century projected warming? Second, how robust are estimated changes to different model assumptions about atmospheric moisture? Third, what are the implications for ecosystem water availability in wet and dry years?

Methods

We used *iSnobal*, a full energy- and mass-balance snowpack numerical model (Marks et al., 1998; Marks et al., 1999b) with minimal calibration to examine the sensitivity of snowpack to uniform temperature increases, coupled with end-member assumptions of atmospheric moisture conditions. Specifically, we examined the impact of assuming constant relative humidity (increased atmospheric moisture consistent with the observations of Dai (2006)) and constant vapor pressure (constant atmospheric moisture), between storms. The model was run at a 100 m spatial resolution in order to produce results that may inform future monitoring and vulnerabilities at a scale appropriate to land management. This scale also meant that model results could reasonably be compared to available snowpack measurements. Forcing data were then perturbed by uniform temperature increases, energy components recalculated for each atmospheric-moisture scenario, and the energy-balance model rerun. Results were compared to the base model, and relative differences in snowpack energy-balance components evaluated.

Study area. This investigation centered on the Merced and Tuolumne River basins in the central Sierra Nevada of California above their respective foothills dams, Exchequer and Don Pedro (Figure 2-1). The area comprises the broad western slope of the range, with elevations ranging from 100 to 3400 m, and encompassing all of Yosemite National Park. Much of the area receiving snowfall (>1500 m) is conifer dominated (73%), with shrubs, bare rock, and alpine tundra making up the rest of the area. Average annual precipitation from 800-m PRISM 1981–2010 climatology (PRISM

Climate Group, Oregon State University, 2012) for the Merced and Tuolumne watersheds is 1060 and 1150 mm, respectively. Both basins are part of the San Joaquin River basin and comprise major sources of water for agriculture and municipalities. These basins were chosen for this study because they were sparsely instrumented, similar to others in the region, and because of the need to develop high-resolution climate-scenario products for Yosemite National Park and downstream stakeholders.

Model description. We ran the model *iSnobal* for water years 2011 and 2013 (beginning October 1st of the previous year), larger and smaller years with respect to average snowpack accumulation and total precipitation. *iSnobal* is a spatially distributed full-energy-balance snowpack model that is part of the Image Processing Workbench (IPW, Frew, 1990; Marks et al., 1999a). Inputs are spatial arrays of hourly air temperature, vapor pressure, wind speed, soil temperature, long-wave radiation, net solar radiation, precipitation amount, precipitation temperature as determined by dew-point temperature, percentage of precipitation that is snow, and its density. The model calculates snowpack depth, density, temperature, melt, and energy balance as well as net radiative, turbulent, and advective energy fluxes. *iSnobal* is a compact numerically efficient representation of snowpack physics with minimal parameterization and as such is a valuable tool for examining snowpack sensitivity to available model inputs. After examining model results with respect to available observations, we then subjected these two model years to climate scenarios with uniform temperature increases of +2, +4, and +6°C and high and low atmospheric-humidity endmembers.

Data. Terrain data were derived from a 100-m digital elevation model sampled from the 1/3 arc-second (~ 10 m) USGS National Elevation Dataset product that yielded a model domain of 1107 by 1296 cells. These data were used to derive slope, aspect, and sky-view fraction layers. Vegetation indices, including height and canopy light penetration, were derived from the U.S. Forest Service 30-m CALVEG (US Forest Service, 2014) geodatabase (hereafter referred to as CALVEG). This layer was resampled to 100-m resolution and aligned to the model grid using nearest-neighbor sampling.

Forcing data for the model were derived from ground-based measurements and supplemented by modeled inputs for the base water years of 2011 (wet) and 2013 (dry). We used a total of 34 weather stations within and immediately adjacent to the Merced and Tuolumne watersheds (Figure 2-1 and Table 2-1) that record on an hourly basis. Sites were operated by the California Department of Water Resources (DWR), Western Regional Climate Center (WRCC), National Interagency Fire Center Remote Automatic Weather Stations (RAWS), or Scripps Institution of Oceanography (SIO). Subsets of these stations were chosen for each input parameter based on knowledge of station locations and data type and quality. Each record was inspected for data continuity and coherence with adjacent stations; and gaps were filled using linear interpolation for periods of a few hours and linear regression with a nearby station for longer gaps.

A study objective was to examine snowpack sensitivity to temperature and humidity changes, and we chose stations that recorded both quantities where the authors were confident in the quality of the data due to knowledge of sensor maintenance (Figure

2-1, Table 2-1). Relative-humidity sensors are particularly prone to drift after one to two years and require regular recalibration for accurate measurements. RAWS stations listed in Table 2-1 received documented maintenance and recalibrated sensors on an annual or biannual basis. SIO stations received a comparable level of maintenance. Other stations such as the Dana Meadows site (DWR) were known by the authors to have been maintained properly for the two model years examined here.

Other station data used included precipitation, solar radiation as an indication of cloudiness, wind speed and direction, and various measures of snowpack used for model-performance evaluation. Precipitation data were derived from eleven stations that recorded both rain and snow accumulation, though notably only two sites were located at the highest elevations and both were rain-shadow affected. Solar radiation recorded at five (WY2011) and six (WY2013) stations with minimal tree and terrain shadowing were used to develop a spatial estimate of cloudiness. Wind-speed data recorded at seven relatively open locations were used to develop spatial wind-speed distributions. Wind direction was derived from a single station (Crane Flat Lookout) and no attempt was made to adjust these values given very limited data on wind direction and highly variable terrain. Twenty-two snow-course and eight snow-pillow locations, distributed snow-depth data from four locations along the Tioga Road, and snow LiDAR data from 2013 were used to also assess spatial model performance (Table 2-2).

Methods used to develop the gridded data inputs for *iSnobal* are detailed in the following paragraphs.

Precipitation. Hourly precipitation grids were generated using data from eleven stations that were first distributed using a modified inverse distance weighting (IDW) and then bias-corrected using daily 800-m resolution PRISM (PRISM Climate Group, Oregon State University, 2012) values. We used an IDW approach that averages weights based on distances to closest stations and distances to stations with the closest monthly PRISM values. This step minimizes the bullseye effect of simple IDW (with so few available stations) while being more computationally efficient that other methods such as co-kriging. These hourly precipitation grids were then bias-corrected using daily 800-m resolution PRISM data, using a simple delta approach. PRISM data has been shown to produce lower bias relative to Daymet and WorldClim datasets in mountainous areas with sparse data in the western U.S. (Daly et al., 2008). Average annual bias was -10.4 and -48.4 mm in dry and wet years, respectively.

Temperature and vapor pressure. Air and dew-point temperature (calculated using IPW) were distributed spatially on an hourly basis using detrended kriging (Garen et al., 1994). For each hour, station values and elevation were linearly regressed and the resulting trend removed from the data. Residuals were then spatially kriged using a linear variogram and the elevation trend added back in. In the case where the regression slope was positive (increasing temperature with elevation), data were distributed using ordinary kriging only. Spatial grids of dew-point temperature were converted to vapor pressure, then to relative humidity, restricting values to 0–100%. To insure internal consistency, vapor pressure and dew point were then recalculated using these relative-humidity spatial fields with air temperature.

Net solar radiation. Hourly solar radiation input to the snowpack was calculated in a manner similar to that of Garen and Marks (2005). The IPW function stoporad (Dozier, 1980) was used to estimate incoming global and diffuse visible (0.28-0.7 μm) and infrared (0.7-2.8 μm) radiation using atmospheric parameters adjusted to match measured clear-sky values at Dana Meadows. Stoporad adjusts these values based on solar zenith and azimuth angles and topographic slope, aspect, and shading from surrounding terrain. Resulting clear-sky grids of visible and infrared, diffuse and beam (global – diffuse) radiation were then adjusted for cloudiness, canopy, and albedo.

Clear-sky radiation was attenuated by cloudiness, estimated as the ratio of measured all-wave solar radiation to the calculated estimate of clear-sky values. We developed hourly ratios at six stations spanning the model domain where topographic and forest-canopy shading was minimal or could be reasonably corrected. Night-time cloud factors were estimated as an interpolation between the last daylight hour minus one hour and the first daylight hour plus one hour. All values were maximized to 1.0.

Next, attenuation due to forest canopy was estimated using the methods of Link et al. (2004) using adjusted optical transmissivity (τ) and extinction coefficient (μ) parameters from Garen and Marks (2005). Transmissivity is the proportion of the sky hemisphere above a point on the forest floor that is unobstructed by canopy elements (also known as the sky view factor). The extinction coefficient is the exponential decay coefficient of beam radiation as it passes through the forest canopy. Pixels were classified

as conifer, mixed conifer and hardwood, hardwood, or open based on CALVEG to match those used by the foregoing references (Table 2-3). Tree height was estimated using diameter at breast height values in CALVEG and an empirical fit for central Sierra Nevada forests from Zhao et al. (2012):

$$\text{Tree height (m)} = \frac{(\text{Diameter at breast height (cm)} - 4.37)}{1.81} \quad (1)$$

Final values assigned to each grid cell were adjusted by the proportion of canopy-covered area from CALVEG.

Finally, estimated snowpack albedo was obtained using the method of Marshall and Warren (1987) as applied by Marks et al. (1999b) in the IPW albedo function. Albedo decay was determined at each model pixel based on the time since last snowfall (greater than 50% of precipitation) exceeding 0.5 mm water equivalent and accounting for solar-illumination angle. A single set of albedo parameters was used to facilitate the application of the model in future climate scenarios (effective grain size of new snow of 300 μm, maximum grain radius from grain growth of 2000 μm, and effective contamination factor of 2.0). Results were snowpack visible and infrared albedos in the range 0.9 to 0.99 and 0.4 to 0.7, respectively, that were then applied equally to diffuse and beam components. Net solar radiation was then determined by summing visible-beam, visible-diffuse, infrared-beam, and infrared-diffuse components.

Thermal radiation. We estimated incoming thermal radiation using the methods of Garen and Marks (2005) by first determining clear-sky longwave radiation, and then

adjusting for cloudiness and forest canopy. Down-welling longwave radiation was determined using the IPW topotherm tool that uses air and dew point temperature and elevation (Marks & Dozier, 1979) and has been shown to perform well in the Sierra Nevada (Marks & Dozier, 1992). Additional thermal input from clouds was estimated based on a relation between proportionalities of measured to clear-sky thermal radiation (*TRR*) versus measured to clear-sky solar radiation (*SRR*), the latter being the cloudiness index referred to in the solar-radiation section above (after Garen & Marks (2005)). We used a modified version of their equation based on further measurements at Reynolds Mountain East experimental catchment (Reba et al., 2011a; Reba et al., 2011b):

$$TRR = mSRR + b \tag{2}$$

where $m = 0.5070$ and $b = 1.5552$. Flerchinger et al. (2009) recommended the use of the cloudiness corrections by Kimball et al. (1982), Unsworth & Monteith (1975), and Crawford & Duchon (1999). Knowledge of cloud temperature precluded use of the Kimball model and comparison of the results of (2) with the other two methods yielded results that were approximately 7 W m^{-2} lower when averaged over December through February and 10 W m^{-2} lower over the March through May period at the Gin Flat and Dana Meadow sites. It was, however, unclear what bias may be introduced by combining the output of topotherm with these cloudiness adjustment factors. In the absence of better longwave data to assess the adequacy of either of these methods, we defaulted to the demonstrated success of (2) by Garen & Marks (2005). Thermal radiation was then adjusted for forest canopy using the same canopy transmissivity value used for solar radiation (Table 2-3) and estimating canopy temperature to be air temperature after the methods of Link & Marks (1999). While canopy temperature may substantially exceed

air temperature (Pomeroy et al., 2009) particularly in more open forests on south slopes in this region, no data existed to improve this estimate.

Wind speed and direction. We used hourly wind speed measured at six locations to create hourly raster grids using IDW to distribute values. The chosen locations are largely open and distributed across the domain. Wind direction was taken from one location (Crane Flat Lookout) and distributed uniformly. Given that one purpose of the investigation was to examine snowpack sensitivity to changes in vapor pressure, a detailed topographic analysis of wind direction was deemed unnecessary. Wind speed, however, was adjusted for upwind terrain and vegetation characteristics using the methods of Winstral et al. (2009). Minimum wind speed was set to 0.447 m s^{-1} for model stability. This value is considerably less than average forest wind speeds (1 m s^{-1}) and changes turbulent energy exchange very little.

Soil temperature. Soil temperature was set to a constant of 0°C at 50-cm depth after Marks & Dozier (1992). While some soil-temperature data existed for the modeled periods, the energy state of soil was not coupled to the snowpack in the available version of *iSnobal* and as such there was little justification to change this boundary condition. Equally, ground heat flux is a minor component of snowpack energy balance (Granger & Male, 1978; Link & Marks, 1999; Marks & Dozier, 1992).

Climate scenarios. To create simplified warming scenarios where we could critically examine the role of temperature and vapor-pressure changes on snow accumulation and melt, we first created air-temperature layers that were 2, 4 and 6°C

greater than those used in the water years 2011 (wet) and 2013 (dry) base-model runs. The chosen values and range are roughly in line with regional end-of-century warming estimates (Cayan et al., 2008).

The first humidity scheme consisted of assuming constant relative humidity, a common approach in climate modeling (Wigmosta et al., 1994). This scheme effectively increased atmospheric moisture during all scenario model intervals, which in turn should increase longwave radiative input to snowpack relative to lower humidity scenarios (next paragraph). Model runs for this scheme were referred to as RH2, RH4, and RH6 for the three temperature scenarios, respectively. From this, we recalculated vapor pressure and dew-point temperature, and then precipitation form, percent snow, and density. The change in dew point and precipitation then necessitated a recalculation of albedo, which is based on time since last snow. Thermal radiation was also recalculated given its dependence on air temperature and vapor pressure.

The second humidity scheme assumed that vapor pressure remained constant between storms (decreased relative humidity) and was sufficiently elevated during storms to achieve relative-humidity values consistent with the base model runs. To implement this, we set relative humidity to base-year values for the entire domain if any cell recorded precipitation. The latter step was necessary to retain physically real conditions during precipitation events where relative humidity was close to 100 percent and dew-point and air temperature were close in value. An underlying assumption inherent in this approach is that the synoptic nature of winter storms affects areas much greater than the

model domain. Model runs for this scenario were termed VP2, VP4, and VP6 for the respective temperature increases. Precipitation, albedo, and thermal-radiation grids were adjusted accordingly.

Results

Base-year results were evaluated by comparing them to ground and LiDAR measurements. We then compared base-year and climate-scenario modeled snow accumulation and melt to assess warming effects across the elevation range of the basins. Additionally, we examined changes in energy forcing that affect the elevational patterns.

Base-year results and comparison to available measurements. Modeled snow depths compared favorably to the mean and standard deviation of snow-depth observations at distributed snow-sensor sites along the Tioga Road (Figure 2-2). Comparing model results with snow-pillow data showed a good match at the higher-elevation sites; however model performance was poorer at elevations below about 2400 m (Figure A1). While performance at the lower elevations will have to be refined in future efforts, the volume of snowpack at these lower elevations comprised less than 5% of the overall snowpack in the years modeled, and as such was very small with respect to the magnitude of changes between temperature scenarios. It should also be noted that the highest snow pillow (Dana Meadows) was only 2990 m, leaving approximately 1000 m and 14% of the snow zone (Figure 2-1) above this elevation without snowpack measurements. Model predictions were also lower than most of the monthly snow-course values (Figure A2). In contrast to snow pillows, which have a footprint of a few meters,

snow courses cover areas similar in size to the 100-m grid cell size used in the model, though parts of multiple model grid-cells overlie a snow course. Snow courses are largely in forest clearings, and typically have more snow than the surrounding forest. Lower model estimates at some locations may also be attributed to underestimates of precipitation amount in PRISM, particularly in WY2013 at Horse and Paradise Meadow sites, an issue highlighted by Henn et al. (2016). Nonetheless, the model produced results that approximate the magnitude and track the seasonal trend of snowpack, consistent with both dry and wet base years (Figures 2-2, A1-2).

In contrast, modeled SWE was consistently higher than the experimental data product from the NASA Airborne Snow Observatory (Painter et al., 2016) in 2013 (Figure A3). Snow depth was measured using laser altimetry during six flights in the spring of 2013 with the main product being a 50-m resolution estimate of snow depth and snow water equivalent (Painter et al., 2016). These results were aggregated and aligned with the 100-m model grid using bilinear resampling. Results were compared by constructing boxplots of values in 300-m elevation bands. Despite our higher modeled SWE, elevational and season trends were similar to those of the ASO products (Figure A3).

Climate-scenario results. Substantial reduction of peak SWE was estimated in all warming scenarios, with the greatest reduction in areas that currently contribute the greatest amount of basin-wide SWE (Figure 2-3). Predicted dry-year SWE declined 38, 73, and 90% on April 1 for RH2, RH4, and RH6 scenarios, respectively (18, 56, and 85%

in wet-year scenarios, not shown). Complete loss of the April 1 snowpack occurred in successive 300-m elevations bands with each 2°C warming. April 1 snowpack exhibited the greatest declines at elevations centered around 2850 m (Figures 2-3 and A4). Integrated over the Merced and Tuolumne watersheds, peak SWE in the 2850-m band, which shifted earlier with warming, was reduced from base values in dry (wet) years by 38 (14)%, 55 (49)%, and 78 (73)% with 2, 4, 6°C warming (wet-year data not shown).

The sensitivity of peak SWE timing was substantially greater in dry versus wet year warming scenarios (Figure 2-4 and Table 2-4). In the Merced basin, the date of peak SWE in a dry year shifted from mid-March to mid-January with 2°C of warming, and was about 200 mm lower (Figure 2-4). Melt rate was lower when compared to the base year and melt-out date was similar. Peak SWE shifted substantially in this case due to storm input early in the year, with little precipitation in February and March. The peak-SWE date shifted little in the +4 and +6°C cases, though the amount of SWE diminished by 100 then 125 mm with each 2°C increment of warming. Melt rates generally declined from 6.6 mm day^{-1} to 2-3 mm day^{-1} in dry-year scenarios and 11 mm day^{-1} to 7-10 mm day^{-1} in wet-year scenarios due to the earlier onset of melt. The +2, +4, and +6°C wet-year cases exhibited little change in peak SWE date from the base case (close to April 1st), with decreases of 250, 800, and 1250 mm SWE, respectively.

The rate of snowline retreat was similar for base and warming scenarios, though lower in the dry versus wet year scenarios (Figure 2-5). Melt-out date shifted 4-39 days at

elevations above 3150 m for each 2°C warming in dry scenarios. Snowline retreat was approximately 9.9 m d^{-1} (12.6 m d^{-1}) in the base dry (wet) case, and 6.4-10.2 m d^{-1} (8.5-11.3 m d^{-1}) in dry (wet) warming scenarios. A change in the melt-out trend was evident around water year day 183 (April 1) in the dry scenarios, with snowline retreat before this date of 2.3-5.1 m d^{-1} and 8.0-18.8 m d^{-1} afterwards across all scenarios. A similar pattern was observed for the wet-year scenarios, though the change in melt rate occurred closer to water year day 240 (May 28).

A close correspondence between the elevation of peak annual melt and peak precipitation persisted in all warming scenarios for the Tuolumne Basin while progressively separating by several hundred meters in the Merced Basin (Figure 2-6). The zone of peak melt contribution contracted substantially and shifted approximately 500 m up in elevation in the Merced for the +6°C case compared to only 100-200 m for the Tuolumne. The contraction was more substantial in the Tuolumne case, with the top two 300-m melt-producing elevation bands exhibiting increased proportional melt contributions of 15-20% in contrast to the Merced (5-10%) and the wet-year case (10-15%). Base-year proportional melt contribution below 2000 m, the lower extent of the rain-snow transition zone, was approximately 10-15% and this largely disappeared once warming exceeded +2°C in both basins.

During the melt period, lower atmospheric moisture scenarios retained a slightly larger snowpack when compared to the constant-relative-humidity scenarios (Figure 2-7). For the +6°C, constant-relative-humidity scenario there was 50-100 mm less SWE during

late winter and spring when compared to the constant-vapor-pressure scenarios, and melt-out 1-2 weeks earlier in elevation bands that produced the most melt. Differences increased with increasing snowpack – greater differences in the wet versus dry year scenarios – and between April and June. Differences were manifest primarily during melt due to the modeling assumption that relative humidity remained constant in the constant-vapor-pressure scenario when there was precipitation.

Discussion

The purpose of this investigation was to examine changes to snowpack in a temperate mountain watershed under climate-warming scenarios using a simplified set of robust model parameters and minimal calibration to current conditions. The spatially fine resolution of the results may permit land managers and scientists to better characterize climate-change vulnerabilities as well as more precisely understand changing snowpack energetics, potentially leading to improved monitoring methods and locations and, thus, to better-informed management actions. In this section, we first examine base model results and available snowpack observations, followed by an interpretation of model results using climate scenarios.

Accumulation and melt patterns. Precipitation amounts and timing substantially affected snowpack sensitivity to temperature increases in modeled results by altering accumulation. The dry base year (2013) was highly sensitive to the rain-to-snow transition because it was a warmer than 2011 and much of the annual snowpack arrived in a warm fall storm that accounted for over one-third of the peak SWE amount in the

2850-m elevation band (Figure 2-4). Warming of 2°C effectively removed this snowfall from the winter SWE balance. Subsequent 2°C warming increments produced less change between the +2 and +4°C scenarios, because the next storm occurred in late December and was much colder. The +6°C scenario reduced the amount of SWE from this storm by 200 mm, substantially removing the snowpack from this elevation band. Nonetheless, integrated SWE losses by April 1st were maximized at elevations with the greatest snow accumulation. The accumulation period in the cooler and wetter base year (2011) was less sensitive to +2°C warming because a greater percentage of the annual snowpack accumulated later and under colder conditions, again primarily during a spate of late-December storms. Additional warming in the +4°C scenario reduced the amount of SWE during these storms by approximately 400 mm, a difference that then increased through the winter. Warming appeared to affect SWE accumulation during colder late-February and March storms under the +4°C scenario. The 6°C warming scenario substantially reduced accumulation during these late-winter storms by 1250 mm. The timing of snowfall in 2013 rendered the base model year more sensitive (reduced peak SWE) to a uniform temperature increase of 2°C than the wetter 2011 base year (smaller decrease in peak SWE).

Melt rate also varied substantially between wet and dry years. At the 2850-m band in 2013 (Figures 2-4 and 2-5, Table 2-4), peak SWE occurred early in March and melt-out occurred in mid-June for an average melt rate of 6.6 mm d^{-1}. A 2°C warming advanced the peak to mid-January given the near absence of snow accumulation after this

month in 2013. The resulting average melt rate was reduced to 2.6 mm d^{-1}, though winter-melt rates were around 1 mm d^{-1}, which accelerated to 5 mm day^{-1} after mid-April. Melt rates in the wet-year case (2011) were modeled to be substantially greater for base and the +2°C temperature increase at approximately 11 mm d^{-1} overall and 22 mm d^{-1} between the beginning of June to melt-out in August and September. At +6°C warming, peak SWE occurred near April 1st, though melt rate was reduced to 9.4 mm d^{-1}, approximately 3 times that for all dry-year scenarios. In general, the lower melt rates that accompany most scenarios may lead to less runoff due to decreased saturated soil water pressure gradient. The increased melt rate for the +2°C wet year scenario could lead to greater spring flooding over the base case, though melt rates were not substantially above those observed in many wet years, and as a result flooding would not be substantially greater than currently observed.

Integrated annual melt originated in an increasingly limited elevation range with warming. Across the model domain in the dry (wet) base-year scenario, greater than 94 (88-92)% of snowmelt originated at elevations above 1200 m, with more than half of melt coming from elevations above 2500 m. These areas correspond to areas of elevated precipitation caused by orographic lifting of synoptic storm systems as they cross the mountain range. Peak proportional precipitation inputs in the snowmelt zone occurred at 2400 and 2800 m in the Merced and Tuolumne River watersheds, respectively, in both wet and dry years, which correspond to peak fractional basin area (note that the peak proportional precipitation 100-m elevation band for the Merced basin actually occurs below the seasonal snowpack zone at 1000 m). Precipitation contributions above these

elevations drop off due to a combination of reduced basin area and rain-shadow effects. Annual melt contribution peaks close to the same elevation as peak precipitation in base-year model runs (Figure 2-6). The elevation of peak-melt contribution shifted upwards in elevation by 17-83 m $°C^{-1}$, with larger shifts modeled in the Merced than the Tuolumne watersheds. This is due to the proportionally greater area above 2800 m in the Tuolumne than the Merced (17 vs 11%) snow zones. The zone of peak-melt contribution contracts with increasing temperature due to a rising rain-to-snow transition elevation, resulting in greater than 95% of melt derived from elevations greater than 2200 m in the Tuolumne and Merced watersheds under the RH6 dry condition.

Sensitivity to humidity scenarios was less than that of temperature increases (Figures 2-7 and A5). As expected, the higher-atmospheric-moisture scenarios (RH2, RH4, RH6) exhibited faster melt-out rates than the respective low-humidity scenarios (VP2, VP4, VP6) resulting in melt-out dates 1-2 weeks earlier. This was mainly the result of increased thermal radiation and turbulent energy flux to the snowpack. For example, the energy balance for snowpack in the 2850-m band differed by +0.9 W m^{-2} from February 1 to May 1 between RH6 and VP6 wet-year scenarios. The difference was driven by greater net thermal radiation (+1.2 W m^{-2}) and turbulent-energy fluxes to the snowpack (+1.2 W m^{-2}) that offset greater solar radiation input for the VP6 scenario, a result of more snow-covered area relative to the RH6 scenario. Dry-year results exhibited a smaller difference due to the smaller snowpack and an energy balance differing by -1.0 W m^{-2} (RH6 – VP6) between February and May, the negative value a result of greater areas of zero SWE in the RH6 scenario.

In contrast, increasing air temperature by 2°C increased the energy flux to the snowpack by an order of magnitude greater than differences between humidity scenarios. Figure 2-8 illustrates the differences in energy components between January and June for the wet base and +2°C scenarios at the 2850 m elevation band. The greater energy flux to the snowpack for the warmer scenario January – May (+24 W m^{-2}) was driven primarily by differences in thermal radiation, with smaller latent heat differences showing up in April and May. Solar radiation (net) to the snowpack is higher for the base model case in May and June due to greater proportional shading of the snowpack for the warmer scenario (energy components were averaged over areas with snowcover only).

Comparison of the 2013 model results to the Airborne Snow Observatory (ASO) snow LiDAR SWE product highlights the challenges of comparing spatial results to ground-based measurements (Figure A3). Model results underestimate SWE at ground measurement locations (Figures A1, A2) and generally over-predict SWE when compared to the spatially continuous ASO product (Figure A3). The latter uses snow density derived from an *iSnobal* model that uses different temperature and precipitation forcing data than that used here (Hedrick et al., in prep). Further, comparison of model or ASO results to snow course and snow pillow data is inherently limited by uncertainty in measurement location, and the spatial resolution and quality of forcing data. While beyond the scope of this investigation, further evaluation of ASO and modeled results relative to improved ground measurements is a critical research area.

Limitations of model approach. Because the purpose of this study was to examine snowpack sensitivity to climate-warming scenarios, limitations that impact this analysis must be noted. The snow model *iSnobal* is independent of the required forcing data – it does not calculate forcing parameters internally – and has been shown to very accurately simulate spatial patterns of snow cover development and ablation (Garen and Marks, 2005; Kormos et al., 2014; Kormos et al., 2017; Marks et al., 1998; Marks et al., 1999b; Marks & Winstral, 2001; Marks et al., 2001; Marks et al., 2002; Nayak et al., 2012). The accuracy of results is largely limited by the accuracy of the forcing data. Precipitation timing, as distributed using inverse-distance weighting, may result in mismatches with dew-point records, resulting in changes in the rain-to-snow transition. This was particularly acute at lower elevations during early fall storms in the 2013 dry-year base-case modeling. Further, precipitation amount is quite uncertain in these basins as described by Henn et al. (2016) and illustrated by snow pillow totals that exceed the estimated precipitation for Horse Meadow in 2011 and 2013 (Figure A1). Ascribing a single set of albedo parameters limited the interpretation of results because it does not adequately account for enhanced albedo decay with the addition of late-season litter and dust accumulation at the snowpack surface (Hardy et al., 2000; Hardy et al., 2004). There was considerable uncertainty in the estimate of longwave radiation given a lack of measured values, which is a common issue in snowpack modeling (Lapo et al., 2015; Raleigh et al., 2015). Longwave radiation was often too high for snow accumulation at lower elevation sites, which retarded the onset of snowpack formation. Similarly, longwave radiation was probably too low at the highest elevations, which resulted in enhanced snowpack retention. While we did not incorporate canopy interception of snow,

evidence suggests that evaporation or sublimation from tree canopies in humid temperate mountain areas is minimal (Storck et al., 2002). Model results are nonetheless useful for evaluation of snowpack sensitivity to climate change at a mountain watershed scale, and this effort plus its limitations highlight avenues for snowpack model improvement over large sparsely instrumented watersheds.

Management implications. Study results are instructive to water and forest management in these and similar mountain basins in that they provide an indication of potential snowpack reduction and complete loss with respect to location and progressive warming. Results suggest that the Tuolumne Meadows area at 2600 m elevation loses much of its snowpack by April 1 under a 4°C increase in a dry year and by April 1 under a 6°C increase in a wet year. Indeed, under these scenarios, the area known for its winter beauty and recreation will shift to a rain-dominated system by mid- to late-century. The meadow wetland environment that has excluded conifers is supported by late snowpack that in turn generates high groundwater levels well into the dry summer months. Once annual snowmelt in contributing basins ceases, groundwater levels drop quickly, leaving only a small amount of water in the upper layers of organic-rich meadows soils (Loheide II et al., 2009). Loss of seasonal snow cover may lead to desiccation and loss of carbon from meadows (Arnold et al., 2014) and decreased hydroperiod essential to maintaining wetland conditions that exclude trees (Lowry et al., 2011), creating the potential to convert meadows to forest, as has been observed already in many mountain meadows in the west (Fites-Kaufman et al., 2007; Millar et al., 2004).

Reduced snowpack storage will affect water storage for downstream users, especially for communities dependent on run-of-the-river water systems where groundwater resources are limited (Lundquist and Roche, 2009). Water supply for the community of Wawona is derived from the South Fork Merced near the southern border of Yosemite National Park, and will likely be substantially affected by snowpack reduction. Model results suggest that the basin may lose approximately 50% of current April 1 snowpack with a 2°C temperature increase relative to the dry base year (Figure 2-3) and nearly all April 1 snowpack with a 4°C warming. Water-use restrictions imposed during recent drought years, of which 2013 was one, will likely become part of normal operations, with new restrictions becoming increasingly necessary as the length of the snow-free season increases. Downstream water users that depend on streamflow in the Merced and Tuolumne Rivers will progressively lose snowpack storage (174 mm or 1.16×10^9 m^3 on April 1, 2013) equivalent to 31% of the combined primary rim dam reservoir capacity: Lakes McClure and Don Pedro on the Merced and Tuolumne Rivers, respectively. Given that a greater proportion of precipitation would fall as rain rather than snow and that reservoirs must be maintained at lower levels during the winter to protect downstream areas from flooding, it will become increasingly difficult to safely fill reservoirs from a diminishing snowpack in the spring and early summer.

SWE scenarios can be combined with evapotranspiration scenarios to estimate changes in the basin-wide water balance. For example, using the relation in Figure 4 of Goulden and Bales (2014), warming of 4°C would increase ET by 179 mm per year, which when combined with a mean annual precipitation of 694 mm and estimated ET of

510 mm in 2013 effectively eliminates runoff. Snowpack storage on April 1 would be reduced from 171 mm to 46 mm implying that virtually all runoff will be derived from snowmelt. Vegetation management to reduce ET will be essential to mitigating effects of increased temperature. Reducing biomass through forest thinning is possible on up to 25% of U.S. Forest Service lands given economic, access, and administrative constraints (North et al., 2015). Remaining areas (U.S. Forest Service and National Park Service) would have to be thinned through managed fire (North et al., 2015), which shows promise of increased or at least sustained water yield (Boisramé et al., 2016).

Fine-scale snow-model results may assist managers in anticipating forest-fire activity. Lutz et al. (2009) documented an inverse relation between the number of fire starts and fire severity in Yosemite National Park and April 1 SWE in Tuolumne Meadows. This observation may reflect the duration of the snow-free period across elevations spanning the mixed-conifer zone (approximately 1500-2400 m), which may in turn determine vegetation and fuel dryness, as well as increased summer convective-storm activity, leading to increased lightning. Using the 300-m elevation band centered at 2550 m in the Tuolumne basin as a proxy for Lutz et al. (2009) Tuolumne Meadows SWE estimates, we found that modeled SWE declined by 38% (48%) in the wet (dry) year case for the 2°C warming scenario. Further warming of +4°C and +6°C resulted in April 1st SWE declines of 69% (86%) and 92% (100%) respectively for wet (dry) year cases examined in this study. This corresponds to advances in the average melt-out date in the 1500–2400 m elevation range from 44 days in the wet year scenario for +2°C (Figure 2-5) to complete snowpack loss in the lowest elevation bands in the +2 and +4°C

dry year warming scenarios (Figures 2-5 and 2-6). Model results suggest avenues for refinement of the Lutz et al. (2009) analysis that may result in a more spatially refined examination of forest fire susceptibility.

Quality precipitation measurements, particularly at high elevations, are essential to water management in a changing climate. Precipitation estimates derived from snow pillow records will become less reliable as the proportion of rain increases. For this study and the PRISM precipitation data used, there were only three (2013) or four (2011) precipitation gauges in the snow zone, three of which were concentrated in a 400 m elevation band in rain-shadow-affected areas of the upper Tuolumne watershed and Walker watershed immediately to the east. Managing increased flood risks due to more rain and less snow, water storage in reservoirs, and natural resources will require a much-improved network of weighing or accumulation gauges capable of accurately measuring mixed precipitation.

Conclusions

For both wet and dry years, changes in snowpack accumulation and melt, and reduced snowpack storage have significant implications for the region. First, snowpack storage on April 1 in a dry year declines 38, 73, and 90% for +2°C, +4°C, and +6°C warming, respectively, in the zone of current snow maximum accumulation. The seasonal snowline retreats upslope 300 m for each 2°C warming, and areas below 2000 m become snow free once warming reaches +4°C. Second, constant-vapor-pressure scenarios increase late-season snowpack up to 100 mm over constant-relative-humidity scenarios,

suggesting one should consider both end-member atmospheric moisture conditions when modeling snowpack under warmer temperatures.

Finally, there are many implications for future management in Sierra Nevada watersheds including transformation of snow- to rain-dominated ecosystems, progressive loss of snowpack storage as a component of water supply, and forest management. Transformation of the snowy subalpine environment to one dominated by rain would allow for more recreational access in many areas of Yosemite National Park requiring year-round rather than seasonal management presence. Loss of seasonal snow cover may also affect animal and bird habitat, carbon storage, and local water supplies in the Sierra Nevada. Reduction of snowpack storage by 2050 could require an additional one billion cubic meters of downstream storage. Considering increases in evapotranspiration with rising temperatures, much of the annual runoff in dry years could be derived solely from dwindling snowpack storage. As a potential mediator of forest-fire potential, changes in snowpack duration could result in drier summer conditions that are more susceptible to lightning due to increased convective storm activity. Some of this drying could be offset through forest thinning, whether mechanical or through managed fire, resulting in reducing evapotranspiration while potentially enhancing accumulation and retention of a seasonal snowpack.

Acknowledgements. Support for this research was provided by the Yosemite Conservancy, the Merced Irrigation District through the California Integrated Regional Watershed Management Program (IRWMP), the Southern Sierra Critical Zone

Observatory (Grant number EAR-1331939), and the University of California Water Security and Sustainability Research Initiative. We acknowledge the contributions of Drs. Scott Havens (Agricultural Research Service) and Adam Winstral (Swiss Federal Institute for Forest, Snow and Landscape Research) for their immense help with the implementation of *iSnobal* and to Xiande Meng and Esther Canal for their assistance with forcing data preparation.

References

Anderson, E. A. (2006). Snow accumulation and ablation model–SNOW-17. http://www.nws.noaa.gov/oh/hrl/nwsrfs/users_manual/part2/_pdf/22snow17.pdf

Andrews, E. D. (2012). Hydrology of the Sierra Nevada Network national parks: Status and trends. Natural Resource Report NPS/SIEN/NRR—2012/500. National Park Service, Fort Collins, Colorado, 196p

Arnold, C., Ghezzehei, T. A., & Berhe, A. A. (2014). Early spring, severe frost events, and drought induce rapid carbon loss in high elevation meadows. *PloS One*, *9*(9), e106058. doi: 10.1371/journal.pone.0106058

Bales, R. C., Molotch, N. P., Painter, T. H., Dettinger, M. D., Rice, R., & Dozier, J. (2006). Mountain hydrology of the western United States. *Water Resources Research*, *42*(8), W08432. doi: 10.1029/2005WR004387

Barnett, T. P., Adam, J. C., & Lettenmaier, D. P. (2005). Potential impacts of a warming climate on water availability in snow-dominated regions. *Nature*, *438*(7066), 303–309. doi: 10.1038/nature04141

Boisramé, G., Thompson, S., Collins, B., & Stephens, S. (2016). Managed Wildfire Effects on Forest Resilience and Water in the Sierra Nevada. *Ecosystems*, 1–16. doi: 10.1007/s10021-016-0048-1

Brown, R. D., & Mote, P. W. (2009). The Response of Northern Hemisphere Snow Cover to a Changing Climate. *Journal of Climate*, *22*(8), 2124–2145. doi: 10.1175/2008JCLI2665.1

Cayan, D. R., Maurer, E. P., Dettinger, M. D., Tyree, M., & Hayhoe, K. (2008). Climate change scenarios for the California region. *Climatic Change*, *87*(1), 21–42. doi: 10.1007/s10584-007-9377-6

Cooper, M. G., Nolin, A. W., & Safeeq, M. (2016). Testing the recent snow drought as an analog for climate warming sensitivity of Cascades snowpacks. *Environmental Research Letters*, *11*(8), 84009. doi: 10.1088/1748-9326/11/8/084009

Crawford, T. M., and Duchon, C. E. (1999). An improved parameterization for estimating effective atmospheric emissivity for use in calculating daytime downwelling longwave radiation, *Journal of Applied Meteorology*, 48, 474– 480. doi: 10.1175/1520-0450(1999)038<0474:AIPFEE>2.0.CO;2

Curtis, J. A., Flint, L. E., Flint, A. L., Lundquist, J. D., Hudgens, B., Boydston, E. E., & Young, J. K. (2014). Incorporating cold-air pooling into downscaled climate models increases potential refugia for snow-dependent species within the Sierra Nevada Ecoregion, CA. *PloS One*, *9*(9), e106984. doi: 10.1371/journal.pone.0106984

Dai, A. (2006). Recent Climatology, Variability, and Trends in Global Surface Humidity. *Journal of Climate*, *19*(15), 3589–3606. doi: 10.1175/JCLI3816.1

Daly, C., Halbleib, M., Smith, J. I., Gibson, W. P., Doggett, M. K., Taylor, G. H., … Pasteris, P. P. (2008). Physiographically sensitive mapping of climatological temperature and precipitation across the conterminous United States. *International Journal of Climatology*, *28*(15), 2031–2064. doi: 10.1002/joc.1688

Dettinger, M. D., Cayan, D. R., Meyer, M. K., & Jeton, A. (2004). Simulated hydrologic responses to climate variations and change in the Merced, Carson, and American River basins, Sierra Nevada, California, 1900-2099 *. *Climatic Change*, *62*(1–3), 283–317. doi: 10.1023/B:CLIM.0000013683.13346.4f

Diffenbaugh, N. S., & Field, C. B. (2013). Changes in Ecologically Critical Terrestrial Climate Conditions. *Science*, *341*(6145), 486. doi: 10.1126/science.1237123

Dozier, J. (1980). A clear-sky spectral solar radiation model for snow-covered mountainous terrain. *Water Resources Research*, *16*(4), 709–718. doi: 10.1029/WR016i004p00709

Feld, S. I., Cristea, N. C., & Lundquist, J. D. (2013). Representing atmospheric moisture content along mountain slopes: Examination using distributed sensors in the Sierra Nevada, California. *Water Resources Research*, *49*(7), 4424–4441. doi: 10.1002/wrcr.20318

Fites-Kaufman, J. A., Rundel, P., Stephenson, N., & Weixelman, D. A. (2007). Montane and subalpine vegetation of the Sierra Nevada and Cascade ranges (pp. 456–501). Berkeley, CA: University of California Press.

Flint, L., Flint, A., Thorne, J., & Boynton, R. (2013). Fine-scale hydrologic modeling for regional landscape applications: the California Basin Characterization Model development and performance. *Ecological Processes*, *2*(1), 1–21. doi: 10.1186/2192-1709-2-25

Frew, J. E. (1990). The image processing workbench. Doctoral dissertation, University of California at Santa Barbara, California. 382p

Garen, D. C., Johnson, G. L., & Hanson, C. L. (1994). Mean Areal Precipitation for Daily Hydrologic Modeling in Mountainous Regions. *JAWRA Journal of the American Water Resources Association*, *30*(3), 481–491. doi: 10.1111/j.1752-1688.1994.tb03307.x

Garen, D. C., & Marks, D. (2005). Spatially distributed energy balance snowmelt modelling in a mountainous river basin: estimation of meteorological inputs and verification of model results. *Journal of Hydrology*, *315*(1), 126–153. doi: 10.1016/j.jhydrol.2005.03.026

Goulden, M. L., & Bales, R. C. (2014). Mountain runoff vulnerability to increased evapotranspiration with vegetation expansion. *Proceedings of the National Academy of Sciences*, *111*(39), 14071–14075. doi: 10.1073/pnas.1319316111

Granger, R. J., & Male, D. H. (1978). Melting of a Prairie Snowpack. *Journal of Applied Meteorology*, *17*(12), 1833–1842. doi: MOAPS>2.0.CO;2

Hannah, L., Flint, L., Syphard, A. D., Moritz, M. A., Buckley, L. B., & McCullough, I. M. (2014). Fine-grain modeling of species' response to climate change: holdouts, stepping-stones, and microrefugia. *Trends in Ecology & Evolution*, *29*(7), 390–397. doi: 10.1016/j.tree.2014.04.006

Hardy, J. P., Melloh, R., Koenig, G., Marks, D., Winstral, A., Pomeroy, J. W., & Link, T. (2004). Solar radiation transmission through conifer canopies. *Agricultural and Forest Meteorology*, *126*(3–4), 257–270. doi: //doi.org/10.1016/j.agrformet.2004.06.012

Hardy, J. P., Melloh, R., Robinson, P., & Jordan, R. (2000). Incorporating effects of forest litter in a snow process model. *Hydrological Processes*, *14*(18), 3227–3237. doi: AID-HYP198>3.0.CO;2-4

Henn, B., Clark, M. P., Kavetski, D., Newman, A. J., Hughes, M., McGurk, B., & Lundquist, J. D. (2016). Spatiotemporal patterns of precipitation inferred from streamflow observations across the Sierra Nevada mountain range. *Journal of Hydrology*. doi: 10.1016/j.jhydrol.2016.08.009

Kimball, B. A., Idso, S. B., and Aase, J. K. (1982). A model of thermal radiation from partly cloudy and overcast skies. *Water Resources Research*, 18, 931–936. doi: 10.1029/WR018i004p00931

Knowles, N., & Cayan, D. (2004). Elevational Dependence of Projected Hydrologic Changes in the San Francisco Estuary and Watershed. *Climatic Change*, *62*(1), 319–336. doi: CLIM.0000013696.14308.b9

Kormos, P. R., Marks, D., McNamara, J. P., Marshall, H. P., Winstral, A., & Flores, A. N.

(2014). Snow distribution, melt and surface water inputs to the soil in the mountain rain–snow transition zone. *Journal of Hydrology*, *519*, *Part*, 190–204. doi: 10.1016/j.jhydrol.2014.06.051

Kormos, P. R., Marks, D., Pierson, F. B., Williams, C. J., Hardegree, S. P., Havens, S., … Svejcar, T. J. (2017). Ecosystem Water Availability in Juniper versus Sagebrush Snow-Dominated Rangelands. *Rangeland Ecology & Management*, *70*(1), 116–128. doi: 10.1016/j.rama.2016.05.003

Lapo, K. E., Hinkelman, L. M., Raleigh, M. S., & Lundquist, J. D. (2015). Impact of errors in the downwelling irradiances on simulations of snow water equivalent, snow surface temperature, and the snow energy balance. *Water Resources Research*, *51*(3), 1649–1670. doi: 10.1002/2014WR016259

Link, T. E., Marks, D., & Hardy, J. P. (2004). A deterministic method to characterize canopy radiative transfer properties. *Hydrological Processes*, *18*(18), 3583–3594. doi: 10.1002/hyp.5793

Link, T., & Marks, D. (1999). Distributed simulation of snowcover mass- and energy-balance in the boreal forest. *Hydrological Processes*, *13*(14-15), 2439–2452. doi: AID-HYP866>3.0.CO;2-1

Loheide II, S. L., Deitchman, R., Cooper, D., Wolf, E., Hammersmark, C., & Lundquist, J. (2009). A framework for understanding the hydroecology of impacted wet meadows in the Sierra Nevada and Cascade Ranges, California, USA. *Hydrogeology Journal*, *17*(1), 229–246. doi: 10.1007/s10040-008-0380-4

Lowry, C. S., Loheide, S. P., Moore, C. M., & Lundquist, J. D. (2011). Groundwater controls on vegetation composition and patterning in mountain meadows. *Water Resources Research*, *47*. doi: 10.1029/2010WR010086

Lundquist, J. & Roche, J. (2009). Climate change and water supply in western national parks. *Park Science*, 26(1), 31-33, Spring 2009, ISSN 1090-9966.

Lutz, J. A., van Wagtendonk, J. W., Thode, A. E., Miller, J. D., & Franklin, J. F. (2009). Climate, lightning ignitions, and fire severity in Yosemite National Park, California, USA. *International Journal of Wildland Fire*, *18*(7), 765–774. doi: 10.1071/WF08117

Marks, D., Domingo, J., & Frew, J. (1999a). Software tools for hydro-climatic modeling and analysis: Image processing workbench, ARS-USGS Version 2. *ARS Technical Bulletin NWRC-99-1,* 1

Marks, D., Domingo, J., Susong, D., Link, T., & Garen, D. (1999b). A spatially distributed energy balance snowmelt model for application in mountain basins. *Hydrological Processes*, *13*(February), 1935–1959. doi: 10.1002/(SICI)1099-1085(199909)13:12/13<1935::AID-HYP868>3.0.CO;2-C

Marks, D., & Dozier, J. (1979). A clear-sky longwave radiation model for remote alpine areas. *Archiv Für Meteorologie, Geophysik Und Bioklimatologie Serie B*, *27*(2–3), 159–187. doi: 10.1007/BF02243741

Marks, D., & Dozier, J. (1992). Climate and energy exchange at the snow surface in the Alpine Region of the Sierra Nevada: 2. Snow cover energy balance. *Water Resources Research*, *28*(11), 3043–3054. doi: 10.1029/92WR01483

Marks, D., Kimball, J., Tingey, D., & Link, T. (1998). The sensitivity of snowmelt processes to climate conditions and forest cover during rain-on-snow: a case study of the 1996 Pacific Northwest flood. *Hydrological Processes*, *12*(10–11), 1569–1587. doi: AID-HYP682>3.0.CO;2-L

Marks, D., Link, T., Winstral, A., & Garen, D. (2001). Simulating snowmelt processes during rain-on-snow over a semi-arid mountain basin. *Annals of Glaciology*, *32*(1), 195–202. doi: 10.3189/172756401781819751

Marks, D., & Winstral, A. (2001). Comparison of Snow Deposition, the Snow Cover Energy Balance, and Snowmelt at Two Sites in a Semiarid Mountain Basin. *Journal of Hydrometeorology*, *2*(3), 213–227. doi: COSDTS>2.0.CO;2

Marks, D., Winstral, A., & Seyfried, M. (2002). Simulation of terrain and forest shelter effects on patterns of snow deposition, snowmelt and runoff over a semi-arid mountain catchment. *Hydrological Processes*, *16*(18), 3605–3626. doi: 10.1002/hyp.1237

Marshall, S. E., & Warren, S. G. (1987). Parameterization of snow albedo for climate models. In Large Scale Effects of Seasonal Snow Cover, B.E. Goodison, R.G. Barry, J. Dozier Eds. IAHS-AIHS Publication 166, International Association of Hydrological Sciences, Wallingford, UK, 43-50.

McMenamin, S. K., Hadly, E. A., & Wright, C. K. (2008). Climatic Change and Wetland Desiccation Cause Amphibian Decline in Yellowstone National Park. *Proceedings of the National Academy of Sciences of the United States of America*, *105*(44), 16988–16993. doi: 10.1073/pnas.0809090105

Millar, C. I., Westfall, R. D., Delany, D. L., King, J. C., & Graumlich, L. J. (2004). Response of Subalpine Conifers in the Sierra Nevada, California, U.S.A., to 20th-Century Warming and Decadal Climate Variability. *Arctic, Antarctic, and Alpine Research*. doi: 10.1657/1523-0430(2004)036[0181:ROSCIT]2.0.CO;2

Moore, R. D., Fleming, S. W., Menounos, B., Wheate, R., Fountain, A., Stahl, K., … Jakob, M. (2009). Glacier change in western North America: influences on hydrology, geomorphic hazards and water quality. *Hydrological Processes*, *23*(1), 42–61. doi: 10.1002/hyp.7162

Mote, P. W., Hamlet, A. F., Clark, M. P., & Lettenmaier, D. P. (2005). Declining mountain snowpack in western north America. *Bulletin of the American*

Meteorological Society, *86*(1), 39–49. doi: 10.1175/BAMS-86-1-39

Nayak, A., Marks, D., Chandler, D. G., & Winstral, A. (2012). Modeling Interannual Variability in Snow-Cover Development and Melt for a Semiarid Mountain Catchment. *Journal of Hydrologic Engineering*, *17*(1), 74–84. doi: 10.1061/(ASCE)HE.1943-5584.0000408

North, M. P., Brough, A., Long, J., Collins, B., Bowden, P., Yasuda, D., … Sugihara, N. (2015). Constraints on mechanized treatment significantly limit mechanical fuels reduction extent in the Sierra Nevada. *Journal of Forestry*, *113*(1), 40–48. doi: 10.5849/jof.14-058

Painter, T. H., Berisford, D. F., Boardman, J. W., Bormann, K. J., Deems, J. S., Gehrke, F., … Winstral, A. (2016). The Airborne Snow Observatory: Fusion of scanning lidar, imaging spectrometer, and physically-based modeling for mapping snow water equivalent and snow albedo. *Remote Sensing of Environment*, *184*, 139–152. doi: 10.1016/j.rse.2016.06.018

Pierce, D. W., Westerling, A. L., & Oyler, J. (2013). Future humidity trends over the western United States in the CMIP5 global climate models and variable infiltration capacity hydrological modeling system. *Hydrology and Earth System Sciences*, *17*(5), 1833–1850. doi: //doi.org/10.5194/hess-17-1833-2013

Pomeroy, J. W., Marks, D., Link, T., Ellis, C., Hardy, J., Rowlands, A., & Granger, R. (2009). The impact of coniferous forest temperature on incoming longwave radiation to melting snow. *Hydrological Processes*, *23*(17), 2513–2525. doi: 10.1002/hyp.7325

PRISM Climate Group. (2012). United States Average Annual Precipitation, 1981-2010. Oregon State University, http://prism.oregonstate.edu

Raleigh, M. S., Lundquist, J. D., & Clark, M. P. (2015). Exploring the impact of forcing error characteristics on physically based snow simulations within a global sensitivity analysis framework. *Hydrology and Earth System Sciences*, *19*(7), 3153–3179. doi: 10.5194/hess-19-3153-2015

Reba, M. L., Marks, D., Seyfried, M., Winstral, A., Kumar, M., & Flerchinger, G. (2011a). A long-term data set for hydrologic modeling in a snow-dominated mountain catchment. *Water Resources Research*, *47*(7). doi: 10.1029/2010WR010030

Reba, M. L., Marks, D., Winstral, A., Link, T. E., & Kumar, M. (2011b). Sensitivity of the snowcover energetics in a mountain basin to variations in climate. *Hydrological Processes*, *25*(21), 3312–3321. doi: 10.1002/hyp.8155

Schimel, D., Kittel, T. G. F., Running, S., Monson, R., Turnipseed, A., & Anderson, D. (2002). Carbon sequestration studied in western US mountains. *Eos, Transactions American Geophysical Union*, *83*(40), 445–449. doi: 10.1029/2002EO000314

Sproles, E. A., Nolin, A. W., Rittger, K., & Painter, T. H. (2012). Climate change impacts on maritime mountain snowpack in the Oregon Cascades. *Hydrology and Earth System Sciences Discussions*, *9*(11), 13037–13081. doi: 10.5194/hessd-9-13037-2012

Stewart, I. T., Cayan, D. R., & Dettinger, M. D. (2004). Changes in snowmelt runoff timing in western North America under a business as usual climate change scenario. *Climatic Change*, *62*(1), 217–232. doi: CLIM.0000013702.22656.e8

Stewart, I. T., Cayan, D. R., & Dettinger, M. D. (2005). Changes toward earlier streamflow timing across western North America. *Journal of Climate*, *18*(8), 1136–1155. doi: 10.1175/JCLI3321.1

Storck, P., Lettenmaier, D. P., & Bolton, S. M. (2002). Measurement of snow interception and canopy effects on snow accumulation and melt in a mountainous maritime climate, Oregon, United States. *Water Resources Research*, *38*(11), 16. doi: 10.1029/2002WR001281

Trujillo, E., Molotch, N. P., Goulden, M. L., Kelly, A. E., & Bales, R. C. (2012). Elevation-dependent influence of snow accumulation on forest greening. *Nature Geoscience*, *5*(10), 705. doi: 10.1038/ngeo1571

Unsworth, M. H., and J. L. Monteith (1975), Long-wave radiation at the ground, *Q. J. R. Meteorological Society*, 101, 13–24. doi: 10.1002/qj.49710142703

U.S. Forest Service. (2014). Existing Vegetation - CALVEG, ESRI personal geodatabase. https://www.fs.usda.gov/detail/r5/landmanagement/resourcemanagement/?cid=stelprdb5347192.

Wigmosta, M. S., Vail, L. W., & Lettenmaier, D. P. (1994). A distributed hydrology-vegetation model for complex terrain. *Water Resources Research*, *30*(6), 1665–1679. doi: 10.1029/94WR00436

Winstral, A., Marks, D., & Gurney, R. (2009). An efficient method for distributing wind speeds over heterogeneous terrain. *Hydrological Processes*, *23*(17), 2526–2535. doi: 10.1002/hyp.7141

Zhao, F., Guo, Q., & Kelly, M. (2012). Allometric equation choice impacts lidar-based forest biomass estimates: A case study from the Sierra National Forest, CA. *Agricultural and Forest Meteorology*, *165*, 64–72. doi: 10.1016/j.agrformet.2012.05.019

Table 2-1. Meteorological stations and data used to force model.

Station name[1]	Elev., m	UTM northing[2], m	UTM easting[2], m	Measurements used[3]	Operator[4]
Green Springs (GRN)	311	4193067	191966	t, rh, p	RAWS
Stanislaus Powerhouse (SPW)	333	4225930	204880	p	PGE
Cathey's Valley (CVR)	366	4151342	224905	t, rh, p	RAWS
Dudley Ranch (DUC)	366	4151264	224864	p	MID
Briceburg (MBB)	452	4165485	237083	p	MID
Mariposa (MRP)	680	4154996	235967	t, rh, p	RAWS
Priest Reservoir (PRR-SIO)	709	4189078	212647	t, rh	SIO
Metcalf Gap (MCF)	938	4143892	255011	t, rh	RAWS
Batterson (BTT)	943	4140575	268301	p	RAWS
Smith Peak (SEW)	1168	4188222	226980	sr, w	RAWS
Smith Peak (SEW-SIO)	1168	4188222	226980	t, rh	SIO
Jerseydale (JSD)	1189	4158967	249214	t, rh	RAWS
Hetch Hetchy (HEM)	1195	4203412	255489	p	HHWP
Wawona (WWN)	1235	4158119	265654	t, rh, sr	RAWS
Yosemite Valley (YYV)	1208	4181238	271843	p	MID
Miami Mountain (MIA)	1321	4144912	257059	t, rh, sr, w	RAWS
Sunset Inn (SUN-SIO)	1371	4188288	245001	t, rh	SIO
Hodgdon (HDG-SIO)	1397	4187075	248304	t, rh	SIO
Mount Elizabeth (MTE)	1504	4217791	215134	t, rh, sr, w	RAWS
Yosemite South Entrance (YOW)	1511	4154480	267291	p	MID
Forty Mile (FTY-SIO)	1723	4184565	247936	t, rh	SIO
Pinecrest (PNW)	1738	4230750	236322	t, rh, sr, w	RAWS
Merced Grove (MEG-SIO)	1810	4183446	249675	t, rh	SIO
Mariposa Grove (MPG)	1951	4154932	269754	t, rh	RAWS
Crane Flat (CFL-CRN)	2017	4182829	251510	p	NOAA
Crane Flat Lookout (CFL)	2026	4182878	251530	t, rh, sr, w	RAWS
Gin Flat (GIN-SIO)	2149	4183578	255577	t, rh	SIO
Fresno Dome (FRS)	2177	4149346	275698	t, rh, w	UCM
Smoky Jack (SMK-SIO)	2182	4188935	261192	t, rh	SIO
White Wolf (WHW)	2408	4193540	266732	t, rh, sr, w	RAWS
Olmsted Quarry (OLM-SIO)	2604	4187768	279089	t, rh	SIO

Table 2-1. (cont.)

Station name[1]	Elev., m	UTM easting[2], m	UTM northing[2], m	Measurements used[3]	Operator[4]
Tuolumne Meadows (TUM)	2622	4194700	293480	p	CA-DWR
Virginia Lakes Ridge (VRG)	2879	4215567	304085	p	NRCS
Dana Meadow (DAN)	2988	4196683	301507	t, rh, sr, w	CA-DWR

[1]Station name abbreviations: Three letter abbreviations are derived from conventions in the California Data Exchange Commission database (http://cdec.water.ca.gov/). Abbreviations ending with "-SIO" indicate stations operated by Scripps Institution of Oceanography that are not currently available through CDEC. CFL-CRN indicates the NOAA Climate Reference Network Station located near the Crane Flat Lookout.

[2]Geographic coordinates are in Universal Transverse Mercator (UTM) projection, North American 1983 Datum, Zone 11.

[3]Variable abbreviations: p, precipitation; rh, relative humidity; sr, solar radiation; t, air temperature; w, wind speed and direction.

[4]Operator abbreviations are: RAWS – Interagency Fire Remote Access Weather Station network managed by the Bureau of Land Management; SIO – Scripps Institution of Oceanography; UCM – University of California Merced; CA-DWR – California Department of Water Resources; MID – Merced Irrigation District; HHWP – Hetch Hetchy Water and Power; NRCS – Natural Resource Conservation Service; PGE – Pacific Gas and Electric; NOAA – National Oceanic and Atmospheric Administration Climate Reference Network.

Table 2-2. Meteorological stations and data used to force model.

Station name[1]	Elev., m	UTM northing[2], m	UTM easting[2], m	Data type[3]
Merced Grove (MEG-SIO)	1810	4183446	249675	distributed snow depth
Bell Meadow (BEM)	1981	4228435	242260	monthly swe
Beehive Meadow (BHV)	1981	4208908	255883	monthly swe
Lower Kibbie (LKB)	2042	4213387	247407	monthly swe
Lake Vernon (VNN)	2042	4211186	261488	monthly swe
Upper Kibbie Ridge (UKR)	2042	4214521	246651	monthly swe
Kerrick Ranch (KRC)	2134	4229596	240718	monthly swe
Gin Flat (GFL)	2134	4183363	255739	monthly swe; hourly swe
Peregoy Meadow (PGM)	2134	4172111	268473	monthly swe
Smoky Jack (SMK-SIO)	2182	4188935	261192	distributed snow depth
Paradise Meadow (PDS)	2332	4214396	265710	monthly swe; hourly swe
Huckleberry Lake (HCL)	2377	4220692	259308	monthly swe
Spotted Fawn Lake (SPF)	2377	4219616	258135	monthly swe
Sachse Spring (SAS)	2408	4219048	251182	monthly swe
White Wolf (WHW)	2408	4193540	266732	hourly swe
Wilma Lake (WLW)	2438	4218298	269071	monthly swe
Tenaya Lake (TNY)	2484	4190665	284584	monthly swe; hourly swe
Ostrander Lake (STR)	2499	4168599	274999	monthly swe; hourly swe
Horse Meadow (HRS)	2560	4226695	266766	monthly swe; hourly swe
Olmsted Quarry (OLM-SIO)	2604	4187768	279089	distributed snow depth
Tuolumne Meadow (TUM)	2621	4194327	293307	monthly swe
Snow Flat (SNF)	2652	4189558	280239	monthly swe
New Grace Meadow (NGM)	2713	4225694	270684	monthly swe
Slide Canyon (SLI)	2797	4218724	286737	hourly swe
Bond Pass (BNP)	2835	4228817	270246	monthly swe
Rafferty Meadow (RFM)	2865	4190277	295406	monthly swe
Dana Meadow (DAN)	2987	4196789	301552	monthly swe, hourly swe

[1]See footnote 1 in Table 1.

[2]See footnote 2 in Table 1.

[3]Data type explanations: monthly swe denotes manually measured snow courses, hourly swe indicates a snow-pillow site, and distributed snow depth indicates sites with 4-6 snow depth sensors distributed across an area of approximately 100 meters square.

Table 2-3. Canopy parameters (adapted from Link and Marks, 1999).

Vegetation class	tau (τ)	mu (μ)
Herbaceous, sparse shrub, non-vegetated	1	0
Conifer forest/woodland	0.2	0.040
Mixed conifer and hardwood	0.3	0.033
Hardwood forest/woodland	0.4	0.025

Table 2-4. Base and climate scenario summary snowpack results for the 300-meter elevation band centered at 2850 m in the Merced basin.[1]

Model run	Dry				Wet			
	Peak SWE mm	Peak day	Melt-out day	Melt rate mm d^{-1}	Peak SWE mm	Peak day	Melt-out day	Melt rate mm d^{-1}
Base	645	160	243	6.6	1484	181	307	10.9
RH2	400	107	223	2.6	1248	179	287	10.6
RH4	311	91	188	2.2	722	179	264	7.3
RH6	150	91	110	2.7	317	177	200	9.4
VP2	402	107	225	2.6	1262	179	292	10.3
VP4	312	91	195	2.0	755	179	270	7.2
VP6	151	91	112	2.4	340	177	212	6.9

[1]Day units are number of days since the start of the water year (October 1st). Melt-out day is the first day after peak SWE that snowpack falls below 100 mm SWE. Melt rate is the peak SWE minus 100 mm divided by the number of days between peak SWE and melt-out.

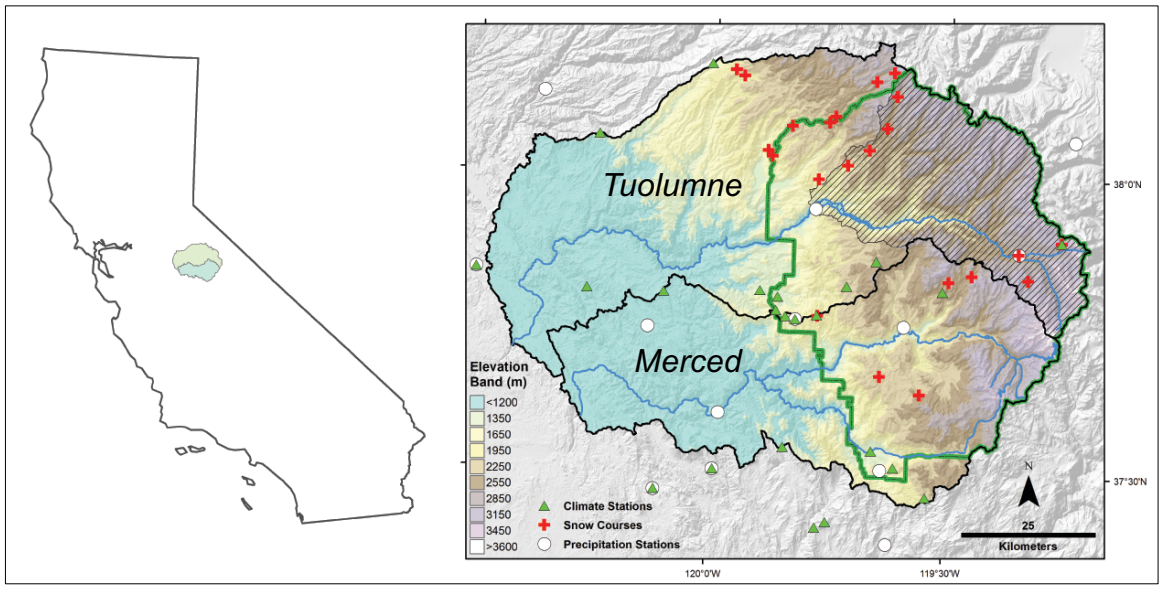

Figure 2-1. Merced and Tuolumne River watersheds in the central Sierra Nevada of California. Climate and precipitation stations used to force model runs are shown, along with snow courses used to evaluate model performance. Yosemite National Park is shown within a green border and diagonal hatching demarks the Hetch Hetchy watershed. The current approximate seasonal "snow zone" exists at elevations above the 1500 m contour.

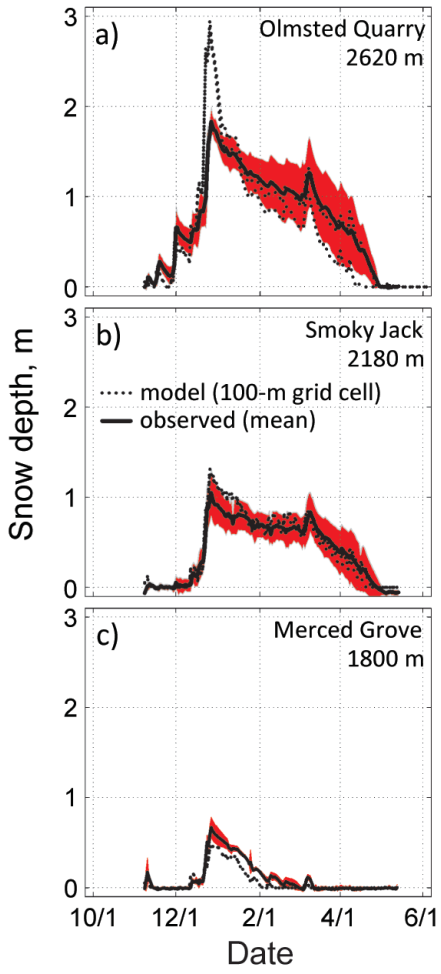

Figure 2-2. Modeled and observed snow depths at three distributed snow depth monitoring locations along an elevational transect for WY2013. Red shading indicates the standard deviation of observations. Each site had 4-6 operational sensors during the period shown. One or more 100-m model grid cells that overlapped sensor locations is depicted separately.

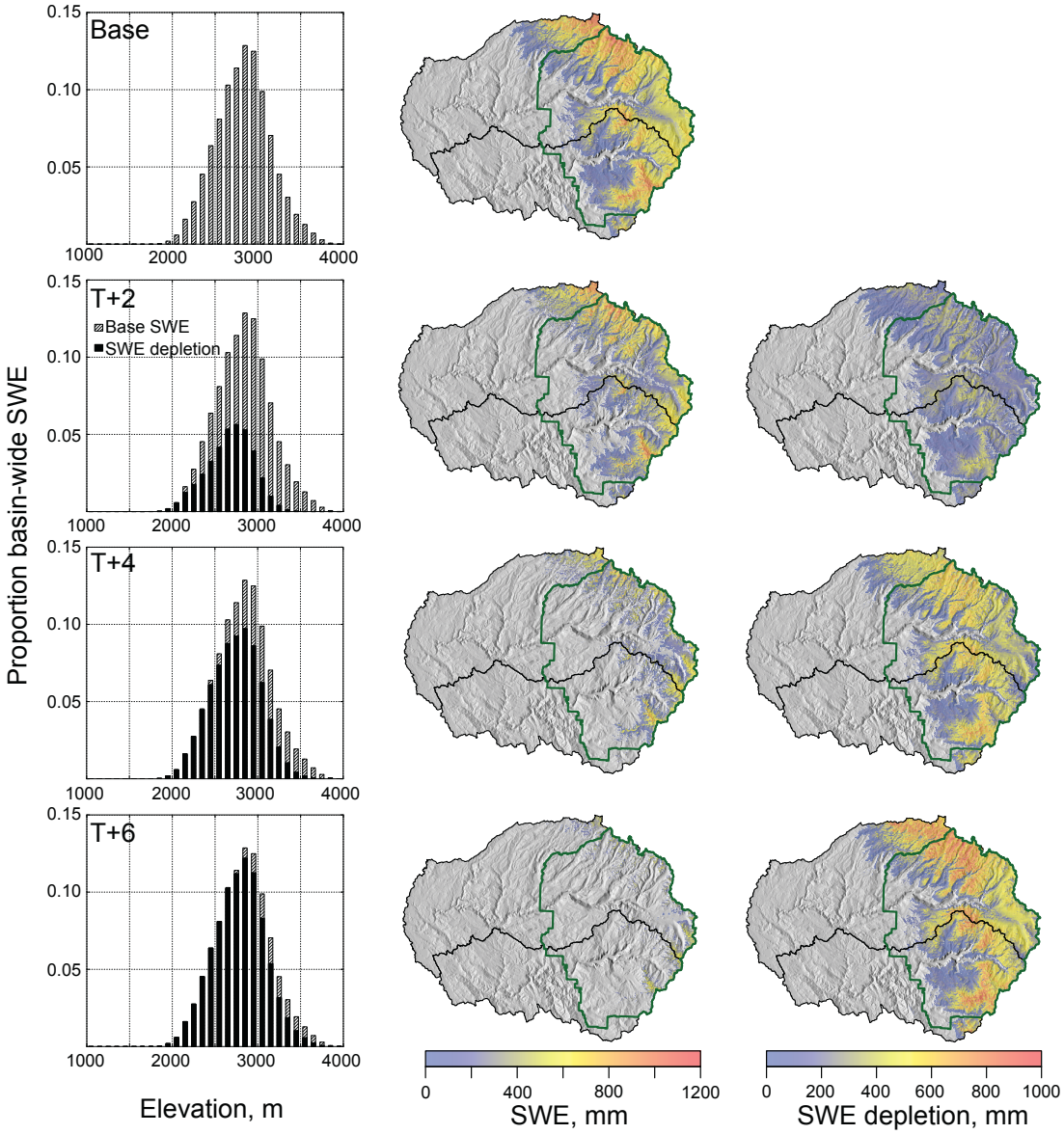

Figure 2-3. Proportion of basin-wide April 1 modeled snow-water-equivalent depletion in constant-relative-humidity temperature increase scenarios for water year 2013 by 100-m elevation band (left), modeled April SWE for each scenario (middle), and spatial absolute SWE depletion (right). Black outlines on watershed maps are the Tuolumne (northern part) and Merced (southern part) watersheds and the green outline is the boundary of Yosemite National Park.

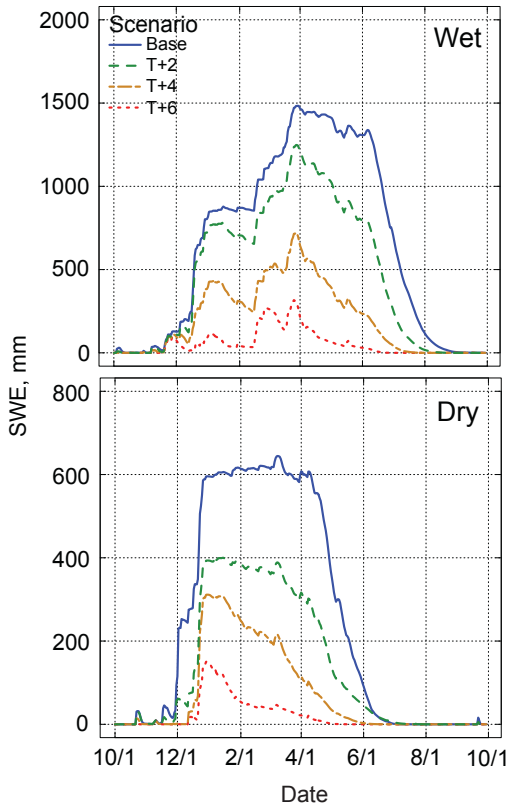

Figure 2-4. Snowpack evolution in the Merced River basin for base modeled wet (WY11) and dry (WY13) years as well as constant relative humidity scenarios (+2, +4, +6°C) for the 2850 m elevation band. Note the different ordinate scales. See Figure S4 in Appendix A for results for other elevation bands.

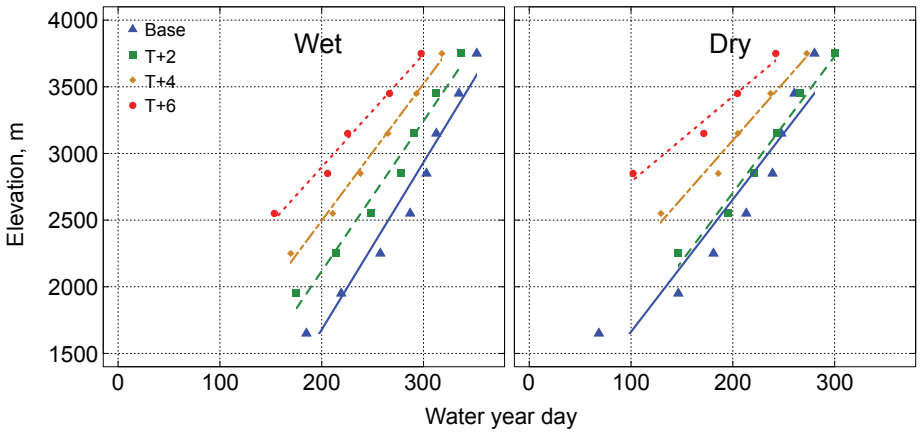

Figure 2-5. Melt-out day (average grid cell value < 100 mm SWE) by 300-m elevation band for base-case wet and dry years and constant-relative humidity warming scenarios in the Tuolumne River basin.

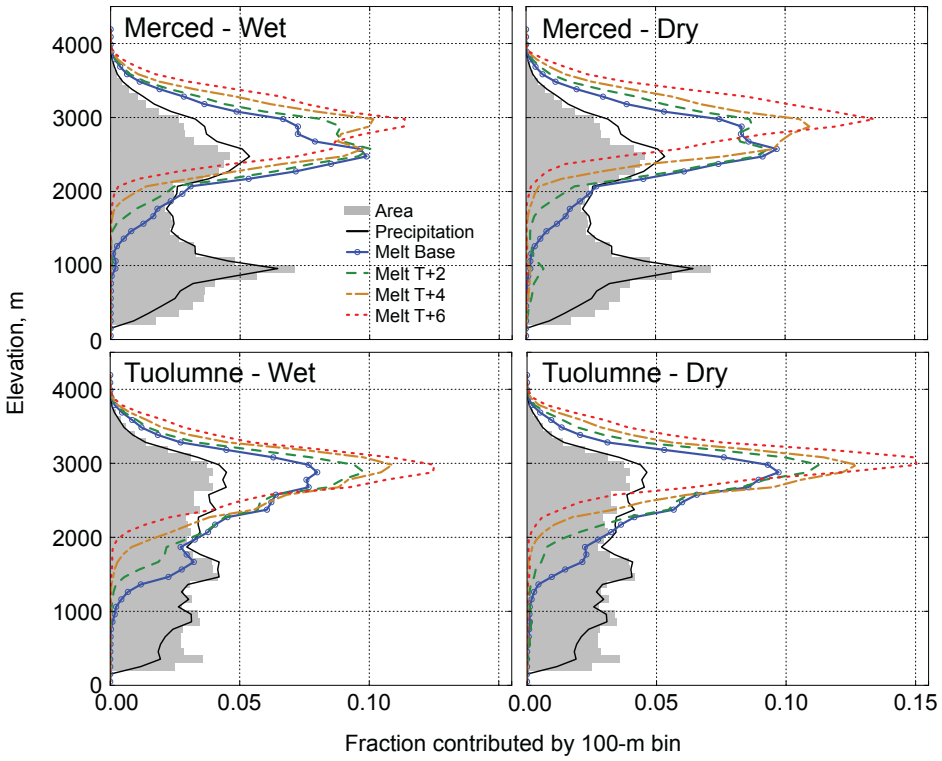

Figure 2-6. Elevational relationship of precipitation (model input) and fractional contribution to basin-wide snowmelt by basin area for base case and constant-relative-humidity temperature increase scenarios.

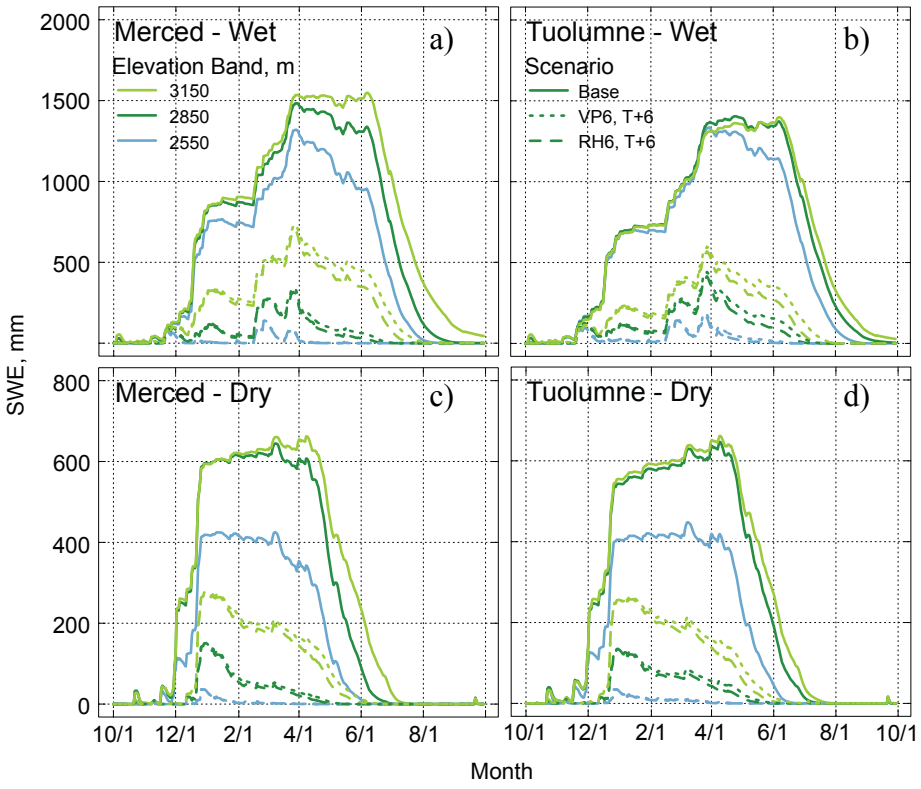

Figure 2-7. Seasonal snowpack progression for 300-m elevation bands that produce the most snowmelt in base (solid lines) and constant-relative-humidity (dashed lines) and constant-vapor-pressure (dotted lines) temperature increase scenarios. Wet and dry year scenarios are shown for the Merced (a, c) and Tuolumne (b, d) watersheds. Note the difference in snow-water-equivalent scales between the wet and dry years. Full results for the Merced basin are shown in Figure A5 in Appendix A.

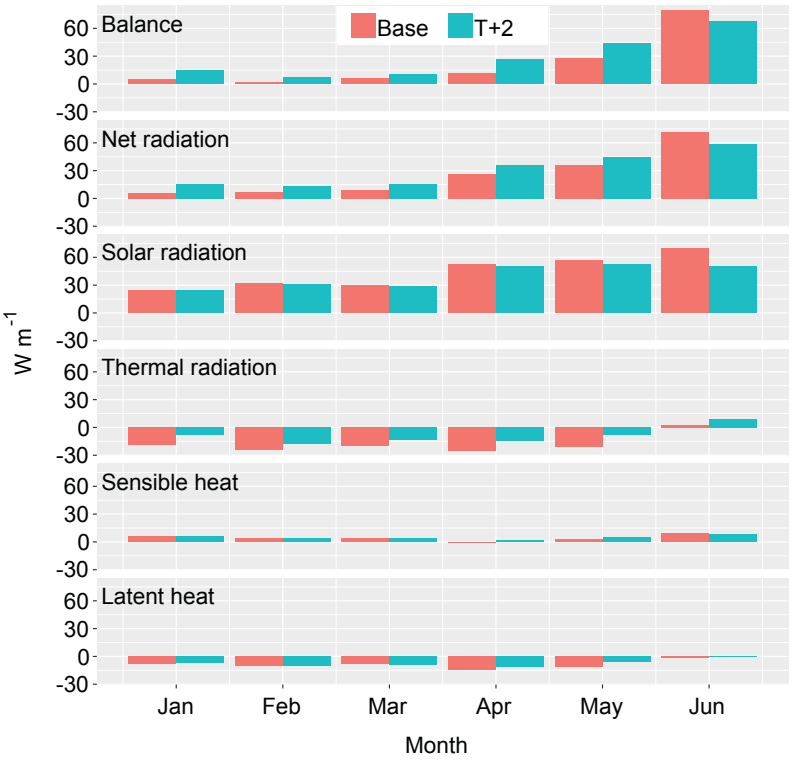

Figure 2-8. Energy balance for the 300-m elevation band centered on 2850 m in the Merced watershed for 2011 (wet base year) and a temperature increase of 2ºC with constant relative humidity (RH2 scenario). Energy components are as follows: snowpack energy balance, net all-wave radiation to the snowpack, net solar radiation, thermal or longwave radiation, sensible, and latent energy (positive toward the snow surface). Net energy to the snowpack in June is less for the RH2 scenario due to reduced net solar radiation to the snowpack.

Chapter 3 Estimating Evapotranspiration Change due to Forest Treatment and Fire at the Basin Scale in the Sierra Nevada, California

James W. Roche[1,2], Michael L. Goulden[3], and Roger C. Bales[2,4]

[1] Yosemite National Park, USDOI National Park Service, El Portal, California

[2]Environmental Systems Graduate Group, University of California, Merced, CA

[3]Department of Earth System Science, University of California, Irvine, California

[4]Sierra Nevada Research Institute, University of California, Merced, Merced, California

Corresponding author: James W. Roche

E-mail: jim_roche@nps.gov

Abstract

We investigated the potential magnitude and duration of forest evapotranspiration (ET) decreases resulting from forest-thinning treatments and fire using a robust empirical relation between Landsat-derived mean-annual normalized difference vegetation index (NDVI) and ET measured at flux towers. Among forest treatments, the minimum observed NDVI change required to produce a significant departure from control plots with NDVI of about 0.70 was -0.07 units, corresponding to a basal-area reduction of 3.1 $m^2\ ha^{-1}$, and equivalent to an estimated ET reduction of 102 mm yr^{-1}. Intensive thinning in highly productive forests that approached pre-fire-exclusion densities reduced basal area by 40-50%, generating estimated ET reductions of 152-216 mm yr^{-1} over five years following treatment. Between 1990 and 2008, fires in American River basin generated more than twice the ET reduction per unit area than those in the Kings River basin, corresponding to greater water and energy limitations in the latter and greater fire severity in the former. A rough extrapolation of these results to the entire American River watershed, much of which would have burned naturally during this 19-year period, could result in ET reductions that approach 10% of full natural flows for drought years and 5% for all years.

Keywords:

Water balance, forest evapotranspiration, forest thinning, forest fire, Sierra Nevada

Introduction

Many western forests are overstocked with live trees, a legacy of successful policies of fire exclusion since the 1920's (Agee & Skinner, 2005; Miller et al., 2012). In areas where fire had previously burned every decade or two, forests transitioned from a mosaic of open areas, and denser and less-dense stands, to areas of continuous canopy cover (Collins et al., 2011; Scholl & Taylor, 2010; Taylor, 2004). This, in turn, has led to increased susceptibility to stand-replacing fires, disease and insect attacks, and increased mortality (Allen, 2007). Implementing a policy of forest thinning using both mechanical treatments and management fire will be essential to managing for ecosystem resilience to climate warming (North et al., 2015), including reduced fire risk and potential changes in water yield (Hopkinson & Battles, 2015; Troendle et al., 2007).

The multi-year California drought that began in fall 2011 highlighted the need to re-examine earlier estimates of the magnitude of water consumption by overstocked forests versus less-dense and healthier forests (e.g. Huff et al., 2000; Kattelmann et al., 1983). There is substantial consensus that forest thinning above a certain threshold reduces evapotranspiration (ET) and increases runoff. Bosch and Hewelet (1982), Stednick (1996), and Brown (2005) demonstrate that changes in density of greater than approximately 20% cause measureable changes the forest water balance. Results such as these have been complicated by limited treatment extent with respect to watershed area at the outlet where runoff is measured. Other challenges included a lack of repeat or follow-up treatments such as underburns to sustain the impact of the initial treatment by limiting understory growth and reducing the seed bank of trees and shrubs. And finally, because

many studies depend on reference watersheds, the adequacy of matched watersheds for this purpose is a substantial source of uncertainty, which makes interpretation of results challenging.

Forest managers and their stakeholders require rigorous estimates of forest benefit before embarking on major forest-thinning projects, and in general these have typically involved estimates of commercial harvest and reduced fire risk to communities and recreational areas. The recent Sierra Nevada Adaptive Management Project (SNAMP) project is a good example of such an endeavor, though limited treatment areas confounded by drought in 2012-2016 limited the conclusions that could be definitively drawn from this research (Fry et al., 2015). Model results extending from this work suggest that runoff in the Central Sierra Nevada could be increased 12% over 20 years with vegetation thinning by 8% and over 50% if fire reduced vegetation by 40% (Conklin et al., 2015; Saksa et al., 2017). A complementary approach to estimating change in forest evapotranspiration is to use remotely sensed information to calculate ET directly (Mu et al., 2011) or indirectly using vegetation indices as they relate to measured ET (Goulden et al., 2012). Relating ET magnitude and its temporal trend to measures of forest change due to fire or mechanical treatment such as leaf area index (LAI), canopy cover, and basal area provides a powerful tool for evaluating ET change at a broad scale (e.g. Vanderhoof & Williams, 2015).

Data-driven remote-sensing measurements of forest evapotranspiration provide a valuable means of quantifying temporal and spatial variability before and following

forest-canopy thinning whether through fire or mechanical thinning. Goulden et al. (2012) demonstrated a tight regression between annual evapotranspiration and annual average of the MODIS satellite-derived normalized differenced vegetation index (NDVI), and that this relationship compared well with mass-balance estimates at the watershed scale (precipitation minus runoff) at an annual resolution. A second important outcome of this work was the demonstration that ET variability is substantially less than precipitation and runoff, arguing that changes in ET are driven largely by changes in vegetation. The method is particularly powerful because it does not require additional parameters such as soil properties and moisture as in many mechanistic models, which are often not available at broad scales. Given that the methods of Goulden et al. (2012) and the subsequent application (Goulden & Bales, 2014) provide a robust means of estimating ET in the Sierra Nevada, we sought to analyze the temporal and spatial variability of ET change in areas of known forest disturbance.

In this paper, we estimated changes in forest water use due to changes in forest density by employing an extension of the previously described work. The work builds on many studies that have shown increases in runoff and/or decreases in ET following forest biomass reduction by estimating ET reductions on a patch basis and then integrating potential impacts to the watershed scale. Specifically, we estimated the magnitude and duration of ET change after forest treatments and fire across a range of elevations and latitude within the Sierra Nevada of California. There were two primary research questions for this study. First, what is the range and variability of NDVI change associated with forest treatments and forest fire in representative watershed areas?

Second, what is the potential range and scale of ET reduction due to forest treatments and forest fires? We conclude with an examination of the research necessary to rigorously extend this analysis to full watershed scale.

Methods

The study area encompasses the central Sierra Nevada, including the lower and wetter American River basin, the drier and colder Kings River basin, and forest treatment areas between these watersheds (Figure 3-1). We examined NDVI change at four forest treatment areas (Figure 3-1a, b, c) as well as in burned and unburned areas over the whole of the American and Kings River watersheds during the 1990-2008 period (Figure 3-1a, d, e). NDVI change, measured using Landsat surface reflectance data, and subsequent calculation of ET were determined using methods described in the following paragraphs.

In order to estimate ET changes at the forest patch scale, we first established a relation between point measurements of evapotranspiration and the remotely sensed NDVI. NDVI maximizes the contrast between strong absorbance of red light by chlorphyll and weaker absorbance of near-infrared light by green vegetation. This index of "greenness" has been shown to be well correlated with in-situ ET measurements using MODIS satellite data (Goulden et al., 2012), a relation that is extended in this paper by making use of the greater spatial-resolution Landsat data. Landsat data offers a 30-m resolution and low image-to-image alignment error (generally less than half a pixel) making it ideal for examining changes in NDVI at the plot scale (1-100 ha) in the case of

forest treatments (Figure 3-1c) and to examine change caused by forest fire, which often impacts forest canopy in a highly heterogeneous way (Figure 3-1e).

Figure 3-2 depicts the primary ET-NDVI relation used in this analysis. Regression data were comprised of water-year annual evapotranspiration (October 1 to September 30) from ten flux towers located in the southern Sierra Nevada and the transverse ranges of California from 2007 to 2016 (see Goulden et al., 2012). Taken together, this data set represents 78 water years (water year is October 1 to September 30). Additionally, points were classified by impacts to the forest patch contributing to each flux tower. A point was classified as drought-affected if the PRISM annual precipitation (PRISM Climate Group, 2012) for the 800 m grid cell encompassing the flux tower was below the 1981-2010 PRISM average for the site. Other classifications pertained to potential changes to the forest structure due to thinning or fire as well as whether this occurred in association with drought conditions (e.g. fire alone and fire with drought). To determine an annual mean NDVI, we used the complete collection of U.S. Geological Survey Landsat Surface Reflectance data (Masek et al., 2006) for the water years of interest following these steps:

1) Determine mean NDVI value in the area of interest for each date. This was accomplished by uploading a Keyhole Markup Language (kml) file of all polygons of interest to a Google fusion file and determining the mean NDVI in Google Earth Engine (Google Earth Engine Team, 2015). Full U.S. Geological Survey Landsat Surface Reflectance collections are available within the Google Earth Engine environment. Specific Landsat tiles were chosen using the World

Wide Reference System 2 for each area of analysis to minimize the influence of different sun and off-nadir angles between images. These were Path 43 and Row 33 for areas in the American River watershed and the Stanislaus-Tuolumne Experimental Forest, and Path 42 and Rows 34 and 35 for the Kings River watershed and Sugar Pine treatment area. Depending on the specific area of analysis, this resulted in approximately 900 available images for analysis of each polygon from 1984 through 2016. NDVI was calculated in the standard way using bands 3 and 4 in Landsat 5 and 7, and bands 4 and 5 from Landsat 8. Pixels were filtered using the Landsat Collection-1 Level-1 Quality-Assessment (QA) Band (CFMask, Foga et al., 2017) removing all pixels with a QA value greater than zero. This filtering removes most pixels containing clouds, cloud shadows, snow, and shadows. NDVI values were further constrained to be between values of 0.2 and 1.0 in order to remove largely unvegetated areas from the analysis.

2) Normalize Landsat Thematic Mapper (Landsat 5 or LT-5) and Landsat Operational Land Imager (Landsat 8 or LC8) values to Landsat Enhanced Thematic Mapper values (Landsat 7 or LE-7) using the following equations (Su et al., in review):

$$NDVI_{Landsat5\_homogenized} = NDVI_{Landsat5} \times 1.1236 - 0.0596$$

$$NDVI_{Landsat8\_homogenized} = NDVI_{Landsat8} \times 0.9938 - 0.0167$$

3) Smooth the resultant time series using a centered moving average spanning five dates.

4) Determine the mid-month value for all months by interpolating between smoothed points

5) Average mid-month values between October 1st and September 30th of the subsequent year to obtain water-year NDVI average values

Smoothing and month-centering reduced the impact of the discontinuous availability of Landsat data due to its 8- and 16-day overpass frequency and substantial excluded data during winter due to clouds and snow. We used a similar process for determining annual NDVI in forest treatment plots and burned areas, as described in the following paragraphs.

We examined select forest treatments spanning the latitudinal range between the American and Kings River basins on the west slope of the Sierra Nevada range (Figure 3-1a, b). Forest-treatment data available for this study from north to south were from the Sierra Nevada Adaptive Management Project (SNAMP) Last Chance fireshed treatment area, select treatment compartments from the Blodgett Experimental Forest, the variable density thinning project at the Stanislaus-Tuolumne Experimental Forest (Figure 3-1b, c), and the SNAMP Sugar Pine fireshed treatment area. Treatments in these forests were well documented and represent a range of treatment intensity (Table 3-1). The portion of

Last Chance treatments burned by the 2013 American fire was excluded from analysis. For each treatment, we estimated the change in NDVI by averaging the five years prior to treatment and comparing this to the five years post treatment for both treated and control units. The significance of the observed change was determined using the before-after-control-impact (BACI) assessment (Stewart-Oaten et al., 1986) as applied by Fry et al, 2015. Specifically, this entailed a two-way ANOVA on treated and control plots before and after treatment with change detection determined by the interaction between treatment type and before after classification at alpha=0.05 (Smith, 2002). Change detection on control plots before and after treatment was determined using a two-sample paired t-test. In order to characterize the general climate for the region, we calculated mean water-year precipitation and temperature using monthly 4-km resolution PRISM data (PRISM Climate Group, 2012). The averaging area covered the full latitude range of our study sites and included the American, Mokelumne, Stanislaus, Tuolumne, Merced, San Joaquin, and Kings watersheds above their respective Sierra-foothill dams.

We examined the role of fire on ET change by using fire-severity data and estimated changes in canopy cover and basal area from the USFS Monitoring Trends in Burn Severity (MTBS, Eidenshink et al., 2007) and Miller et al. (2009) geodatabases (http://www.mtbs.gov/, https://www.fs.usda.gov/detail/r5/landmanagement/gis/?cid=STELPRDB5327833), respectively. We selected all forest fires in the American and Kings watersheds between 1990 and 2008, excluding those fires at lower elevations in largely unforested areas of the watersheds. The date range chosen included at least five years of baseline NDVI data

prior to the first fire (the earliest full annual Landsat Thematic Mapper data are available starting in 1985) and five years after the last fire (2013), and avoided the extreme forest mortality of the California drought (2012-2015) and associated very large fires (the American (2013) and Rough (2015)) in these watersheds. In order to examine effects by severity, we used 1-year post-fire severity classification polygons from the MTBS database directly and applied an area-weighted mean of severity classes to determine average NDVI-change within an individual fire perimeter.

In order to investigate the role of elevation on NDVI change after fire, we required better-defined elevations within the fire perimeter. To do this, we created a 90-m mesh over each fire area assigning each 90-m square polygon an elevation based on the 30-m Shuttle Radar Topography Mission elevation dataset (Farr et al., 2007). The mesh was created within a buffer of 75 meters inside the fire perimeter to avoid sampling of unburned areas (Figure 3-1d). Additionally, we created a set of randomly selected 90-m polygons in areas that remained unburned between 1990 and 2008 that accounted for approximately 20% of each watershed area. Annual NDVI values were determined for all polygons for the period 1985-2013 and burned area polygons records were summarized as 5-year pre-fire mean NDVI, 1-year post-fire NDVI, and 5-year post-fire mean NDVI. The water year of the fire was excluded from analysis because mean annual NDVI could include both burned and unburned conditions. We chose to characterize fire severity using the one-year post-fire classification rather than the immediate post-fire classification to better capture fire effects on vegetation including delayed fire-caused mortality (Miller & Thode, 2007). Each burned polygon was additionally attributed with

an area-weighted estimate of basal-area and canopy-cover change from Miller et al. (2009).

The magnitude and trend of ET change was estimated for fire and forest treatment areas using the regression equation in Figure 3-2. To account for post-fire interannual variability, we used the following equation:

$$\Delta ET = (ET_{postfire_{burned}} - ET_{postfire_{unburned}}) - (ET_{prefire\_burned} - ET_{prefire\_unburned}) \quad (1)$$

where ET in unburned areas was determined as the mean of all unburned polygons in the watershed within 250 m in elevation of the target burned polygon. In this way, ET change was calculated for each water year and then averaged for subsequent analysis. In order to estimate post-impact ET, we subtracted ET change determined using the above equation from a 5-year average of pre-disturbance ET. Finally, we estimated the cumulative ET reduction for fires where ΔET recovered to a zero or positive value or to the end of the available record (water year 2016) if fires were recent. Change in ET for all burned areas was averaged each year in order to estimate the influence of forest fire on basin-wide ET with respect to mean annual runoff.

Results

Forest Treatments. At Blodgett Forest, two intensively thinned compartments (basal-area reductions of 68 and 45%) yielded NDVI changes that were readily evident

(Figure 3a); however, the statistical significance of these changes could not be evaluated due to the small sample size. Moderate thinning (change in basal area = 27%) at Blodgett resulted in an NDVI change that barely exceeded the standard deviation of control plots and was non-significant at the alpha = 0.05 level (Table 3-1).

The highly productive STEF sites exhibited an obvious and statistically significant change in NDVI accompanying basal-area reductions of 41-46% across all treatments, except on those plots treated with only an underburn (Figures 3-2b and 3-3b). Control plots with an underburn treatment changed less than did control plots that received no treatment, associated with a difference in the change in basal area of +5% for control-only versus +0.6% for control-plus-underburn plots. It should also be noted that all STEF plots exhibited a drop in NDVI during an extended period of lower-than-average precipitation in the late 1980's and early 1990's that was similar in magnitude to that observed in the treatment plots.

Among the SNAMP treatment areas, only tractor-thin treatments in Last Chance basin (a decrease in basal area of 9%) exhibited a significant change in NDVI between 2008 and 2013 (Figure 3-3c and 3-3d). Despite larger decreases in basal area in the Sugar Pine basin (11 and 15%, respectively), there were no apparent changes in NDVI. There was no change in NDVI associated with negligible changes in basal area resulting from controlled burns. It should be noted that mastication treatments at Last Chance may have been treated as early as 2008 as seen in Figure 3-3d, though had mostly recovered by 2013 and, hence did not result in a significant change. Though beyond the scope of this

study, most areas exhibited pronounced changes in NDVI in 2015 and 2016, presumably due to lower than average precipitation and higher temperatures over the period 2012-2015 (Figure 3-3e,f).

Forest Fire. Figure 3-4a depicts a typical forest-fire NDVI time-series and Figure 3-4b shows change in NDVI distribution before the fire and during recovery for both burned and adjacent unburned areas. Areas with a burn severity classified as low or none changed little, which is probably the result of low initial vegetation density that included areas of bare rock and soil. Similarly, the broader NDVI distribution and smaller median value of unburned versus pre-fire areas (Figure 3-4b) indicates more heterogeneous and lower forest densities outside of the burned area. The overall change in NDVI of approximately 0.13 units in the first year following the fire corresponded with a change in basal area of 51% over the area of the Choke fire (Table 3-2). Decreased NDVI persisted for over 10 years across much of the fire area. As with the forest-treatment data, substantial drought effects were apparent in 2015-2016.

Figure 3-5 illustrates NDVI and ET elevational variability in burned and unburned areas during the 1990-2008 period. Burned area NDVI was broken into mean NDVI five years prior to the year of the fire, one year post-fire, and mean NDVI over the five years following fire for all fires that occurred in each elevation band. Pre-fire area NDVI followed a similar elevation trend to unburned areas, though it was substantially higher than unburned areas below 500 m in the American. Fire shifted one-year post-fire NDVI means by 0.2 units or more at elevations below 2000 m. The shift was less

dramatic at higher elevations in the Kings. Note that there were no large fires above 2000 m in the American between 1990-2008. NDVI recovery was greatest below 2000 m in the Kings and below 1000 m in the American.

ET change due to forest fire was estimated to be substantial in both watersheds. Pre-fire annual ET values averaged 680 mm and 510 mm between the 1000-2000 m elevations in the American and Kings, respectively (Figure 3-6a). ET peaked at around 660 mm at the 100-m elevation band centered at 1450 m in the Kings and declined to about 440 mm near 2700 m (18 mm per 100 m) and then dropped below 300 mm at 2900 m and above. This pattern corresponds to energy limitation and thus lower vegetation density at higher elevations (Goulden & Bales, 2014). In the American, pre-fire annual ET peaked close to 830 mm at the 950-m elevation band and declined to near 560 mm at 2150 m (22 mm per 100 m). While there is substantial area above 2000 m elevation in the American, no fires over 100 ha occurred in this elevation range during the study period.

ET reduction due to forest fire was greater per unit reduction in basal area in the American than the Kings at a given elevation (Figure 3-6a, c) and persisted for longer periods in the American than in the Kings (Figure 3-6b, d). High basal-area reduction (75-100%), which corresponds with high-severity fire, resulted in a decrease in ET of 320-440 mm yr^{-1} in the 1000-2000 m elevation range of the American compared to 200-310 mm yr^{-1} in the Kings. This difference was substantially less for respective 25-50% basal area reduction (190-260 mm yr^{-1} versus 100-190 mm yr^{-1}). Differences were smaller when compared to unburned areas of the watershed. Overall, the mean 5-year

post-fire ET reduction was 265 mm in the American and 113 mm in the Kings. Recovery following fire appeared to take about 9 years post-fire for basal-area reduction of 0-25% in the American versus 3 years for the Kings. Areas experiencing 75-100% basal-area reduction recovered at 17 and 9 mm yr^{-1} in the Kings and American basins, respectively.

Finally, the net ET reduction in burned areas from all timber fires in the 1990-2008 period in the American was about double that in the Kings River basin (210 vs. 100 mm ha^{-1}). Expressed as a volume per year, the maximum estimated net ET reduction was 65 million m^3 yr^{-1} in the American versus 14 million m^3 yr^{-1} in the Kings in 2009 (Figure 3-7). It is important to note that these values peak in 2009, the year after the last fire in the analysis, and would continue to climb if subsequent fires were included.

Discussion

NDVI vs. ET. The NDVI-ET relation shown in Figure 3-2 appears to be sensitive to drought, while changes due to forest disturbance such as fire and management (thinning) are less clear. Measurements associated with drought, including fire/drought, and management/drought appear to plot slightly lower than the regression line, similar to observations with MODIS data (Goulden et al., 2012). Points associated with just fire or management appear to exhibit a similar relation, though presently there are too few observations to fully describe this impact. Management and fire-impacted areas that were also associated with drought appeared to track more closely with other drought-affected measurements. In summary, the fundamental relation used in this study appears to be

robust to changes wrought by forest disturbance, especially considering that half of the observations (39 of 78) used in construction of the regression were affected by drought or forest disturbance.

Forest Disturbance. Changes in NDVI and thus ET of Sierra conifer forests following thinning or fire were observed to be consistent with changes in forest density indicated by basal area and canopy cover. The small NDVI change of 0.07 units was detectable for tractor thinning at Last Chance, but thinning of a similar or larger magnitude at Sugar Pine yielded no significant NDVI change, likely the result of canopy retention greater than 60% in adherence with the Pacific fisher conservation strategy (Fry et al., 2015). Mastication treatments at Last Chance may have produced significant changes in NDVI had they occurred in 2008 as suggested by Figure 3-3d. However, information about the timing of those treatments was lacking and by 2013 there was no longer a significant different from prior to 2008.

The duration of NDVI change following treatment lasted longer for both more-intensively thinned areas (Blodgett) as well as those treatments that were subsequently burned after thinning (STEF). While, measured basal area and canopy cover appeared to be correlated with annual mean NDVI for the year of measurement in treated and control areas, the additional data and analyses required to elucidate these relations were beyond the scope of the study. Specifically, more information is needed about the nature of thinning (e.g. thin from below or above, canopy retention or removal, etc.) as it relates to

NDVI change in order to more rigorously estimate impacts of treatment with respect to change in ET.

The magnitude and duration of NDVI change due to forest fire varied substantially by elevation and watershed, however the maximum change was in the 1000-2000 m range in both. Unburned conifer forests in the American and Kings watersheds exhibited peak NDVI at 1050 m (0.71 ± 0.09) and 1650 m (0.61 ± 0.09), respectively. Pre-fire NDVI during 1985-2013 tracked the unburned-forest elevation trend in each watershed, while post-fire NDVI below 2000 m dropped approximately 0.1-0.2 units below that of unburned forests after one year. Mean NDVI recovery over 5 years post-fire was 0.06 units in both watersheds. Due in part to the limited number of fires at high elevations, NDVI change following fire was minimal above 2700 m in the Kings (no fires occurred above 2000 m in the American during the study period).

Areas that burned in the American River watershed exhibited a greater reduction in estimated ET per proportional reduction in basal area than in the Kings. At 1000 m in the American, annual ET decreased nearly 320 mm with a 50% decrease in basal area, compared to around 200 mm in the Kings. This difference between the watersheds was roughly consistent between 1000 and 2000 m. Differences between pre-fire and post-fire 5-year ET means remained roughly consistent for the entire range of elevations burned during the study period in the American (1990-2008), which is a somewhat surprising result. Below 2000 m, one would expect little energy limitation to ET and so the decline in ET from 1000 to 2000 m must be driven by a decreasing forest density. However, a

decrease in basal area of 75-100% reduced ET about 400 mm at 1000 m, which diminishes to 300 mm at 2000 m, suggesting that more rapid recovery rates at lower elevations may offset the expect difference (results not shown). In contrast, the small differences between pre- and post-fire ET above 2700 m in the Kings indicates increasing energy limitation and low vegetation density.

Tracking overall changes in basin-wide ET due to forest fire revealed interesting temporal trends. First, on a per unit area burned basis, ET reduction in the American basin was approximately double that of the Kings after 2008, consistent with the 5-year post-fire estimates (Figure 3-7a). Coupling this with the fact that 1.8 times more area burned in the American watershed than in the Kings (36,824 vs. 19,088 ha), net ET reduction due to fires between 1990-2008 peaked in the American at over four times that of the Kings (Figure 3-7b; 65 vs. 14 million m^3 yr^{-1}). Given that the area burned was only 11 and 9% of the conifer forest in the American and Kings watersheds, respectively, one could anticipate much greater ET reduction if fires burned more closely to the expected fire return interval for forested areas. For example, almost all of the American River forests have a historical mean fire return interval of less than 20 years (Safford & Van de Water, 2013), which is far more frequent that actual fire return interval of 85 years. Hence, during the 1990-2008 period, all forests would have burned historically, potentially resulting in nearly 10 times the net annual ET reduction, or 650 million m^3 yr^{-1}. This amount is greater than 10% of the mean annual unimpaired runoff from the basin during the 1992 and 1994 drought years, and on average 5.4% for the 1990-2008 period (California Department of Water Resources, 2016). In contrast, only 43% of forests in the

Kings have mean historic fire return intervals of less than 20 years, which is five times what burned in 1990-2008, and had this area burned it could have resulted in an ET reduction of 4.5% of the unimpaired runoff.

An important caveat to the above analysis is that most of the ET reduction in the American was driven by large 7000-8000 ha fires in 1992 (Cleveland), 2001 (Gap, Ponderosa, and Star), and 2008 (Government). All of these fires except the Government Fire contained large areas of high-severity burn, and over half of the fire area during the period 1990-2008 burned at high severity (compared to only 9% in the Kings watershed). While this is undesirable for ecological as well as human health and safety reasons, we estimate that shifting the high-severity burn class (>75% reduction in basal area) to moderate severity (25-75%), perhaps better reflecting historically less dense forests that burned at lower intensities, would only decrease estimated ET reduction by 20%.

Limitations to current work and opportunities for future research. The key limitation to this work is the lack of readily available and high-quality forest-treatment data that span the range of forest types, treatments, and/or climate zones of the Sierra Nevada. The four data sets obtained for this study demonstrate the potential for relating remote sensing of NDVI or other vegetation indices with accurate assessments of forest density, and subsequently, the potential to scale these observations to full watershed treatment potential. Obtaining a larger dataset was beyond the scope the present work. While the US Forest Service Activity Tracking System (FACTS) database is a starting point, much additional work will be required to obtain exact treatment dates as well as

pre- and post- treatment forest-density metrics. Data for forest fires, on the other hand, are much more complete and available, providing a solid basis for future analyses of this type. Indeed, given that approximately 75% of the forested landscape in the Sierra Nevada may be treated only by fire (North et al., 2015), it will be critical to estimate the further effects of more-extensive managed fire on evapotranspiration.

Estimating the full impact of forest treatments on evapotranspiration, whether fire or mechanical, may be estimated by the following heuristic equation:

$$\text{Cumulative ET reduction} = \text{Area treated} \times \text{Initial ET change} \times \text{Effective duration of the change}$$

Using the examples of Figures 3-3 and 3-4, we see that beyond a certain threshold of thinning, the duration of NDVI change is likely to be the most-sensitive parameter for estimating integrated change in ET. Area is generally known to within a few percent and the initial change should be easy to estimate if the treatment date is known. The subsequent forest recovery and evolution of NDVI depends on follow-up treatments, the intensity of the initial treatment, ensuing climate, forest type, and potential other factors such as bug kill. In the case of the Choke fire in Figure 3-4, NDVI recovered nearly 50% of its original value within 3-4 years of the fire, though full recovery took approximately 10 years. Hence, the effective duration of the initial change was five years. Integrating forest change as was done in Figure 3-7 for future treatment and managed fire scenarios could be a valuable component of funding justification for watershed restoration projects.

Research questions stimulated by this initial investigation may be grouped into three primary areas. First, there is a need to further evaluate factors affecting the relation between NDVI or remotely sensed indices and ET at measurement locations. This may include examining the impact of seasonal and inter-annual temperature and precipitation patterns on the correlation and the sensitivity of the correlation to changes in forest density or the nature of thinning. Second, in order to scale measures of forest density with observed NDVI across the region, we require better estimates of recovery rate and how this varies by treatment type and intensity as well as elevation, latitude, and climate. Third, having refined our understanding of the foregoing processes, there exists the potential to predict forest response to treatments and disturbance, particularly in areas where there has been a fundamental shift in vegetation type due to disturbance and climate change. Potential areas of investigation include estimating ET and CO_2 variation during forest succession following disturbance and, using space-for-time substitution, predicting forest trajectories under different climate regimes with associated management implications.

Central to the utility of methods introduced here is the assumption that forest disturbance and resulting changes in NDVI translate to changes in ET of similar magnitude to those observed at flux tower sites. Ongoing observations and drought-induced forest mortality at these and other sites suggest that this may be the case (Figure 3-2; Bales et al., submitted). Also, as noted in Figure 2 of Goulden et al. (2012), drought years do tend to reduce ET for a given NDVI level, which would need to be accounted

for in future analyses. Finally, it is evident in Figure 3-2 that the regression underestimates ET in higher productivity forests, which tend also to be those forests of highest management concern due to over-stocking and fire risk, as well as species recovery. These middle-elevation mixed-conifer forests are also where forest thinning may have the greatest impact on ET. Changes in the ET-NDVI relation due to forest fire and forest management will require better experimental data, particularly as forest densities recover to pre-suppression-era densities, with fewer and larger trees.

Conclusions

There are many potential benefits to reducing forest overstocking that has occurred during the era of fire exclusion over the past century, including the potential ET reductions explored in this paper. Here, we have identified that for NDVI values around 0.7, changes of 0.2-0.3 units can occur in high-fire-severity burn areas, corresponding to declines in ET from 800 to 280-450 mm yr^{-1}. The potential for NDVI and thus ET changes peaks in middle elevations around 1000-2000 m where NDVI and ET also peak. Estimated ET reductions due to forest treatment ranged from 102 mm at the minimum detection limit for NDVI change (0.07 units) to over 300 mm in the intensive thinning units in the Blodgett Forest. Intensive thinning in Blodgett and the Stanislaus-Tuolumne Experimental Forests was similar in magnitude to moderate- and high-severity fire, particularly in the American River basin. Returning fire to areas that once burned frequently has the potential to reduce forest ET by approximately 5% of full natural outflows from the American and Kings River watersheds. Finally, in order to predict ET

change due to forest treatment and managed fire will require an improved understanding of the climate and vegetation factors that affect the relation between remotely sensed vegetation indices and measured ET over the range of elevation, latitude, and vegetation types in mountain forests.

References

Agee, J. K., & Skinner, C. N. (2005). Basic principles of forest fuel reduction treatments. *Forest Ecology and Management*, *211*(1–2), 83–96. doi: 10.1016/j.foreco.2005.01.034

Allen, C. D. (2007). Interactions across spatial scales among forest dieback, fire, and erosion in northern New Mexico landscapes. *Ecosystems*, *10*(5), 797–808. doi: 10.1007/s10021-007-9057-4

Bosch, J. M., & Hewlett, J. D. (1982). A review of catchment experiments to determine the effect of vegetation changes on water yield and evapotranspiration. *Journal of Hydrology*, *55*(1–4), 3–23. doi: 10.1016/0022-1694(82)90117-2

Brown, A. E., Zhang, L., McMahon, T. A., Western, A. W., & Vertessy, R. A. (2005). A review of paired catchment studies for determining changes in water yield resulting from alterations in vegetation. *Journal of Hydrology*, *310*(1–4), 28–61. doi: 10.1016/j.jhydrol.2004.12.010

California Department of Water Resources. (2016). Estimates of Natural and Unimpaired Flows for the Central Valley of California: Water Years 1922-2014. (pp. 256). Retrieved from https://msb.water.ca.gov/documents/86728/a702a57f-ae7a-41a3-8bff-722e144059d6

Collins, B. M., Everett, R., & Stephens, S. L. (2011). Impacts of fire exclusion and recent managed fire on forest structure in old growth Sierra Nevada mixed-conifer forests. *Ecosphere*, *2*(4), 14. doi: 10.1890/ES11-00026.1

Conklin, M. H., Bales, R. C., Saksa, P. C., Martin, S. E., & Ray, R. (2015). Appendix E: Water Team Final Report. (pp. 104). *Learning how to apply adaptive management in Sierra Nevada forests: An integrated assessment. Final report of the Sierra Nevada Adaptive Management Project (P. Hopkinson and J.J. Battles, eds.)*. Berkeley, CA.

Eidenshink, J., Schwind, B., Brewer, K., Zhu, Z.-L., Quayle, B., & Howard, S. (2007). A Project for Monitoring Trends in Burn Severity. *Fire Ecology Special Issue*, *3*(1). Retrieved from http://www.mtbs.gov/files/articles/Eidenshink final.pdf

Farr, T. G., Rosen, P. A., Caro, E., Crippen, R., Duren, R., Hensley, S., … Alsdorf, D. E. (2007). The shuttle radar topography mission. *Reviews of Geophysics*, *45*(2), 1–33. doi: 10.1029/2005RG000183

Foga, S., Scaramuzza, P. L., Guo, S., Zhu, Z., Jr, R. D. D., Beckmann, T., … Laue, B. (2017). Cloud detection algorithm comparison and validation for operational Landsat data products. *Remote Sensing of Environment*, *194*, 379–390. doi: //doi.org/10.1016/j.rse.2017.03.026

Fry, D. L., Battles, J. J., Collins, B. M., & Stephens, S. L. (2015). Appendix A: Fire and Forest Ecosystem Health Team Final Report. . *Learning how to apply adaptive management in Sierra Nevada forests: An integrated assessment. Final report of the Sierra Nevada Adaptive Management Project (P. Hopkinson and J.J. Battles, eds.)*. Berkeley, CA.

Google Earth Engine Team. (2015). Google Earth Engine: A planetary-scale geospatial analysis platform. Retrieved from https://earthengine.google.com

Goulden, M. L., Anderson, R. G., Bales, R. C., Kelly, A. E., Meadows, M., & Winston, G. C. (2012). Evapotranspiration along an elevation gradient in California's Sierra Nevada. *Journal of Geophysical Research: Biogeosciences*, *117*(G3). doi: 10.1029/2012JG002027

Goulden, M. L., & Bales, R. C. (2014). Mountain runoff vulnerability to increased evapotranspiration with vegetation expansion. *Proceedings of the National Academy of Sciences*, *111*(39), 14071–14075. doi: 10.1073/pnas.1319316111

Hopkinson, P., & Battles, J. J. (2015). Learning how to apply adaptive management in Sierra Nevada forests: An integrated assessment. Final report of the Sierra Nevada Adaptive Management Project. . Berkeley, CA. Retrieved from http://snamp.cnr.berkeley.edu/snamp-final-report/

Huff, D. D., Hargrove, B., Tharp, M. L., & Graham, R. (2000). Managing Forests for Water Yield: The Importance of Scale. *Journal of Forestry*, *98*(12), 15–19.

Kattelmann, R. C., Berg, N. H., & Rector, J. (1983). The Potential for Increasing Streamflow from Sierra Nevada Watersheds. *JAWRA Journal of the American Water Resources Association*, *19*(3), 395–402. doi: 10.1111/j.1752-1688.1983.tb04596.x

Masek, J. G., Vermote, E. F., Saleous, N. E., Wolfe, R., Hall, F. G., Huemmrich, K. F., … Lim, T.-K. (2006). A Landsat surface reflectance dataset for North America, 1990-2000. *IEEE Geoscience and Remote Sensing Letters*, *3*(1), 68–72. doi: 10.1109/LGRS.2005.857030

Miller, J. D., Collins, B. M., Lutz, J. A., Stephens, S. L., van Wagtendonk, J. W., & Yasuda, D. A. (2012). Differences in wildfires among ecoregions and land management agencies in the Sierra Nevada region, California, USA. *Ecosphere*, *3*(9), 1–20. doi: 10.1890/ES12-00158.1

Miller, J. D., Knapp, E. E., Key, C. H., Skinner, C. N., Isbell, C. J., Creasy, R. M., & Sherlock, J. W. (2009). Calibration and validation of the relative differenced Normalized Burn Ratio (RdNBR) to three measures of fire severity in the Sierra Nevada and Klamath Mountains, California, USA. *Remote Sensing of Environment*, *113*(3), 645–656. doi: 10.1016/j.rse.2008.11.009

Miller, J. D., & Thode, A. E. (2007). Quantifying burn severity in a heterogeneous landscape with a relative version of the delta Normalized Burn Ratio (dNBR). *Remote Sensing of Environment*, *109*(1), 66–80. doi: 10.1016/j.rse.2006.12.006

Mu, Q., Zhao, M., & Running, S. W. (2011). Improvements to a MODIS global terrestrial evapotranspiration algorithm. *Remote Sensing of Environment*, *115*(8), 1781–1800. doi: 10.1016/j.rse.2011.02.019

North, M. P., Brough, A., Long, J., Collins, B., Bowden, P., Yasuda, D., … Sugihara, N. (2015). Constraints on mechanized treatment significantly limit mechanical fuels reduction extent in the Sierra Nevada. *Journal of Forestry*, *113*(1), 40–48. doi: 10.5849/jof.14-058

North, M. P., Stephens, S. L., Collins, B. M., Agee, J. K., Aplet, G., Franklin, J. F., & Fulé, P. Z. (2015). Reform forest fire management. *Science*, *349*(6254), 1280–1281. doi: 10.1126/science.aab2356

PRISM Climate Group (Oregon State University). (2012). United States Average Annual Precipitation, 1981-2010.

Safford, H. D. & Van de Water, K. M. (2013). Using Fire Return Interval Departure (FRID) analysis to map spatial and temporal changes in fire frequency on National Forest lands in California. (pp. 1-59). *Pacific Southwest Research Station - Research Paper PSW-RP-266*. Retrieved from http://www.fs.fed.us/psw/publications/documents/psw_rp266/psw_rp266.pdf

Saksa, P.C., Conklin, M.H., Battles, J.J., Tague, C.L. and Bales, R.C. (2017). Forest thinning impacts on the water balance of Sierra Nevada mixed conifer headwater basins. *Water Resources Researc*h, 53. doi: 10.1002/2016WR019240

Scholl, A. E., & Taylor, A. H. (2010). Fire regimes, forest change, and self-organization in an old-growth mixed-conifer forest, Yosemite National Park, USA. *Ecological Applications*, *20*(2), 362–380. doi: 10.1890/08-2324.1

Smith, E. P. (2002). BACI Design. In *Encyclopedia of Environmetrics* (Vol. 1, pp. 141–148). doi: 10.1002/9780470057339.vab001.pub2

Stednick, J. D. (1996). Monitoring the effects of timber harvest on annual water yield. *Journal of Hydrology*, *176*(1–4), 79–95. doi: 10.1016/0022-1694(95)02780-7

Stewart-Oaten, A., Murdoch, W. W., & Parker, K. R. (1986). Environmental Impact Assessment: "Pseudoreplication" in Time? *Ecology*, *67*(674), 929–940. doi: 10.2307/1939815

Taylor, A. H. (2004). Identifying forest reference conditions on early cut-over lands, Lake Tahoe Basin, USA. *Ecological Applications*, *14*(6), 1903–1920. doi: 10.1890/02-5257

Troendle, C. A., Nankervis, J. M., & Peavy, A. (2007). The Herger-Feinstein Quincy Library Group Project - Impacts of Vegetation Management on Water Yield. (pp. 23).

Vanderhoof, M. K., & Williams, C. A. (2015). Persistence of MODIS evapotranspiration impacts from mountain pine beetle outbreaks in lodgepole pine forests, south-central rocky mountains. *Agricultural and Forest Meteorology*, *200*, 78–91. doi: 10.1016/j.agrformet.2014.09.015

Table 3-1. Summary forest treatment data

Name	Treatment type (number of units)	Year of treatment	Basal area, m^2 ha^{-1} ± std. dev.		Canopy cover, %		NDVI change[1]	ET change, mm yr^{-1}
			before	after	before	after		
Last Chance[2]	Control (294)	NA	39.8 ± 16.9	42.1 ± 17.3	60.7 ± 16.8	56.8 ± 17.5	**-0.021**	+23
	Mastication (19)	2008-2013	28.3 ± 8.5	26.2 ± 7.1	45.5 ± 7.9	37.3 ± 7.8	-0.026	-42
	Tractor thin (6)	2008-2013	33.6 ± 5.5	30.5 ± 4.4	49.9 ± 3.0	39.1 ±3.8	**-0.068**	-102
	Underburn (2)	2008-2013	34.3	34.3	59.9	54.8	+0.021	-1
Blodgett[3]	Control (6) (before: 2001-2004) (after: 2014)	NA	73.8 ± 9.6	81.14 ± 9.8	77.2 ± 5.1	74.9 ± 3.5	+0.032	+74
	Moderate thin (6)	2005-2011	49.1 ± 4.0	35.9 ± 2.3	68.6 ± 3.6	58.6 ± 3.4	-0.0065	+1.4
	Intensive thin (1)	1998	58.9	19.1	-	29.1	-0.18	-306
	Intensive thin (1)	2008	44.1	24.3	69.1	45.1	-0.11	-216
STEF[4]	Control, unburned (4)	NA	63.8 ± 8.6	67.0 ± 9.1		65.1 ± 4.0	**+0.040**	+72
	Even thin, unburned (4)	2011	65.0 ± 11.8	35.9 ± 6.6		40.5 ± 2.5	**-0.088**	-152
	Variable thin, unburned (4)	2011	71.3 ± 6.2	38.4 ± 4.0		35.0 ± 2.2	**-0.11**	-197
	Control, burned (4)	2014	67.2 ± 10.8	67.6 ± 15.4			-0.021	-43
	Even thin, burned (4)	2011, 2014	70.5 ± 12.3	40.8 ± 9.5			**-0.096**	-169
	Variable thin, burned (4)	2011, 2014	67.2 ± 10.6	39.4 ± 11.9			**-0.12**	-202
Sugar Pine[2]	Control (182)	NA	71.4 ± 33.0	65.4 ± 34.1	73.7 ± 13.5	71.5 ± 14.0	**-0.021**	-40
	Mastication (11)	2008-2013	60.8 ± 9.6	54.2 ± 10.2	77.2 ± 3.7	74.3 ± 4.2	-0.0058	-11
	Tractor thin (15)	2008-2013	63.9 ± 17.5	54.6 ± 16.2	75.6 ± 5.7	71.3 ± 6.3	-0.015	-45
	Underburn (4)	2008-2013	64.9 ± 23.0	59.3 ± 23.1	76.9 ± 4.8	74.5 ± 5.6	-0.012	-4

[1]In treatment units, this is relative to the change in the control: $(\mu_{tb} - \mu_{ta}) - (\mu_{ca} - \mu_{cb})$ where μ is the mean NDVI value for either 5 years before or 4-5 years after treatment in treated and control units, *t* indicates treated, *c* indicates untreated, *a* is after treatment, and *b* is before treatment. For control units, the value indicates difference in control units before and after treatments only. Bold type indicates a significant difference at p=0.05 or less using a 2-way ANOVA with significance determined by interaction between treatment and before and after designation. Statistical significance for change in controls used a pair-wise t-test.

[2]Last Chance and Sugar Pine treatments took place between 2008 and 2013. Pre-treatment NDVI was taken as an average of 2004 to 2008 annual NDVI values. Post-treatment NDVI was taken as an average of 2013-2016 annual values (P. Saksa, pers. comm., 2017).

[3]Blodgett control and moderate-thin compartments were evaluated for mean annual NDVI for 2000-2004 and 2012-2016. Control and intensive-thin sites were evaluated for 1993-1997 (before) and 1999-2003 (after) for the site treated in 1998 and for 2003-2007 (before) and 2009-2013 (after) for the site treated in 2008 (A. Thompson, pers. comm., 2017).

[4]STEF treatments were evaluated for NDVI change by averaging annual NDVI for the period 2006-2010 (before) and 2012-2016 (after) (E. Knapp, pers. comm., 2017).

Table 3-2. Kings River watershed fires 1990-2008

Fire	Year	Area, ha	Elevation range, m	Basal area reduction class, %	% Area by class	5-year post-fire mean ET change, mm	Years to recovery[1]
Avalanche	1990	1186	1790-3035	0-25	56.3	-90	13
				25-50	15.6	-172	21
				50-75	15.2	-217	23
				75-100	12.9	-251	23
Buck Peak	1993	880	1899-2842	0-25	64.1	-89	14
				25-50	18.7	-135	17
				50-75	13.2	-190	18
				75-100	4.1	-235	18
Choke	1997	1612	1905-3140	0-25	31	-20	5
				25-50	16.6	-92	13
				50-75	21.3	-158	16
				75-100	31.1	-244	17
Sugarloaf	1997	152	2192-2408	0-25	69.3	-41	8
				25-50	15.9	-71	11
				50-75	10.2	-95	12
				75-100	4.5	-161	11
Williams	1999	259	2443-2874	0-25	92.8	-46	10
				25-50	5.1	-133	16
				50-75	2.1	-110	17
				75-100	0	NA	NA
Millwood	2000	110	1107-1512	0-25	30.7	-43	5
				25-50	12.5	-180	15
				50-75	28.4	-244	15
				75-100	28.4	-241	15
Burnt	2001	973	1698-3019	0-25	61.6	-48	8
				25-50	15.7	-103	11
				50-75	15.6	-142	13
				75-100	7.1	-187	14
Highway	2001	1719	932-1679	0-25	45.7	-101	11
				25-50	17.5	-193	14
				50-75	25.5	-246	15
				75-100	11.4	-287	15

Table 3-2. (cont.)

Fire	Year	Area, ha	Elevation range, m	Basal area reduction class, %	% Area by class	5-year post-fire mean ET change, mm	Years to recovery[1]
Palisade	2002	637	2565-3297	0-25	37.9	-28	6
				25-50	29.1	-47	10
				50-75	17.4	-75	13
				75-100	15.6	-82	13
Williams	2003	1516	2303-2901	0-25	77.9	-79	10
				25-50	13.5	-119	12
				50-75	6.8	-143	12
				75-100	1.9	-168	13
Comb	2005	4222	1485-2904	0-25	48.7	-40	6
				25-50	20.1	-101	9
				50-75	20.9	-150	10
				75-100	10.3	-210	11
Burnt	2006	275	2147-2844	0-25	85.2	-56	7
				25-50	8.3	-93	9
				50-75	6.5	-123	10
				75-100	0	NA	NA
Roaring Ridge	2006	753	1676-2749	0-25	97.3	-80	8
				25-50	2.3	-132	10
				50-75	0.4	-140	10
				75-100	0	NA	NA
Tehipite	2008	5020	1267-2850	0-25	70.8	-98	7
				25-50	13.3	-152	8
				50-75	11.6	-197	8
				75-100	4.2	-255	8

[1]Years to recovery was defined as the number of years post-fire until mean annual NDVI equaled or exceeded the pre-fire 5-year mean.

Table 3-3. American River watershed forest fires 1990-2008.

Fire	Year	Area, ha	Elevation range, m	Basal area reduction class, %	% Area by class	5-year post-fire mean ET change, mm	Years to recovery[1]
Cleveland	1992	9338	1002-1876	0-25	14.7	-44	8
				25-50	10.9	-195	16
				50-75	18.2	-263	18
				75-100	56.1	-382	20
Kelsey	1994	514	574-771	0-25	22.1	-90	10
				25-50	12.3	-151	14
				50-75	24.3	-258	18
				75-100	41.3	-374	19
Mill	1995	51	1639-1721	0-25	2.9	-77	4
				25-50	2.9	-108	5
				50-75	41.2	-235	13
				75-100	52.9	-347	18
Gap	2001	1034	1538-1863	0-25	9.3	-38	6
				25-50	8.3	-156	13
				50-75	16.4	-253	15
				75-100	66	-304	15
Ponderosa	2001	1224	284-820	0-25	21.6	-119	11
				25-50	18.8	-214	13
				50-75	25.6	-297	14
				75-100	34	-395	15
Star	2001	6332	1089-2150	0-25	22.3	-124	11
				25-50	13.6	-206	14
				50-75	21.6	-273	14
				75-100	42.5	-397	15
Hunter	2002	283	1599-1798	0-25	39.2	-148	12
				25-50	30.4	-269	13
				50-75	23.8	-344	14
				75-100	6.6	-396	14
Plum	2002	767	1254-1652	0-25	73.9	-87	9
				25-50	12.9	-270	13
				50-75	10.4	-390	14
				75-100	2.8	-530	14

Table 3-3. (cont.)

Fire	Year	Area, ha	Elevation range, m	Basal area reduction class, %	% Area by class	5-year post-fire mean ET change, mm	Years to recovery[1]
Cod Fish	2003	355	782-1285	0-25	62.2	-135	10
				25-50	18.2	-271	12
				50-75	14.9	-331	13
				75-100	4.8	-465	13
Freds	2004	3194	1227-2128	0-25	6.9	-174	10
				25-50	8.5	-220	12
				50-75	19.8	-289	12
				75-100	64.8	-379	12
Stevens	2004	401	370-854	0-25	21.2	-131	11
				25-50	20	-222	12
				50-75	31.9	-310	12
				75-100	27	-426	12
Ralston	2006	3586	361-1411	0-25	60.7	-109	8
				25-50	15.3	-211	9
				50-75	16.5	-295	10
				75-100	7.6	-392	10
Government	2008	8467	714-2046	0-25	38.6	-149	7
				25-50	17.9	-219	7
				50-75	21.2	-291	8
				75-100	22.3	-393	8
Peavine	2008	272	1342-1551	0-25	49.2	-154	6
				25-50	16.3	-262	8
				50-75	17.1	-367	8
				75-100	17.4	-473	8

[1]Years to recovery was defined as the number of years post-fire until mean annual NDVI equaled or exceeded the pre-fire 5-year mean.

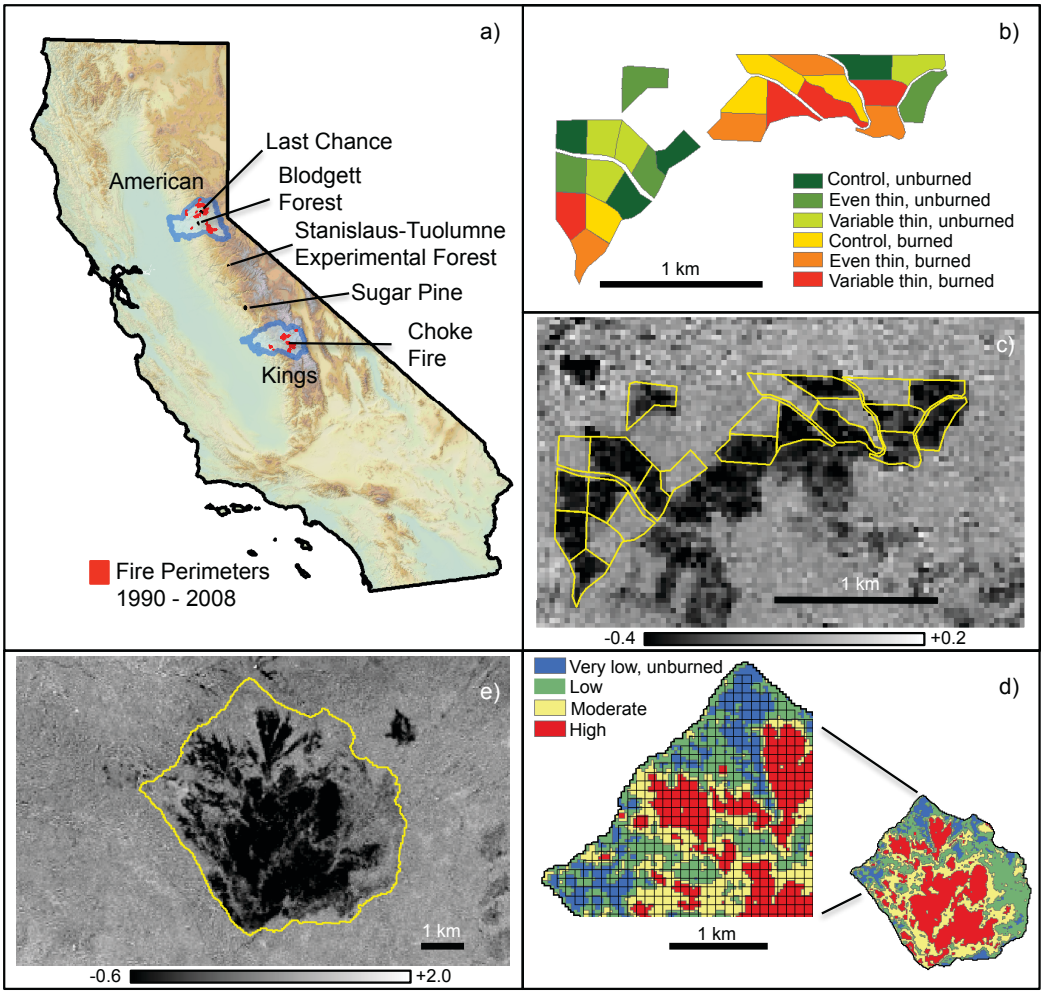

Figure 3-1. Location of forest fires and treatments examined in this study, clockwise from top left: a) overview map showing all fires in the American and Kings watersheds for the 1990-2008 period as well as selected forest treatment areas, b) experimental forest thinning treatment design for the Stanislaus-Tuolumne Experimental Forest Variable Thinning Project (STEF), c) NDVI change at STEF between July 22, 2010 and July 30, 2013, pre- and post-treatment, d) perimeter and burn severity of the 1997 Choke Fire (lower right) and an expanded region of the fire that illustrates the 90-m polygon mesh used to sample Landsat NDVI imagery, and e) NDVI change of Choke Fire between July 24, 1996 and July 30, 1998.

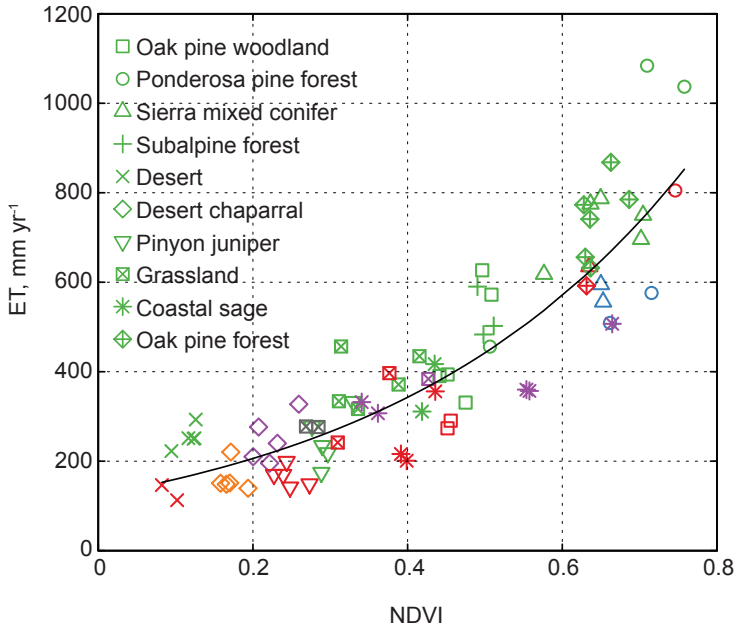

Figure 3-2. Annual water year evapotranspiration (ET) at ten flux towers versus annual average Landsat-derived normalized difference vegetation index (NDVI) for upwind contributing areas at each location for water years 2007-2016. Point colors represent impacts to vegetation at each site as follows: none (green), drought (red), drought and management action (blue), fire (purple), drought and fire (orange), and management action (grey). See text for a more complete description. Best fit regression for all years is ET (mm yr^{-1}) = 123.8243 × $e^{(2.5456 \times NDVI)}$, where NDVI ranges from 0 to 1 (R^2 = 0.7917). For information on the flux towers used, see Goulden et al. (2012).

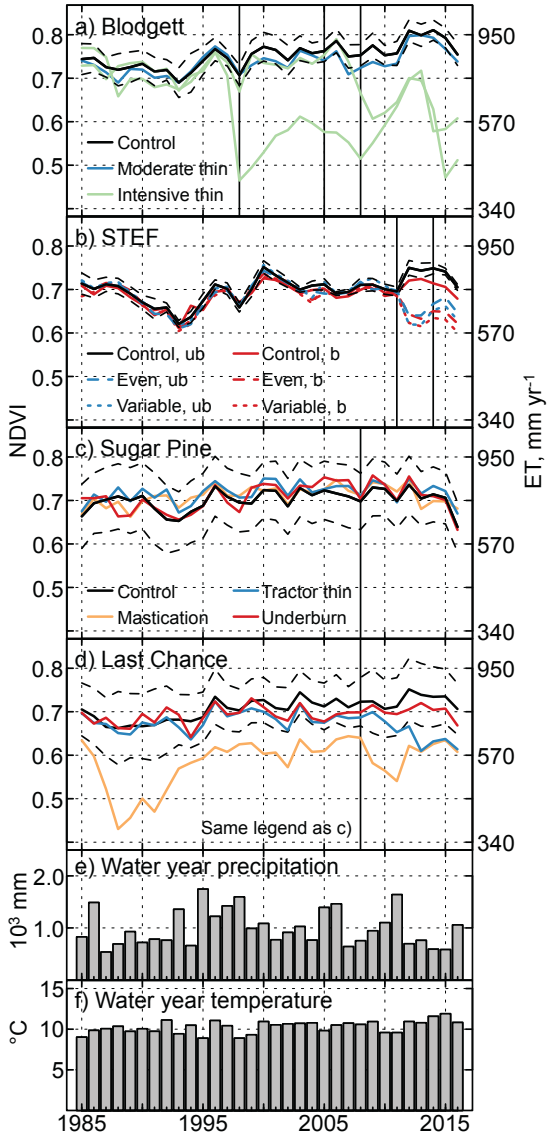

Figure 3-3. NDVI change for forest treatments shown by vertical lines. a) Blodgett Experimental Forest, where vertical lines from the left indicate intensive thinning in 1998, moderate thinning 2004-2006, and intensive thinning in 2008, b) Stanislaus-Tuolumne Experimental Forest (STEF), where vertical lines from the left indicate initial thinning in 2011 followed by underburns in half of the units in 2014, b=burned and ub=unburned, c) SNAMP Sugar Pine site and d) SNAMP Last Chance site, where the vertical line indicates initial year of treatments in 2008. Dashed lines indicate standard deviation around the control blocks. Panels e) and f) show mean annual precipitation and temperature for the central Sierra Nevada area. Note that tick labels for ET are based on Figure 3-2, and thus the axes are non-linear. See Table 3-1 for information on treatments.

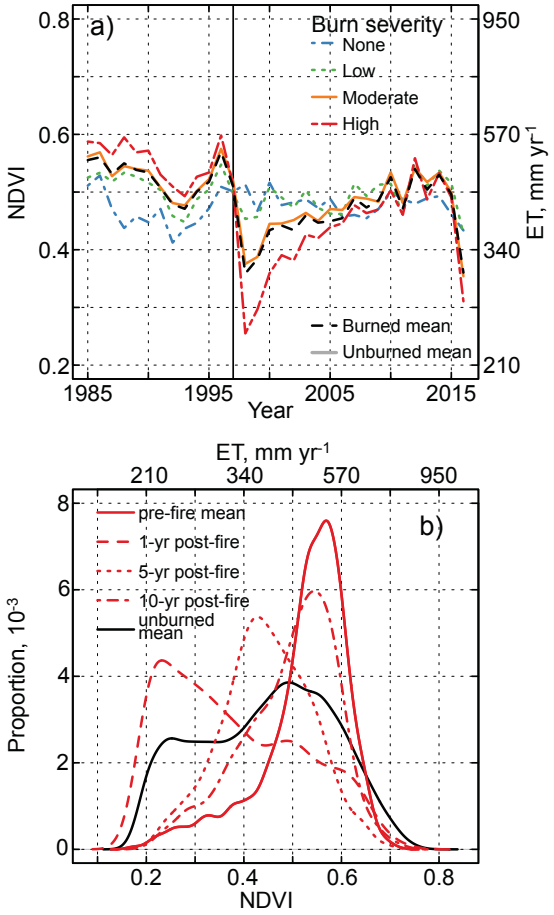

Figure 3-4. a) NDVI progression for the area of the 1997 Choke Fire in the Kings River watershed. The unburned mean was derived from randomly located 90-m square polygons within the same elevation range as the Choke Fire and outside of all areas burned during the 1990-2008 period. Year of the fire is marked by a vertical black line. b) NDVI distribution within the Choke Fire perimeter before the fire, 1, 5, and 10 years post burn, and the mean of unburned areas (black line) for the 10 years post-burn (1998-2007). Note that tick labels for ET are based on Figure 3-2, and thus the axes are non-linear. See Tables 3-2 and 3-3 for information on fires.

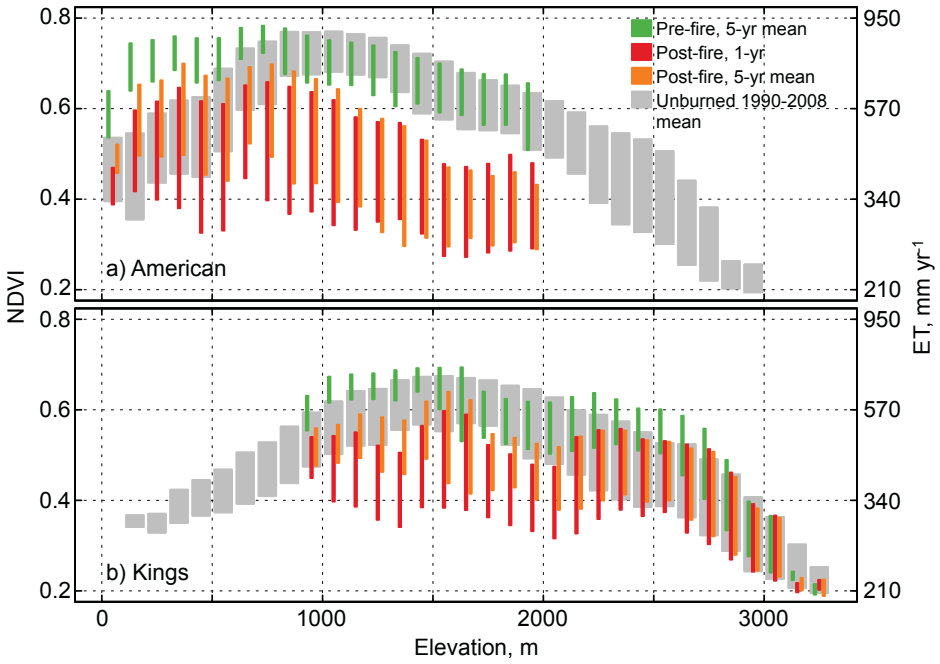

Figure 3-5. NDVI and ET change due to fire by 100-m elevation band for all fires greater than 100 ha 1990-2008 in the American (a) and Kings (b) watersheds. Bars span the 25th to 75th percentiles. Green bars indicate the NDVI mean in areas that burned over the 5 years prior to the fire. Grey shaded area indicates the mean 25-75 percentile of NDVI values for the entire watershed that did not burn during this period.

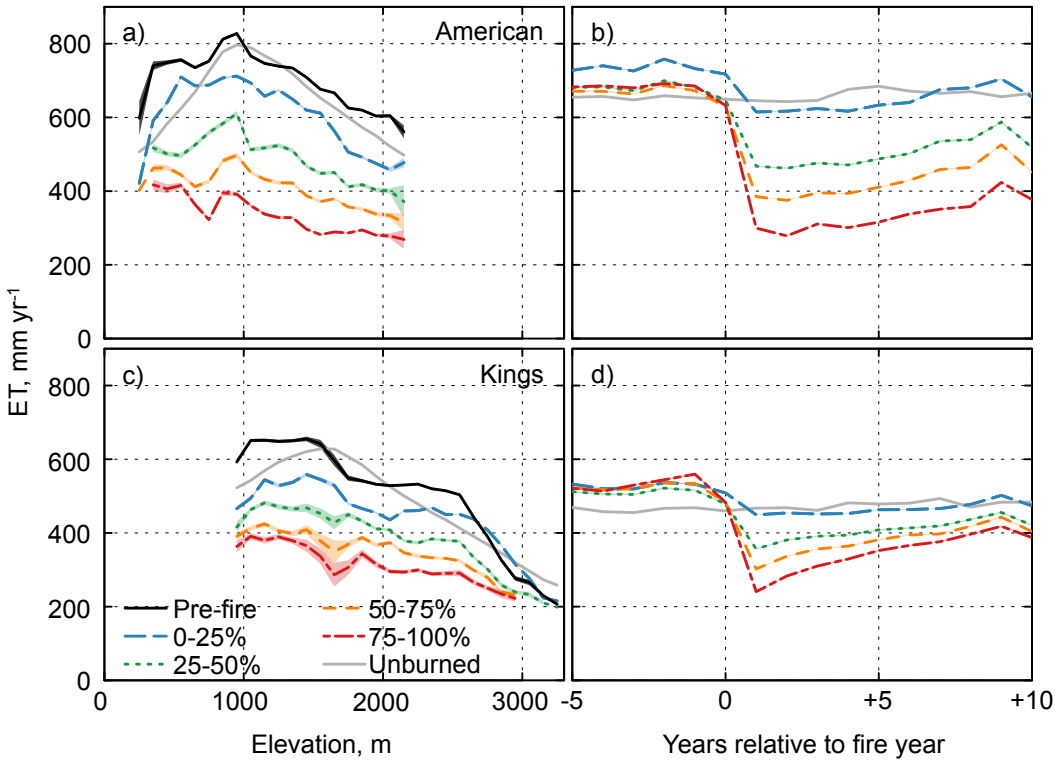

Figure 3-6. Impact of basal area reduction by forest fire on estimated evapotranspiration change, as determined by the mean 5-year change in ET difference between burned and unburned areas before and after the fire. Left panels (a, c) depict variation by 100-m elevation band. Only elevations with fires in the 1985-2013 period are shown. The black line is the estimated pre-fire 5-year mean ET. Right panels (b, d) illustrate the variation temporally from 5 years prior to 10 years after the fire. Shaded areas indicate plus and minus the standard error where greater than the thickness of lines (about 10 mm yr^{-1}). Data for these plots are summarized in Tables 3-2 and 3-3.

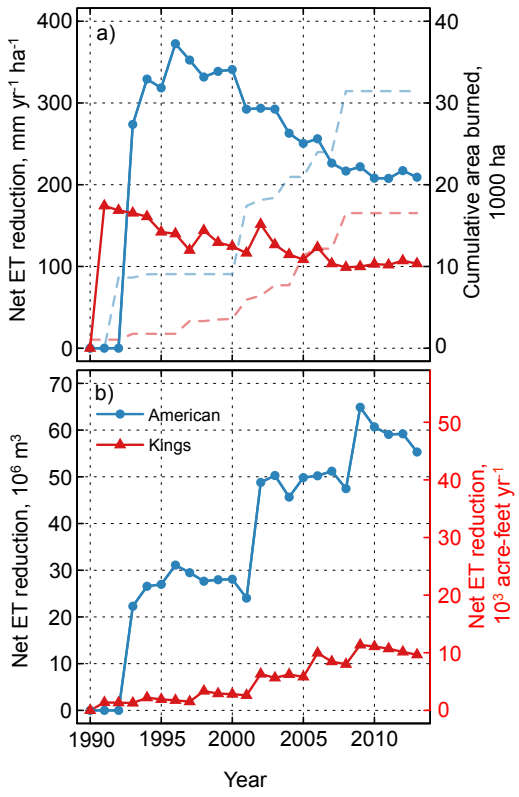

Figure 3-7. a) Net annual ET reduction depth per unit area burned (bold lines) and cumulative area burned (dashed lines), and b) net annual ET reduction volume resulting from fires in the American and Kings River watersheds 1990-2008. Note the only fires through 2008 were included in the analysis.

Summary Conclusion

Study Results

Estimating snowpack sensitivity to temperature increases and alternative atmospheric moisture scenarios in the Merced and Tuolumne River watersheds required assembling hourly forcing data and measured snow depth and water content for recent water years (2010-2014) that exhibited typical climatic variability. Climate data included temperature, relative humidity, precipitation, wind speed and direction, and solar radiation data from stations that spanned the area of interest, and were known to receive regular maintenance and calibration. The time series were quality controlled for outliers and continuity and then gap filled where possible. Snow data received similar treatment. Included with the data set were soil moisture data from sensors collocated with snow depth measurements that, while not used here, provide a means of more fully evaluating both snow and soil water storage components across the rain-to-snow transition zone. Spatial data layers in the data set were basin polygons and co-registered 100-m rasters of elevation and vegetation type, height, cover, and transmissivity to light properties.

The foregoing data were used to force the distributed energy- and mass-balance snowpack model (iSnobal; Marks et al., 1999) in order to assess the sensitivity of snowpack to changing climatic conditions using recent wet and dry years as starting points. Model results for water years 2011 and 2013 tended to under estimate snow water equivalent (SWE) when compared to available measurements, particularly at lower elevations and in the dry year (2013), compared well with measured snow depth

measurements, and over-estimated SWE when compared to the NASA Airborne Snow Observatory SWE product. Maximum sensitivity to temperature increases was observed at the 2800-2900 m elevation band, which was also the band of maximum accumulation, with modeled decreases in April 1 SWE of 38 (14)%, 55 (49)%, and 78 (73)% from base dry (wet) years for +2, 4, 6°C warming. Peak SWE timing shifted from mid-March to mid-January with a 2°C increase in temperature for the dry year scenario and exhibited no shift for the wet year. The zone of peak melt contracted upwards 500 m with 6°C warming in the Merced basin, while there was little change in the Tuolumne. SWE was reduced by 50-100 mm after April 1 and meltout occurred 1-2 week earlier in the wet +6°C constant relative humidity scenario relative to the constant vapor pressure scenario.

We estimated changes in forest "greenness" following treatment and wildfire in order to determine potential changes in evapotranspiration. Significant NDVI change resulting from forest treatment in the American watershed ranged from 0.07 to 0.18 units, corresponding to basal area reductions of 9 and 58% and estimated ET change of -102 to -306 mm yr^{-1}, respectively. For tractor thinning treatments on Sierra Nevada Adaptive Management Project (SNAMP) sites, NDVI remained unchanged in the water-limited Sugar Pine area, despite greater reductions in basal area (15%) than those in the Last Chance area (9%) where change was detected. Peak pre-fire ET estimates were 830 and 650 mm yr^{-1} in the 900-1000 and 1400-1500 m elevation bands in the American and Kings watersheds, respectively. A 50% reduction in basal area due to forest fires in the American and Kings watersheds from 1990 to 2008 corresponded with respective reductions of 320 and 200 mm yr^{-1} in mean 5-year post-fire ET at 1000 m elevation.

Major Findings

Snowpack sensitivity to climate warming was observed to be much larger in the dry- versus wet-year scenarios due to a combination of warmer temperatures and precipitation timing, especially during early fall storms in the dry year. Dry-year April 1 SWE decreased 38, 73, and 90% basin wide for the +2, 4, 6°C warming scenarios. The lower elevation limit of the seasonal snowpack retreated upslope approximately 300 m per 2°C warming and disappeared below 2000 m elevation with 4°C warming. Finally, assuming vapor pressure between storms remains constant with rising temperatures resulted in up to 100 mm more late season SWE (+6°C wet year scenarios) than the usual modeling approach that assumes constant relative humidity.

Among forest treatments and fires assessed, water-limited areas exhibited lower NDVI change per unit change in basal area when compared to less-water-limited areas. Intensive thinning projects at Blodgett and the Stanislaus-Tuolumne Experimental Forest, where stands were thinned to historic densities (40-50% basal area reduction), reduced mean 5-year post-treatment NDVI by 0.09-0.12 units from pre-treatment and control NDVI values of 0.7-0.8. The corresponding estimated ET reduction was 152 to 216 mm yr^{-1}. SNAMP treatments exhibited a minimum significant NDVI change of 0.07 units from control plots with a mean NDVI value of 0.7 in the Last Chance area (American basin) and non-significant changes in NDVI in the more water-limited Sugar Pine area. Mean 5-year post-fire ET rate reduction for burned areas in the American River watershed was twice that of the Kings River watershed from 1990 to 2008. During this

period, twice as much area burned in the American basin and net annual ET reduction in the American grew to nearly five times that in the Kings watershed (65 versus 14 million m^3 yr^{-1}). If one assumes that nearly 10 times this area would have burned historically during this period, ET reduction in the American could approach 10% of full natural runoff from the watershed in dry years.

Limitations

Limited precipitation measurements in the seasonal snow zone and a lack of quality shortwave and longwave radiation measurements does necessarily constrain our direct application of the data to snow modeling. As demonstrated in Chapter 2, however, coupling the point time series with an ever-improving suite of spatial distribution tools and modeled radiation inputs, allows an analysis at scales relevant to landscape management. The addition of 2-3 weighing or accumulation precipitation gauges could substantially improve our understanding of variability in rain versus snow accumulation, especially in the 2000-3000 m elevation range where most of the snowpack forms. Improvements to California Department of Water Resources (DWR) stations, most of which were excluded from the data used in snow modeling for quality and continuity reasons, is taking place as of this writing and includes the addition of overflow tipping bucket precipitation gauges as well as net shortwave radiometers. Longwave measurements remain lacking, though the addition of these measurements could substantially improve snowmelt prediction (Lapo et al., 2015). Beyond snowpack modeling, the soil-moisture data included in the data set, will permit future analyses of

soil water storage as it becomes an increasingly important part of water storage in the basins.

The adequacy of snow modeling is largely limited by the quality of the forcing data and the means by which it is distributed. Spatial distribution of sparse precipitation point data resulted in mismatches between precipitation timing with respect to dew point, which changed the precipitation state. Moreover, precipitation amount as scaled by PRISM data (PRISM Climate Group, 2012) was clearly under estimated in the northern part of the model domain, as has been pointed out by Henn et al. (2015). All radiation input to the model was modeled using available pyranometer measurements just to estimate cloudiness. We ascribed a single set of albedo parameters, which failed to adequately account for late-season litter and dust accumulation at the snow surface. Finally, computational constraints limited the analysis to a single set of input parameters, which makes error propagation difficult if not impossible.

Estimating forest ET using Landsat NDVI promises to help quantify benefits of forest treatments, though advances are required in several areas to more accurately constrain estimates and permit robust scaling from experimental treatments to the watershed scale. Most limiting were a lack of readily available forest-treatment data, whether experimental or not, to investigate the range and variability of the impacts of different treatment types on NDVI across the Sierra Nevada. Assembling a data set for regional forests that included date of treatment, type of treatment, and measured changes in canopy cover, basal area, and biomass would greatly aid future investigation. Finally,

further elucidating the impact of forest treatment, drought, and mortality on measured ET at flux-tower locations will be required to adequately extend these results to other areas.

Management Implications

The data assembled for snow modeling could be used to refine the methods used in Chapter 2 to predict snowmelt runoff. Recently developed tools will facilitate using ensemble scenarios with respect to measurement uncertainty or climate variability in order to generate probabilistic results (Havens et al., in prep). The data set also contributes to the archive of quality-controlled climate data in the Yosemite region beyond WY2010-2014 (Edwards & Redmond, 2011; Lundquist et al., 2016) that could be used for other analyses requiring detailed weather observations such as fire behavior or mixed rain-snow runoff modeling. Finally, the data set highlights the critical need for improved precipitation and radiation data, both in real-time and for long-term monitoring. During numerous wet and warm storms in the winter of 2017, river flood forecasts were severely hampered by uncertainty in the amount and phase of precipitation falling across the broad middle elevations between 2000 and 3000 m.

A reduced snowpack and earlier meltout timing will require adaptive management in the areas of mountain meadow and wetland habitat maintenance, recreation, water supply, and forest fire. Subalpine meadows such as the iconic high-elevation Tuolumne Meadows in Yosemite National Park will lose much of its annual snowpack with +4 and +6°C warming in dry years and wet years, respectively, reducing the time that soils are saturated and making conditions favorable for conifer growth. Increased recreational

access to the high-country area due to reduced snowpack will require adjustments to current management practices in order to protect national park and forest resources. Wildlife dependent on late melting snows to create breeding habitat such as Yosemite Toad could experience reduced reproductive opportunities. Mountain communities, dependent on surface water, will experience greater reductions in late-season water availability due to a shift from snow- to rain-dominated winter conditions and loss of snowpack storage. Further downstream, almost all spring and summer runoff would originate from increasingly diminished snowpack as increased ET demand reduces input from groundwater at lower elevations. Finally, much of Yosemite's forests that are currently in the seasonal snowpack zone could become more available to fire due to a lack of sustained snowmelt input to soils in the early spring and summer. Increased ET demand and a lengthening fire season will require a substantial shift in forest management to prevent catastrophic wildfire and sustain perennial stream flow.

Forest resilience to drought, climate warming, and high-severity fire could be enhanced through intensive thinning that approximates historic forest densities. The work presented here suggests that overstocked forests in the American and Kings River watersheds use more water than those areas that were thinned by treatment or fire. Moreover, if forested areas in both watersheds had burned close to their original fire return interval, nearly all of the basins would have experienced fire at some point in the 1990-2008 period resulting in a greater than 5% decrease in average ET, which increases to greater than 10% in drought years. Intensive forest thinning examined in this study is similar to moderate severity forest fire in terms of basal area and estimated ET reduction.

Given that less than 25% of forested areas in the Sierra Nevada could be mechanically thinned due to physical, economic, and administrative constraints (North et al., 2015), managed fire will be essential to mitigating increased forest ET demand as the climate warms. Indeed, fire is the only tool available for managing national parks, such as Yosemite, and wilderness areas throughout the Sierra Nevada. Land managers may use these results to help build stakeholder support for planned and managed lightening-caused fires over larger portions of the landscape.

References

Edwards, L. M., & Redmond, K. T. (2011). Climate Assessment for the Sierra Nevada Network Parks. Natural Resource Report. NPS/2011/NRR—2011/482. (pp. 178). National Park Service, Fort Collins, Colorado. Retrieved from https://irma.nps.gov/DataStore/Reference/Profile/2181911

Havens, S. C. (in preparation). Spatial Modeling for Resources Framework. Retrieved from http://smrf.readthedocs.io/en/latest/index.html

Henn, B., Clark, M. P., Kavetski, D., & Lundquist, J. D. (2015). Estimating mountain basin-mean precipitation fromstreamflow using Bayesian inference. *Water Resources Research*, *51*, 8012–8033. doi: 10.1002/2014WR016736

Lapo, K. E., Hinkelman, L. M., Raleigh, M. S., & Lundquist, J. D. (2015). Impact of errors in the downwelling irradiances on simulations of snow water equivalent, snow surface temperature, and the snow energy balance. *Water Resources Research*, *51*(3), 1649–1670. doi: 10.1002/2014WR016259

Lundquist, J. D., Roche, J. W., Forrester, H., Moore, C., Keenan, E., Perry, G., … Dettinger, M. D. (2016). Yosemite Hydroclimate Network: Distributed stream and atmospheric data for the Tuolumne River watershed and surroundings. *Water Resources Research*, *52*(9), 7478–7489. doi: 10.1002/2016WR019261

Marks, D., Domingo, J., Susong, D., Link, T., & Garen, D. (1999). A spatially distributed energy balance snowmelt model for application in mountain basins. *Hydrological Processes*, *13*(February), 1935–1959. doi: 10.1002/(SICI)1099-1085(199909)13:12/13<1935::AID-HYP868>3.0.CO;2-C

North, M. P., Brough, A., Long, J., Collins, B., Bowden, P., Yasuda, D., … Sugihara, N. (2015). Constraints on mechanized treatment significantly limit mechanical fuels reduction extent in the Sierra Nevada. *Journal of Forestry*, *113*(1), 40–48. doi: 10.5849/jof.14-058

PRISM Climate Group. (2012). United States Average Annual Precipitation, 1981-2010. Oregon State University.

Appendix A. Supplemental figures to Chapter 2.

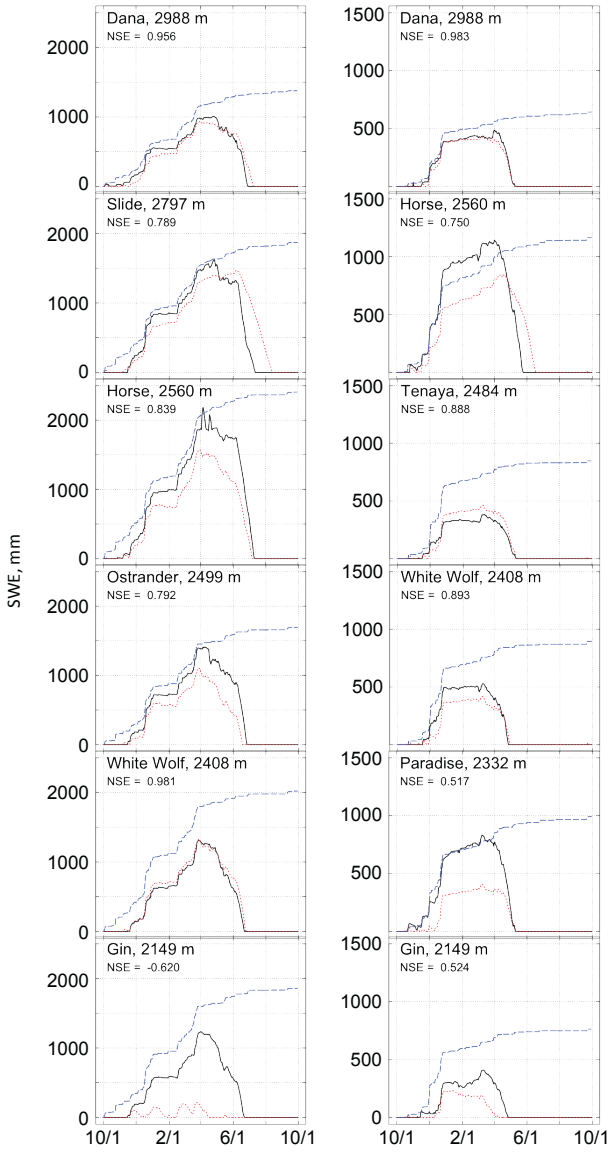

Figure A1. Observed (solid black) and modeled (dotted red) SWE at snow pillows Water Year 2011 (left) and 2013 (right). Dashed blue line depicts cumulative precipitation from daily 800 m PRISM dataset. NSE refers to the Nash-Sutcliffe coefficient indicating the level of agreement. Note different SWE scales for the two water years.

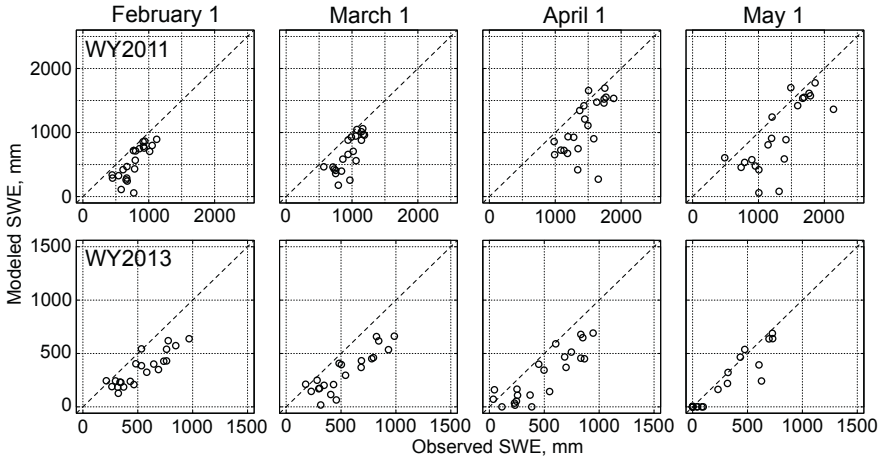

Figure A2. Observed and modeled SWE results at snow courses. See Table 2.2 for site information.

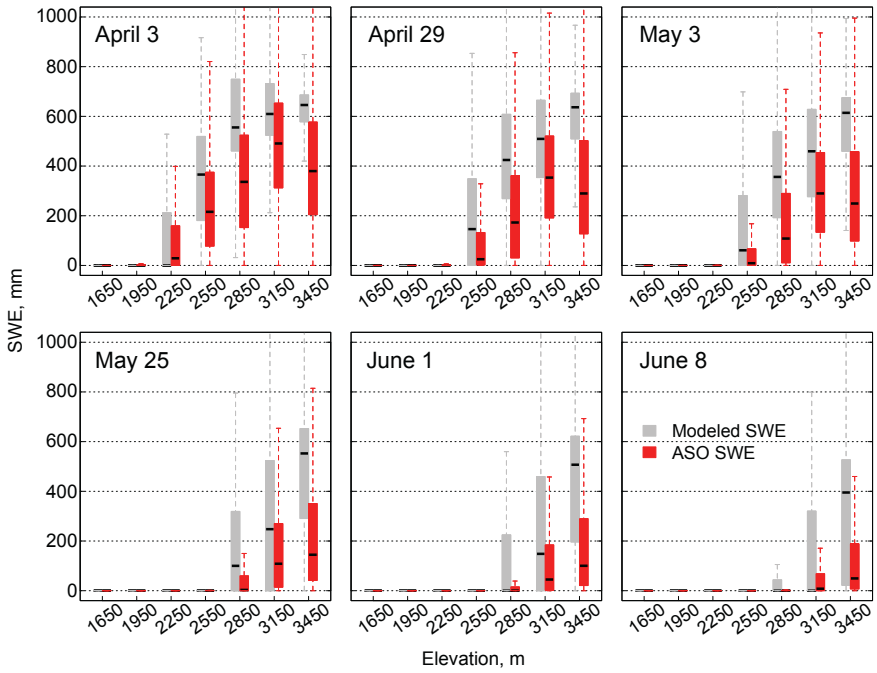

Figure A3. Box and whisker plots of modeled (gray) and NASA Airborne Snow Observatory derived SWE (red) by 300-m elevation bands in the Hetch Hetchy Watershed for water year 2013. Boxes span the 25th to 75th percentile values, with the black bar indicating the median and whiskers spanning the range of data.

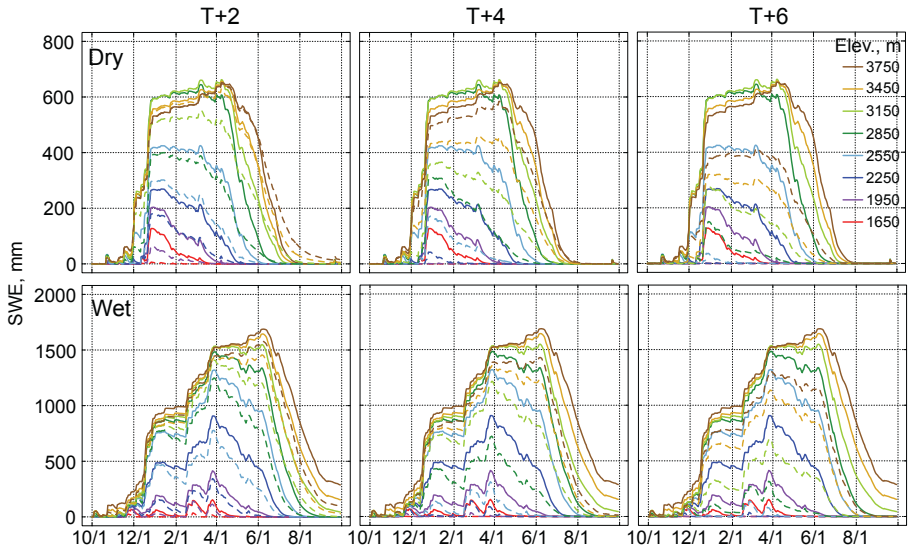

Figure A4. Snow water equivalent by 300-meter elevation band for base and climate scenarios in the Merced River basin. Solid Lines = Base model years (Dry = 2013, Wet = 2011) Dashed Lines = Constant-relative-humidity temperature increase scenarios.

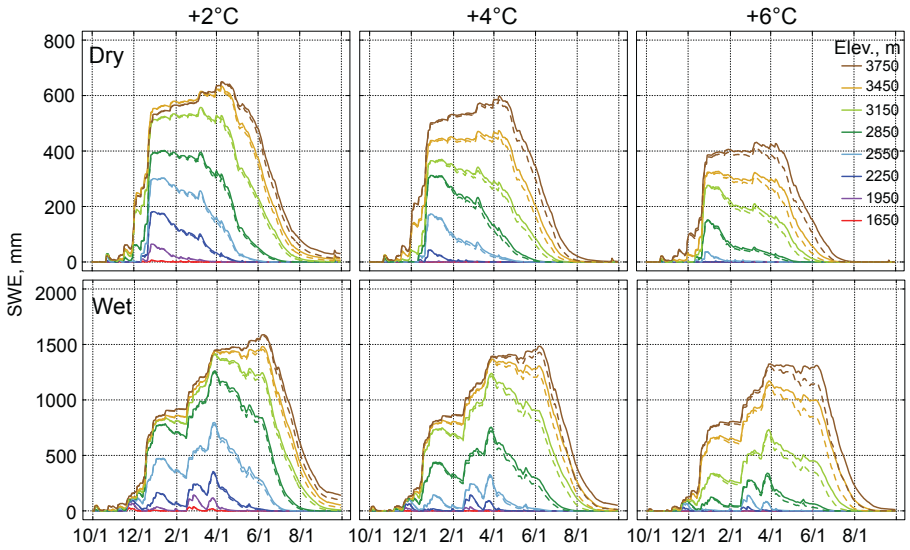

Figure A5. Modeled snow water equivalent by 300-meter elevation band comparing atmospheric moisture scenario results in the Merced River basin in dry and wet years. Solid lines = Constant vapor pressure. Dashed lines = Constant relative humidity.